UNCLASSIFIED

AD NUMBER
AD872866

LIMITATION CHANGES

TO:

Approved for public release; distribution is unlimited. Document partially illegible.

FROM:

Distribution authorized to U.S. Gov't. agencies and their contractors; Critical Technology; JUL 1970. Other requests shall be referred to Air Force Rome Air Development Center, EMATE, Griffiss AFB, NY 13440. This document contains export-controlled technical data.

AUTHORITY

radc, usaf, ltr, 17 sept 1971

THIS PAGE IS UNCLASSIFIED

AD872866

RADC-TR- 70-132
Final Technical Report
July 1970

C-BAND PHASED ARRAY CROSSED-FIELD AMPLIFIER DEVELOPMENT

Contractor: Varian/Eastern Tube Div.
Contract No.: F30602-68-C-0055
Effective Date of Contract: 2 Oct 67
Contract Expiration Date: Dec 69
Amount of Contract: $239,750.00
Program Code No.: 7E30
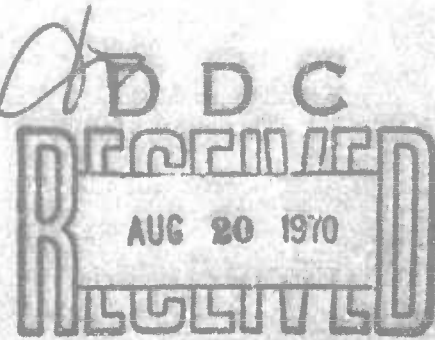
Principal Investigator: A. Wilczek
Phone No.: 201 687-0250

Project Engineer: D. Bussey
Phone No.: 315 330-7057

Sponsored by
Advanced Research Projects Agency
ARPA Order No. 136, Amendment 15

The views and conclusions contained in this document are those of
the authors and should not be interpreted as necessarily repre-
senting the official policies, either expressed or implied, of the
Advanced Research Projects Agency or the U.S. Government.

Rome Air Development Center
Air Force Systems Command
Griffiss Air Force Base, New York

DDC
RECEIVED
AUG 20 1970

C-BAND PHASED ARRAY CROSSED-FIELD AMPLIFIER DEVELOPMENT

A. Wilczek

Varian/Eastern Tube Division

Union, New Jersey

FOREWORD

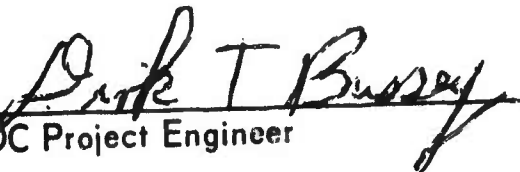Distribution of this report is restricted under the U. S. Mutual Security Acts of 1949.

This report has been reviewed and is approved.

RADC Project Engineer

ABSTRACT

This program has two main objectives. The first is to demonstrate the feasibility of an RF turn on, RF turn off, reentrant stream crossed-field amplifier. The second objective of this program is to increase the power output capability previously demonstrated under Contract AF 30(602)-4082 by a factor of two.

The first objective was met very successfully as RF turn on and RF turn off were demonstrated reliably in a number of experiments in two different amplifier types. The second objective was partially accomplished with very significant results.

TABLE OF CONTENTS

iv

LIST OF ILLUSTRATIONS

*Tradename, S-F-D laboratories/A Varian Division

vii

LIST OF TABLES

1.0 INTRODUCTION

This program effort had two main objectives. The first objective was to demonstrate the feasibility of an RF turn-on, RF turn-off reentrant crossed-field amplifier (CFA) to minimize or eliminate any modulation requirements. RF turn on, on previous programs at S-F-D laboratories under ARPA Order 136*, has been demonstrated to be quite reliable and needs very little, if any, further effort. Turn off in previous designs was obtained by pulsing a control electrode and also has been demonstrated on the previous programs. However, the objective of this program was to obtain RF turn off with a significantly reduced control electrode requirement (e.g. with dc bias) or by eliminating the turn off electrode voltage completely. To this end, twelve experiments were performed using two SFD-237 amplifiers which were developed on Contract AF 30(602)-4082, which immediately preceded this contract. (The SFD-237 was developed to be operated in C-band at a peak power of 1 Mw and an average power of 10 kw with RF turn on and with turn off accomplished by a pulsed control electrode.) The twelve experiments performed did indeed demonstrate RF turn off using only a dc bias voltage. The self-turn-off mechanism was demonstrated reliably in seven of the twelve experiments performed, as well as in the SFD-252 which uses a different slow wave circuit configuration. This type of self-turn-off operation, which we will refer to as AutoMod** operation, has been demonstrated at power levels of 800 kw to 1000 kw peak with constant cathode voltage and 1000 kw or better at fixed cathode current (where the cathode voltage was adjusted for maximum power). Both modes of operation were accomplished with

---

* Contract Numbers AF 30(602)-2533, AF 30(602)-3633, and AF 30(602)-4082.
** Tradename, S-F-D laboratories/A Varian Division

1

a fixed bias voltage and RF input power across a frequency band of
500 MHz from 5.4 GHz to 5.9 GHz. Average power output was limited to
approximately 3.5 kw by the equipment being used. At this power level,
no degrading effects had been observed, and it is expected that the
vehicle can achieve at least twice this average power output without
serious modification.

The second objective of this program was to increase the
power output capability previously demonstrated[*] by a factor of two.
The performance goals are given in Table I. A new slow wave circuit
was designed, i.e., different from that used on AF 30(602)-4082. This
circuit is generically a helix derived circuit in which the interaction
height has been extended and the thermal impedance reduced. More
specifically, it is a double helix coupled bar circuit in which the
coolant is passed directly through the elongated anode bars. The
electrical design parameters are given in Table II.

Because of the complexity of this type of vehicle and the
limited funds available, only one vehicle was constructed. The
results obtained with this vehicle were very significant, but its
evaluation was not as extensive as would be desired. The vehicle,
designated as the SFD-252, was operated across the 500 MHz band with
a peak power output in excess of 1 Mw with an input power of
approximately 100 kw. This limit on peak output performance was
imposed by equipment limitations during cathode pulsed conditions and
by the expiration of funds during the dc control electrode testing.
The tube was operated with pulse modulation and also under dc control
electrode operation, and all indications are that this design is quite
capable of obtaining the full objective power. But most significantly,
the tube was also operated successfully with RF turn off using some
of the preliminary information obtained from the first AutoMod
experiments.

---
[*]Contract AF 30(602)-4082

TABLE I

SPECIFICATIONS FOR EXPERIMENTAL MODEL
FORWARD WAVE CROSSED-FIELD AMPLIFIER

Center frequency	5.675 GHz
Instantaneous bandwidth	500 MHz
Peak power output	2 Mw
Average power output	20 kw
Pulse duration capability	50 μsec
Gain	13 db
Efficiency	40%
Operating voltage	30 kv
Package size (PM focusing)	10" diameter

TABLE II

PRELIMINARY ELECTRICAL DESIGN

Frequency - GHz	5.425	5.675	5.925
Phase shift per section - degrees	115	123	132
Synchronous voltage - kv	5.32	5.02	4.76
Anode-cathode transit angle- radian	2.31	2.47	2.65
Number of wavelengths	20	21	22
Characteristic magnetic field- gauss	885	862	840
Characteristic current - amps	222	203	188
Interaction impedance - ohms	38	34	31

2.0 RF TURN OFF

In an amplifier utilizing a "cold" secondary emitting cathode, it is possible to apply the operating voltage to the amplifier without drawing current until an RF input pulse is supplied. Upon the application of the RF input pulse, a secondary emission multiplication process causes a rapid buildup of space charge. The process requires RF as well as dc electric fields to occur. Current is drawn by the amplifier and amplification takes place through the normal crossed-field mechanisms. In reentrant stream amplifiers in which electrons circulate from the amplifier output to the input via a drift space, the starting process is extremely rapid and reliable and amplification begins in a matter of a few nanoseconds. At the conclusion of the RF drive pulse, however, the space charge which remains in the amplifier must be cleared from the interaction area or the amplifier via the circulating electrons can become an oscillator or noise generator. The amplifier will not generate spurious outputs prior to the application of the RF pulse because there is no way for electron emission to get started. Low level noise fields cannot energize the few available electrons enough to start the secondary emission buildup. The transition from the driven condition to the self-oscillation or noise generating condition can occur at the end of the RF drive pulse because a space charge cloud exists which can support and amplify the noise fields and in turn cause the secondary emission process to continue.

In the past, the space charge remaining after the removal of the RF pulse has been collected on a third electrode called a control electrode. The control electrode is normally situated on the cathode assembly and during the pulse is kept at approximately cathode potential. At the conclusion of the RF input pulse, a voltage is applied to make the control electrode positive with

5

respect to the cathode to collect the remaining space charge and to prevent recirculation. The ratio of applied dc voltage to the peak control electrode voltage is generally about 3 to 1, and the control electrode is then said to have a mu of 3.

Figure 1 shows the usual pulsing sequence for a control electrode amplifier. The absence of the control electrode voltage pulse will result in the amplifier operating in essentially a CW noise mode. Figure 2 shows the detected RF envelope of the output with the control voltage pulse delayed so that the amplifier operates for a short time without the drive signal to control it. The fuzzy lower level of RF envelope at the trailing edge is the spurious output. The voltage pulse applied to the control electrode may have any length provided that the voltage remains on until the RF pulse has ended. The energy consumed by the control electrode is quite small compared with the energy in the long pulse output of the amplifier. Further, the energy consumed per pulse depends upon the rate of rise of control voltage pulse, higher rates of rise lead to lower energy consumption. There is a practical upper limit to the rate of rise of control voltage because of the currents required to charge the stray and interelectrode capacities. Also, as the amplifier pulse width decreases the control electrode consumes proportionately larger amounts of power, thereby limiting its usefulness in pulse burst applications.

One obvious way of removing the space charge would be to insert an electrode which would collect the remaining current and destroy the reentrancy. This device would now be essentially a circular format non-reentrant amplifier. By destroying the reentrancy, the advantage of rapid and reliable starting is reduced and there is a loss in efficiency. The loss in efficiency increases the thermal problems because more of the input power is dissipated

6
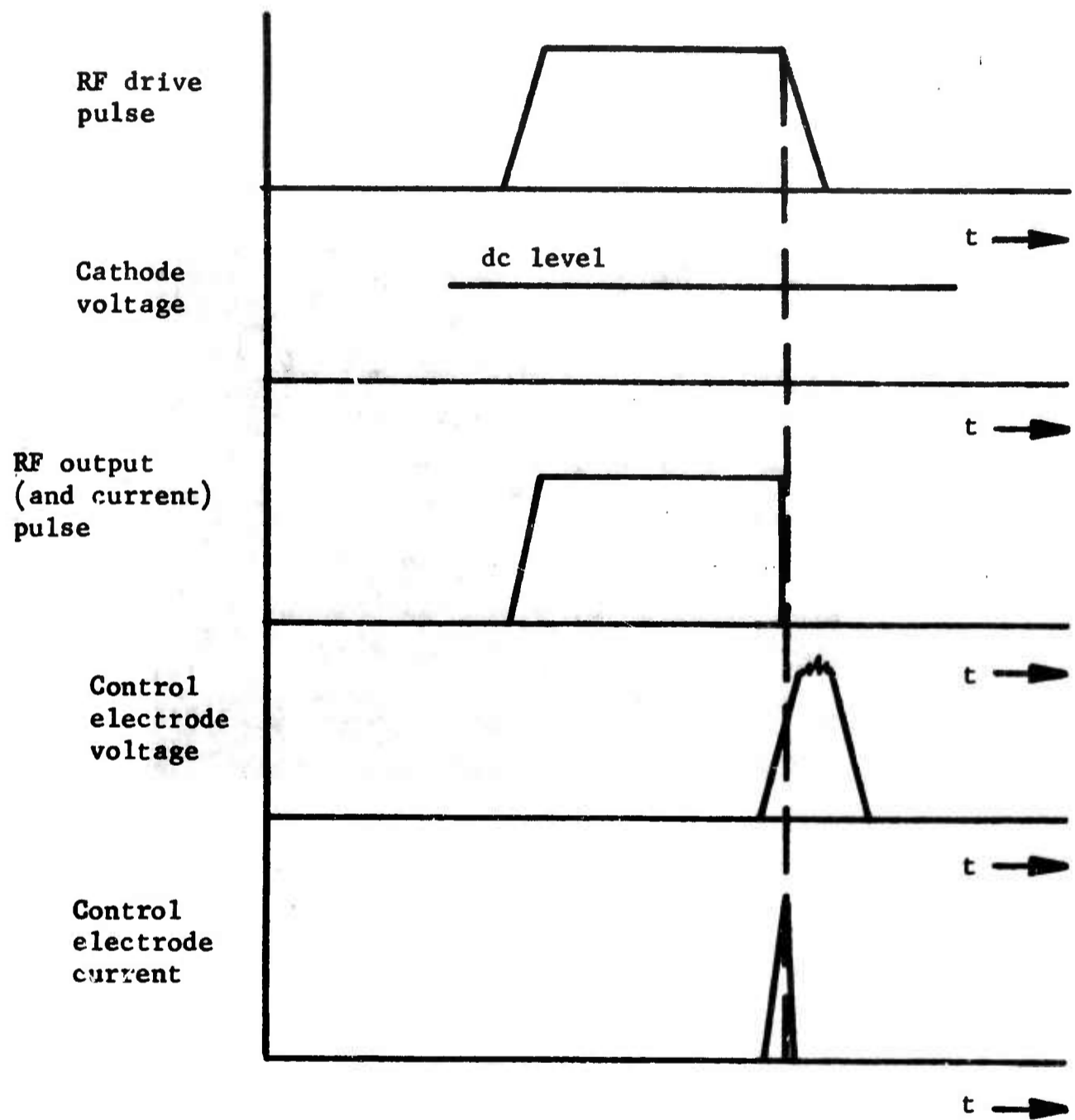
FIGURE 1   CONTROL ELECTRODE PULSING SEQUENCE

FIGURE 2   RF ENVELOPE SHOWING DELAYED CONTROL
ELECTRODE OPERATION

8

in the structure. In order to avoid these limitations, some preliminary experiments were performed on an S-band amplifier to see if the control voltage pulse could be reduced or replaced by a fixed dc voltage which would greatly relax or eliminate the requirements of the control modulator. Indeed, the results of these early experiments indicated that with the application of a dc voltage to the control electrode the amplifier did turn on reliably and did turn off when the RF signal was removed. Figure 3 is a photograph of oscilloscope traces made with such an amplifier operating. A control voltage pulse is used which is sufficiently long to start before the RF drive signal and to end after the RF drive signal. This was used to simulate a dc voltage on the control electrode and is shown as the upper trace. The lower trace shows a superposition of the amplified RF output and the RF drive signal. The amplifier turns itself on and off. It was felt that by further experimentation with the C-band amplifiers having variations in the location and the geometry of the control electrode and of the value of bias voltage, full performance could be achieved with self-turn on and self-turn off while still maintaining the advantages of the reentrant format.

In a series of four experiments the location of the bias electrode was progressively advanced from the input portion of the RF slow wave circuit to the output portion. The results of these experiments indicated that slightly better performance was achieved with the electrode located under the first half of the RF slow wave circuit. The observed results of RF turn off were encouraging but the actual turn off was not very reliable and indicated that a geometrical perturbation might be necessary. Experiments with control electrodes in previous programs indicated that the equipotential contours could be varied with geometric perturbation with correspondingly significant effects on the electron stream.

9

FIGURE 3   OSCILLOSCOPE TRACES FOR AMPLIFIER WITH
dc VOLTAGE APPLIED TO CONTROL ELECTRODE

10

2.1 Self-turn Off

An experiment with the first geometrical perturbation on the bias electrode was performed with the electrode located under the first half of the RF slow wave circuit. The perturbation was significant in that the surface of the bias electrode was located well below the cathode surface and covered an arc length equivalent to approximately one-sixth of the RF slow wave circuit. This experiment, which combined position and geometrical variations, gave evidence of the first reliable self-turn off operation.

RF turn on and RF turn off had now been reliably demonstrated in a reentrant stream crossed-field amplifier. The vehicle used in this experiment was a modified SFD-237, specifically, the amplifier designated as J35H. This amplifier used a bias electrode to which a simulated dc voltage was applied. Under this condition the amplifier could be operated with a dc voltage applied between anode and cathode while the modulation was achieved solely by the application of the RF drive pulse.

In this experiment the dc bias for the amplifier was simulated by the use of a voltage pulse applied between the control electrode and cathode, as shown schematically in Figure 4. The bias voltage pulse was made longer than the RF drive pulse and was applied before the RF drive pulse as shown in the figure. The simulation of the dc bias was necessary because of equipment limitations, and subsequently was proven to be a completely valid technique for these experiments. Figure 5 is a photograph of an oscilloscope presentation of the RF input pulse (lower trace) and the simulated dc bias (upper and longer trace). Upon application of the dc voltage between the anode and cathode, amplification takes place and results in the presentation shown in Figure 6. The amplified RF output pulse is seen to be the shorter of the two pulses. The bias

11
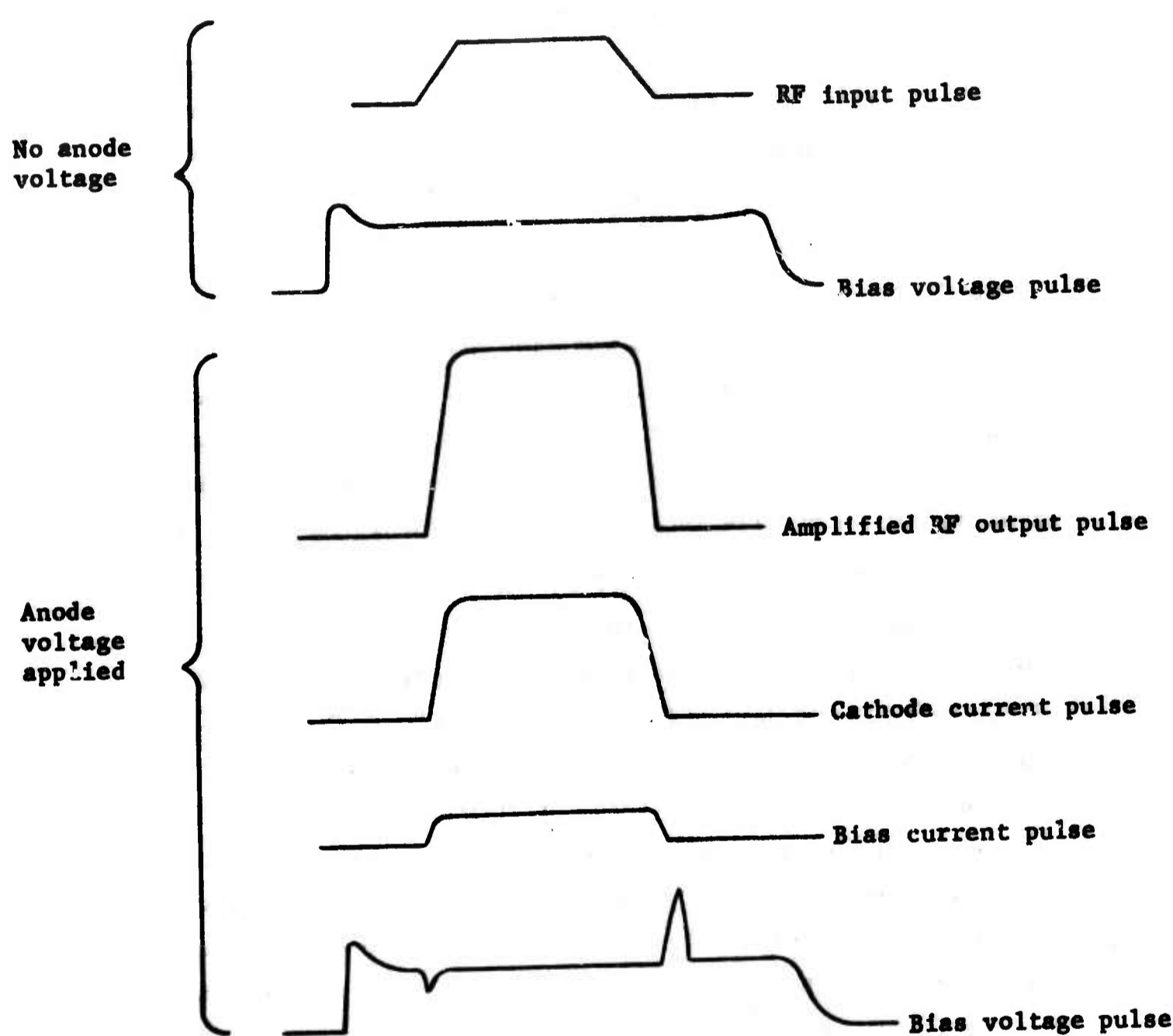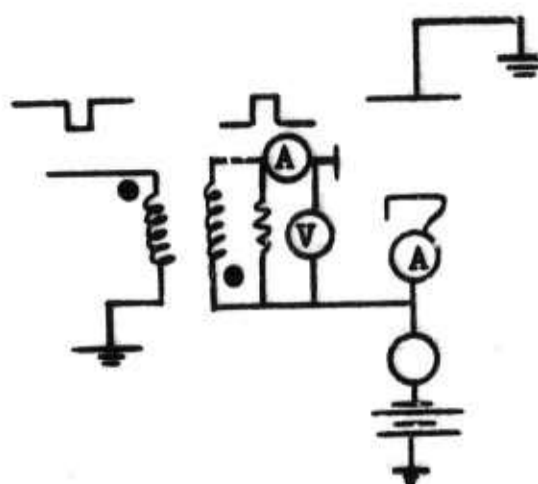
FIGURE 4 PULSING SEQUENCE FOR SIMULATED dc BIAS USED IN
SELF-TURN OFF EXPERIMENTS

12

FIGURE 5   BIAS VOLTAGE PULSE (UPPER TRACE) AND RF
INPUT PULSE (LOWER TRACE) BEFORE dc
SELF-TURN OFF EXPERIMENTS

FIGURE 6   BIAS VOLTAGE PULSE (LOWER TRACE) AND
AMPLIFIED RF OUTPUT PULSE (UPPER TRACE)
INDICATING SELF-TURN OFF

14

electrode voltage pulse shape has changed slightly because of the current drawn by the electrode. This current produces a slight loading on the bias modulator during the amplification process. The rapid buildup and decay of current at the beginning and end of the RF pulse cause the ringing effect seen on the voltage pulse. This ringing is due to the inductance in the bias electrode circuit and it is primarily the inductance of the inverting transformer which is used to provide the positive going bias pulse. Figure 7 is a photograph of the bias voltage pulse and bias current pulse. The bias current pulse is shown with the vertical scale expanded by a factor of 4 to bring out the detail. It can be seen that the ringing effects follow the current changes. As further evidence of self-turn off, the amplified RF output envelope and the total cathode current pulse are shown in Figure 8. The RF envelope is seen as the upper trace and the total cathode current pulse is the lower. These data show that the cathode current flow is initiated by the RF input signal and is terminated with the removal of that signal, clearly indicating the complete RF modulation.

Operation of this type has been obtained across the frequency band from 5.4 GHz to 5.9 GHz at power levels from 300 kw to 500 kw and at several values of constant magnetic fields to insure the reliability of operation. All the tests were conducted at a low duty factor (0.0004) because of equipment limitations. The maximum peak power level which has been observed under the RF modulated conditions and the other performance parameters are shown in Table III. Anode efficiency, η_a, is defined as

$$\eta_a = \frac{P_o}{E_{dc} i_b}$$

where P_o is peak power output

E_{dc} is the dc anode-cathode voltage

i_b is the peak anode current

15
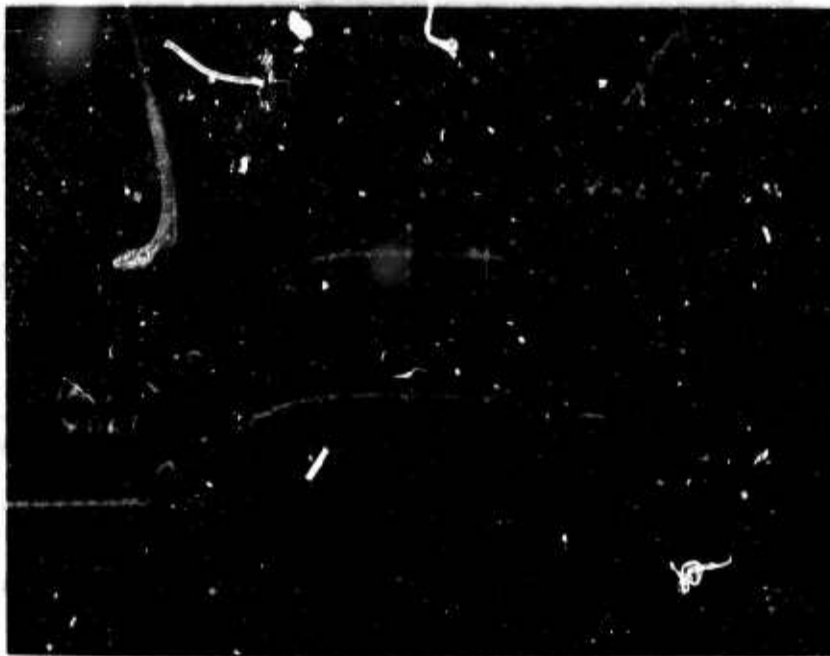
FIGURE 7   BIAS VOLTAGE PULSE (UPPER TRACE) BIAS
            CURRENT PULSE (MIDDLE TRACE), AND AMPLIFIED
            RF OUTPUT PULSE (LOWER TRACE) SHOWING
            SELF-TURN OFF
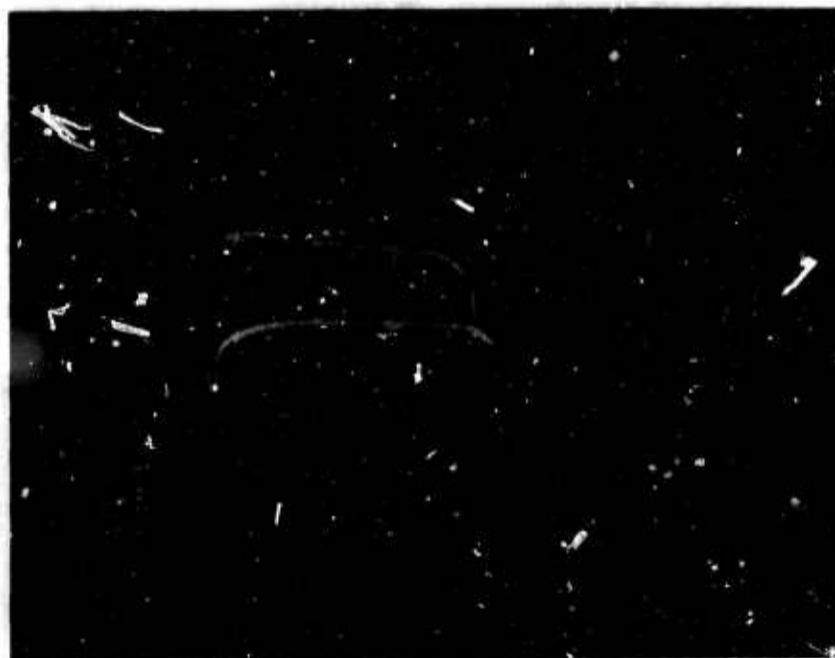
FIGURE 8   CATHODE CURRENT (LOWER TRACE) AND AMPLIFIED
RF OUTPUT PULSE (UPPER TRACE) DURING
SELF-TURN OFF EXPERIMENTS

17

TABLE III

PERFORMANCE PARAMETERS
UNDER SELF-MODULATED CONDITIONS

Frequency	5.6 GHz
Pulse length	4 μsec
Duty factor	0.0004
Operating voltage	24.2 kv, dc
Peak cathode current	100 amps
Peak anode current	75 amps
Peak bias current	25 amps
Peak output power	700 kw
Peak input power	67 kw
Net gain	10^+ db
Bias voltage	12.3 kv (simulated dc)
Anode efficiency	38%
Overall efficiency	33%

Overall efficiency, η_o, is defined as

$$\eta_o = \frac{P_o}{E_{dc}i_b + E_{be}i_{be}}$$

where e_{be} is the peak (simulated dc) bias electrode voltage

i_{be} is the peak bias electrode current

Several aspects of the performance achieved at this time were encouraging. The peak currents were higher than any previously obtained with this vehicle, but more significantly, the high currents were successfully controlled by the biased electrode. The biased electrode operation gave evidence (although not conclusive) that noise due to spurious oscillations were markedly reduced, which would lead to increased dynamic range. The most encouraging result was that the efficiency was as high as it was in the first experiments in which complete RF modulation had been reliably demonstrated.

The overall efficiency of operation with the biased electrode appeared to be about 85% of the anode efficiency. This decreased efficiency was due to the current being drawn by the bias electrode. The anode efficiency remained the same whether the amplifier was operated with the biased electrode for RF modulation or with the control electrode pulsed after removal of the RF input signal. It is significant to note that since the anode efficiency was not affected by the presence of the biased electrode, the thermal properties of the anode circuit and the cathode remained unchanged. This indicated that the vehicle would be capable of operating at the high average power previously demonstrated under Contract AF 30(602)-4082. The anode dissipation and the cathode back bombardment power are directly dependent upon the anode efficiency and since the anode efficiency was not changed, the dissipations were not changed. The additional current, which caused the lower total efficiency, flowed between the cathode and bias electrode and resulted in the additional power being dissipated

19

on the bias electrode. This dissipated power was removed by passing the coolant directly through the bias electrode. This amplifier was now being operated with only dc voltages applied, thereby eliminating the need for a pulsed modulator.

The connection of the amplifier and its dc power supply for this type of operation is shown schematically in Figure 9. The anode and cathode are connected across the principal energy storage system of the dc power supply while the bias electrode is connected across part of that voltage. The mid-point of voltage in our experiments was a convenient value to apply to the bias electrode until a variable floating bias supply was constructed.

The technique for operating the self-modulated amplifier under these conditions was simply to apply the operating voltage and bias electrode voltage before applying RF drive. Upon the application of RF drive, normal amplification and self-modulation occurred. Figure 10 shows the envelope of the RF drive pulse being delivered to the amplifier (lower trace) on a time base of 1 μsec per cm. The envelope of the amplifier RF output is shown as the upper trace. The operating conditions shown for this oscillogram and those to follow are approximately

Duty factor	0.001
Pulse width	5 μsec
Pulse repetition frequency	200 pulses per second
Operating voltage	21.5 kv dc
Bias voltage	11 kv dc
Peak output power	500 kw
Gain	8 db to 10 db

Both the RF input and RF output detectors were broad banded so that spurious outputs, if present, would be detected.

20
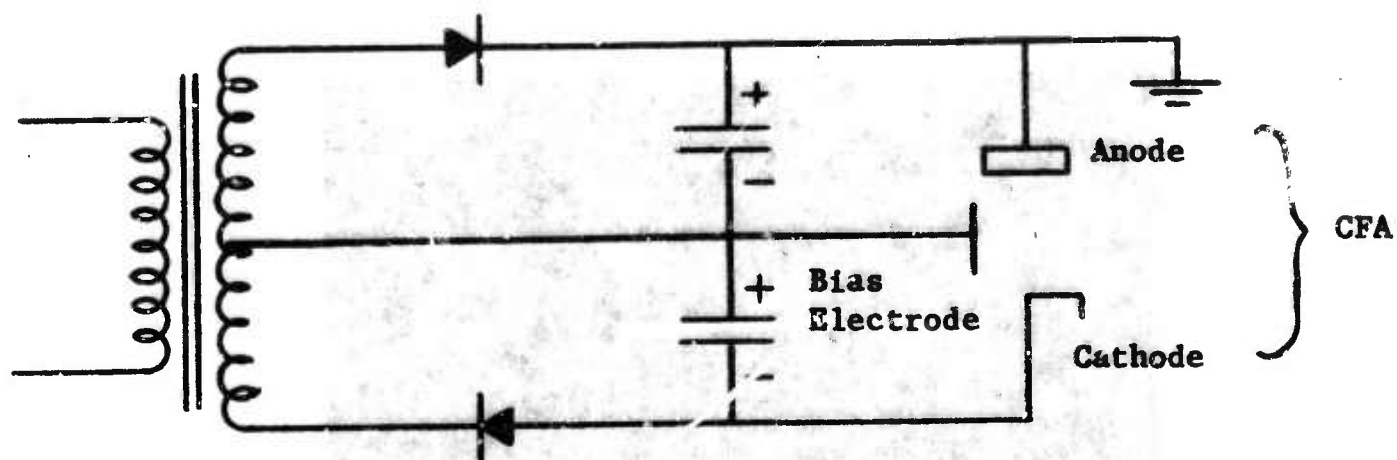
FIGURE 9 SCHEMATIC OF BIAS ELECTRODE CIRCUIT CONNECTION
IN SELF-MODULATED AMPLIFIER

This simplified circuit diagram shows the connection of a
self-modulated CFA to the dc power supply. The bias electrode
operates from a portion of the transformer secondary. Our
present experiments utilize a transformer center tap giving
a bias voltage equal to half anode-cathode voltage. This
value is expected to become lower as work with the technique
proceeds.

FIGURE 10   RF ENVELOPE OF AMPLIFIED PULSE UNDER SELF-
MODULATION CONDITIONS

The lower trace shows the RF envelope of the drive pulse
applied to the amplifier operating solely from a dc source.
The time scale is 1 μsec/cm. The upper trace is the
envelope of the RF output at 500 kw peak. The leading edge
ripples are video effects produced by the RF input as it
rises and falls. The amplifier is non-linear but has
dyn mic range. Gain under these conditions is more than
8 db.

22

Figure 11 shows the RF envelope of the amplified output pulse (upper trace) and the cathode current pulse (lower trace). The close similarity of the shape of these pulses is apparent. Note particularly that the cathode current and the RF output cease at the same time. This is a more positive indicator that the amplifier has turned off than the cessation of the RF output alone. It is possible for amplifiers of this type to continue to operate and draw cathode current without necessarily generating, in the output waveguide system, an easily measurable amount of power. This can occur through the excitation of spurious modes on the internal structure which are not coupled to the output system. The absence of cathode current, however, indicates the absence of this type of interaction when the RF drive is removed.

Figure 12 shows the three parameters of input, output and cathode current on the same display.

2.2 Self-modulation Performance

After the demonstration of reliable self-modulated operation, the performance of the amplifier under these conditions was examined in a number of ways for possible limitations. First, the RF drive signal was tuned over the entire 5 GHz to 5.9 GHz frequency range of the SFD-237 and the self-modulation was shown to be completely insensitive to frequency. Any variations in performance which were observed were accountable from sources other than the self-modulation technique.

Second, the RF drive level was varied over a range of about 7 db without producing instability in the output of the amplifier. The variation in drive ranged from 3 db below the normal level of 50 kw to 4 db above it. The amplifier as expected was not linear over this variation in drive amplitude. For each db variation in RF drive level, the output power changed by approximately 0.7 db.

23

FIGURE 11   RF ENVELOPE AND CATHODE CURRENT PULSE UNDER
SELF-MODULATION TECHNIQUES

The upper trace is the RF output at 500 kw. The lower trace
is the cathode current of about 60 amps peak. The ripples on
the leading edges are video effects caused by external circuitry.
Power output and current appear directly proportional. The
cessation of cathode current at the end of the RF pulse is
the most direct evidence that the amplifier has turned off and
is no longer operating in any unusual mode. The RF detector
used is broad band to show spurious output if it occurred.

24
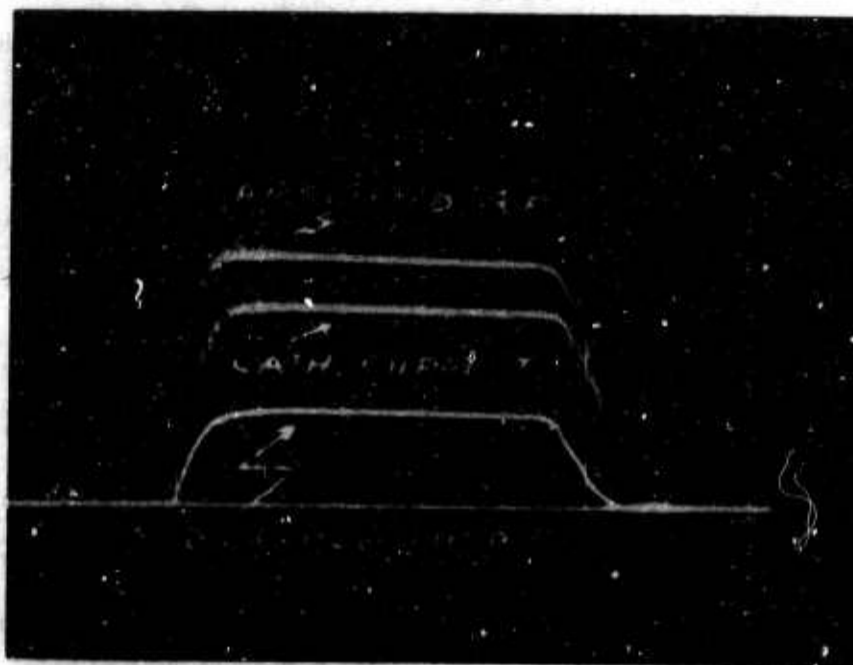
FIGURE 12   RF INPUT, RF OUTPUT AND CATHODE CURRENT PULSES
UNDER SELF-MODULATION CONDITIONS

This photograph displays the three most pertinent parameters
together during self-modulated operation at 500 kw output.
Leading edge ripples in the current and RF output pulses are
caused by power supply inductance. This produces a current
ripple which then produces a ripple in the RF output. The
absence of current following the end of the RF drive pulse
is evidence of the turn off of the tube.

Third, the voltage level applied to the amplifier was varied in order to produce cathode current variations. The amplifier was stable for all voltage levels from the Hartree voltage out to that which produced maximum available current (the maximum current boundary). This corresponded to peak cathode current levels of approximately 100 amperes. This experiment verified that the self-modulation effect was not voltage sensitive and could be used for a range of power output and gain levels.

Fourth, the starting jitter was examined on this first experimental vehicle to see if the existence of voltage on the bias electrode produced unusual behavior during starting. The jitter was found to be equal to or less than 4 nsec.

2.3 Spectral Data

Following these experiments, the relative purity of the amplification was examined to determine whether any basic sacrifice in amplifier performance was required in order to achieve self-modulation. The pulse spectrum of the RF drive source was photographed from a spectrum analyzer display with a spectrum width of approximately 300 kHz per division and a vertical sensitivity of 10 db per division (a logarithmic display). The driver spectrum is shown in Figure 13. The asymmetry of the driver spectrum is caused by frequency modulation from the finite rise and fall time of the voltage pulse being applied to the driver magnetron and the pushing figure of that magnetron. Nevertheless, the drive pulse has a 10 db or better side lobe ratio. Figure 14 shows the pulse spectrum of the amplified RF output. As far as can be discerned from these photographs there is no spectrum distortion produced by the self-modulation process.

Broad band spectrum data were also obtained to examine the possible generation of unwanted spurious output by the self-modulation process. These broad band data were obtained in several different
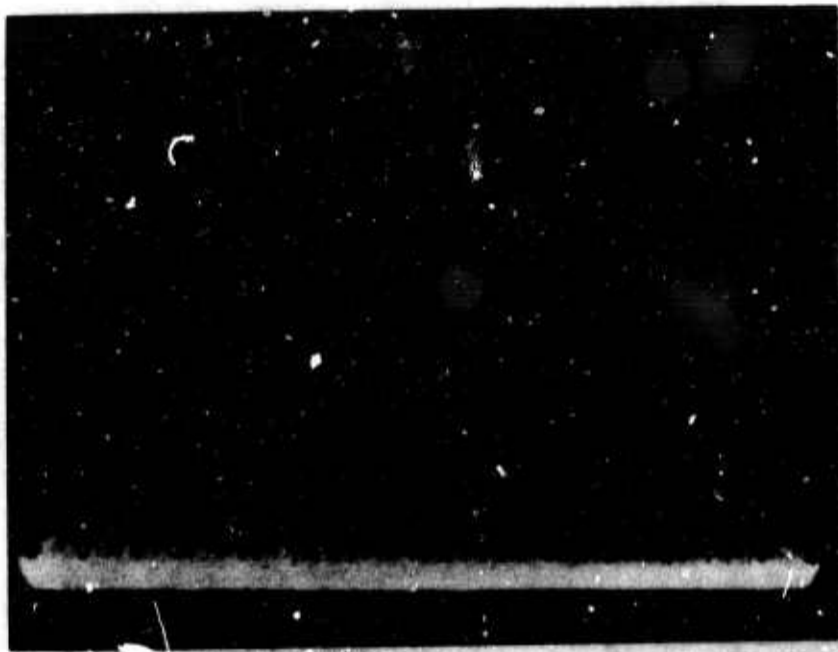
**FIGURE 13   SPECTRUM OF RF INPUT PULSE TO SELF-MODULATED
AMPLIFIER**

A drive pulse of 5 μsec is used. The spectrum shown here is
on a logarithmic display with a vertical sensitivity of
10 db/cm. The drive pulse spectrum has a better than
10 db side lobe ratio. The asymmetry of the spectrum is caused
by frequency modulation of the magnetron used to generate the
pulse. The spectrum is distorted from the more well-known
magnetron spectrum shape because of the logarithmic display.
The spectrum width is approximately 300 kHz/cm.
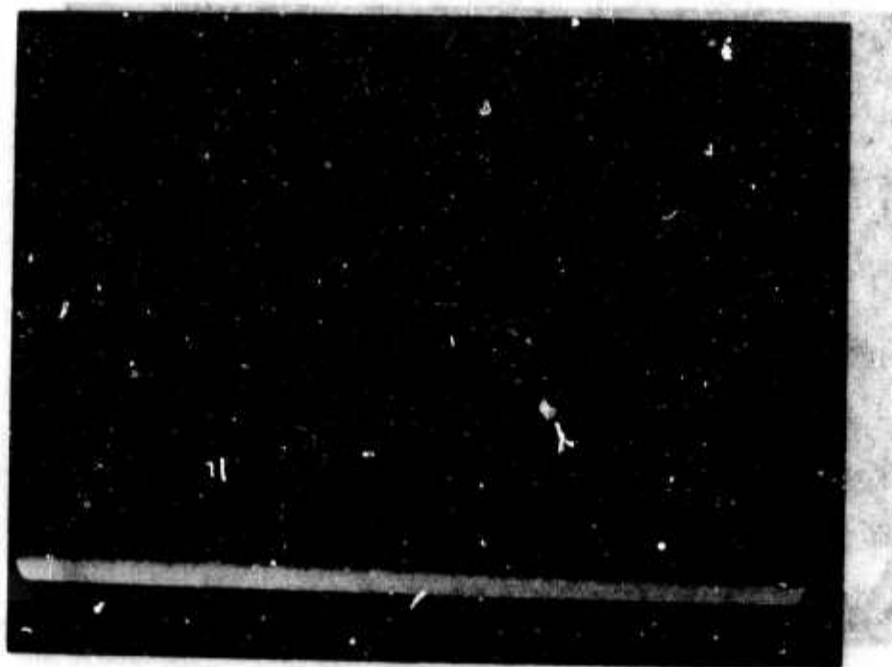
FIGURE 14   SPECTRUM OF RF OUTPUT PULSE FROM SELF-MODULATED
AMPLIFIER

This spectrum photograph was made with the same analyzer
settings as used in Figure 13. A comparison of the two
photographs will show the gain of the amplifier to be 8 db
to 10 db. Note that the side lobe ratio of the spectrum is
still 10 db or more and that the many side lobes visible are
still clearly defined. In both figures, there is an amplitude
decay of about 22 db from the main lobe to the left hand
edge of the display. The amplification produces no apparent
spectrum distortion.

ways. The measurments were made using a Hewlett-Packard 8551B
spectrum analyzer and a Hewlett-Packard 8441A preselector. The
differences in the data to be presented are the result of either the
selection of different spectrum widths or the selection of different
IF bandwidths. The 8551B analyzer has an "automatic" IF bandwidth
selector through which the IF bandwidth is determined by the sweep
speed and spectrum width which have been selected. The IF bandwidth
may also be selected at fixed values such as 100 kHz or 1 MHz.
According to the manufacturer's instructions, the IF bandwidth which
the analyzer would select on "automatic" in Figures 15 and 16 is
100 kHz.

The amplifier was operated at 5.6 GHz and a number of spectra
were photographed. Figure 15a shows the spectrum of the RF drive
pulse to the amplifier displayed over 1 GHz. The spectrum width is
100 MHz/cm and the vertical sensitivity is 10 db/cm. This spectrum
would reveal the generation of any spurious power by the RF drive.
Figure 15b shows the spectrum of the RF output from the amplifier under
the same analyzer conditions. The IF bandwidth for both Figures 15a
and 15b is "automatic" and is selected by the analyzer according to the
combination of spectrum width (1 GHz) and sweep speed (4.5 sec/cm)
which was used for this display.

Figures 16a and 16b are similar spectra except for a spectrum
width of 2 GHz, also with the IF bandwidth on "automatic". For this
display, the sweep speed was selected as 7.5 sec/cm.

A third spectrum display was obtained by selecting a fixed
1 MHz IF bandwidth and a spectrum width of 2 GHz. Figures 17a and 17b
show the spectra of the RF drive and RF output respectively from the
amplifier. The sweep speed here is also 7.5 sec/cm. From this value
it follows that the background spurious output power in Figure 17 would
be approximately 10 db higher because the bandwidth of integration in
the analyzer is 10 db higher. Even with a 1 MHz IF bandwidth, however,

29
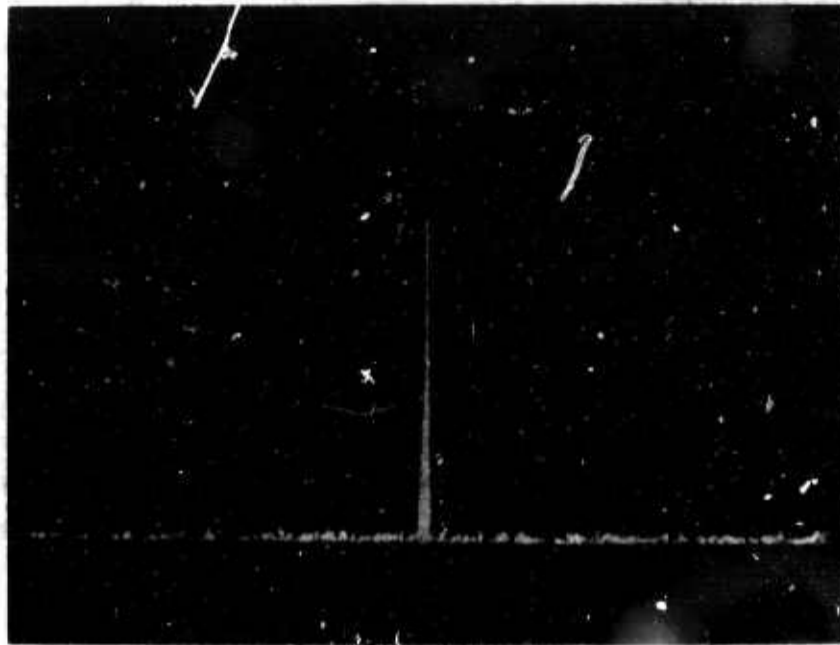
a. 1 GHz spectrum of RF drive pulse
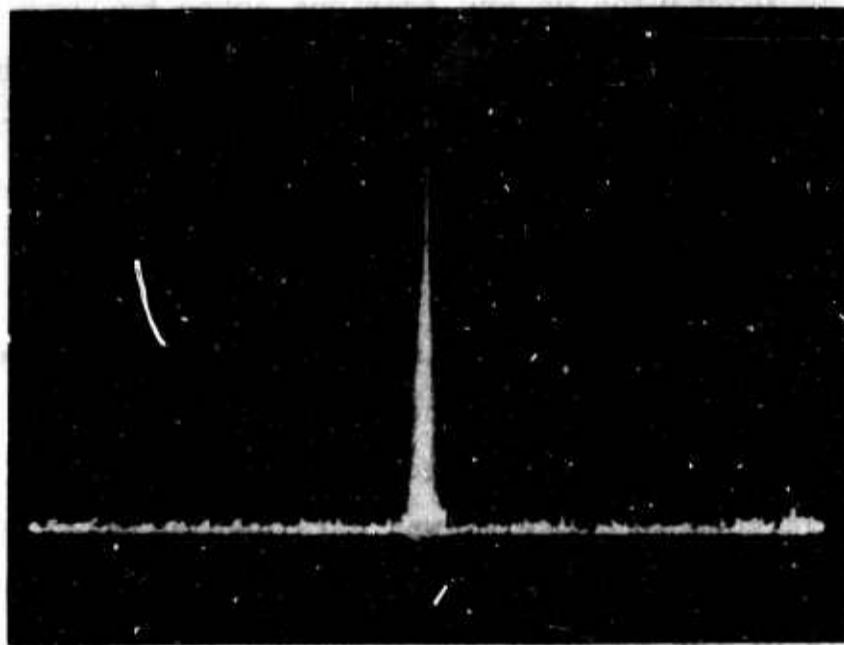
b. 1 GHz spectrum of RF output pulse from
    self-modulated amplifier

FIGURE 15   1 GHz SPECTRA USING 100 kHz BANDWIDTH

The spectrum analyzer using 100 kHz bandwidth shows spurious
output more than 40 db below carrier. Self-modulation produces
no spurious outputs, indicating the turn off is complete.
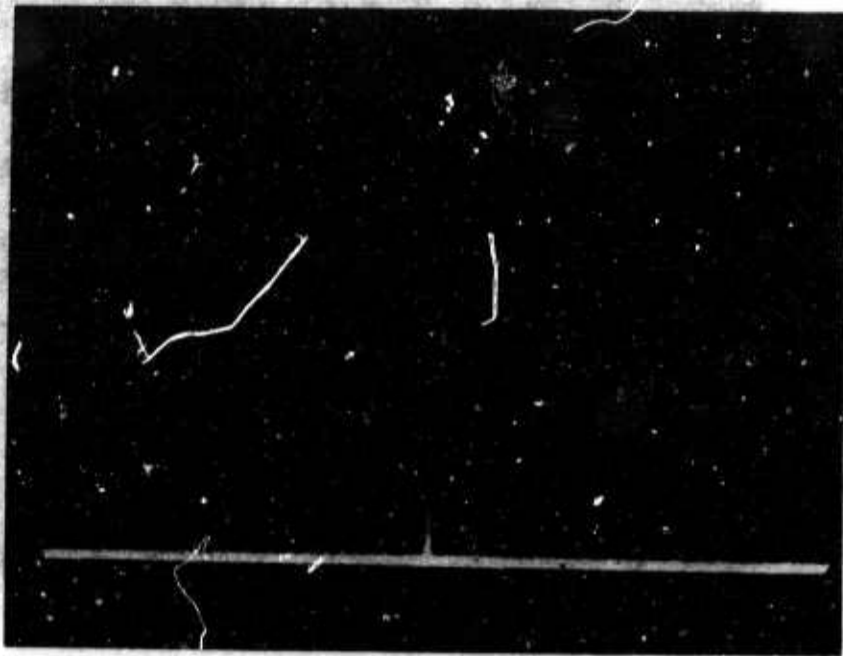
a. 2 GHz spectrum of RF drive pulse
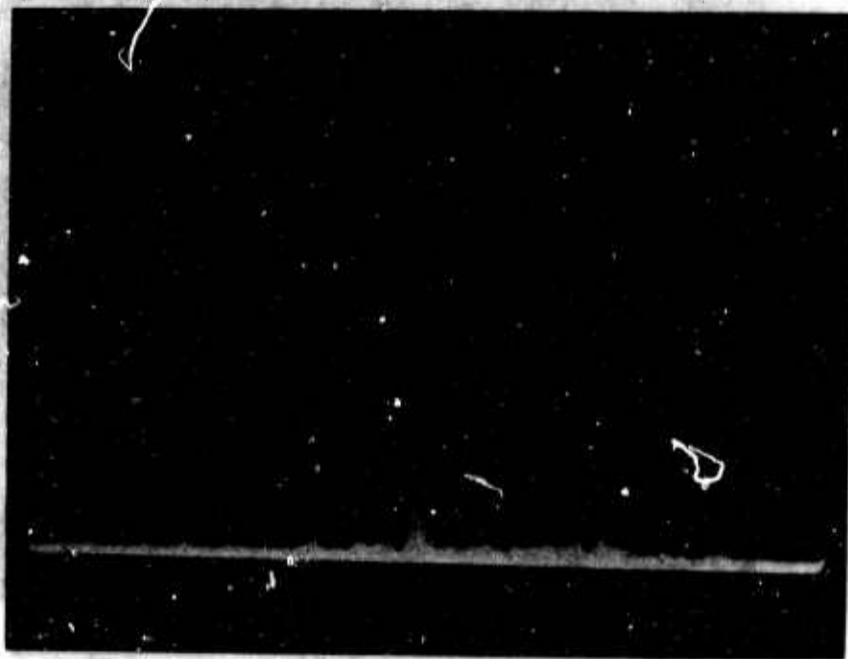
b. 2 GHz spectrum of RF output pulse from
    self-modulated amplifier

FIGURE 16   2 GHz SPECTRA USING 100 kHz BANDWIDTH

The broad spectrum width used here reduces the intensity of the carrier
on the spectrum display. The carrier peak in the top picture is 50 db
above the base line; in the bottom picture about 58 db above the base
line. Spurious outputs using 100 kHz bandwidth are 45 db or more below
the carrier.

31

a.   2 GHz spectrum of RF drive pulse
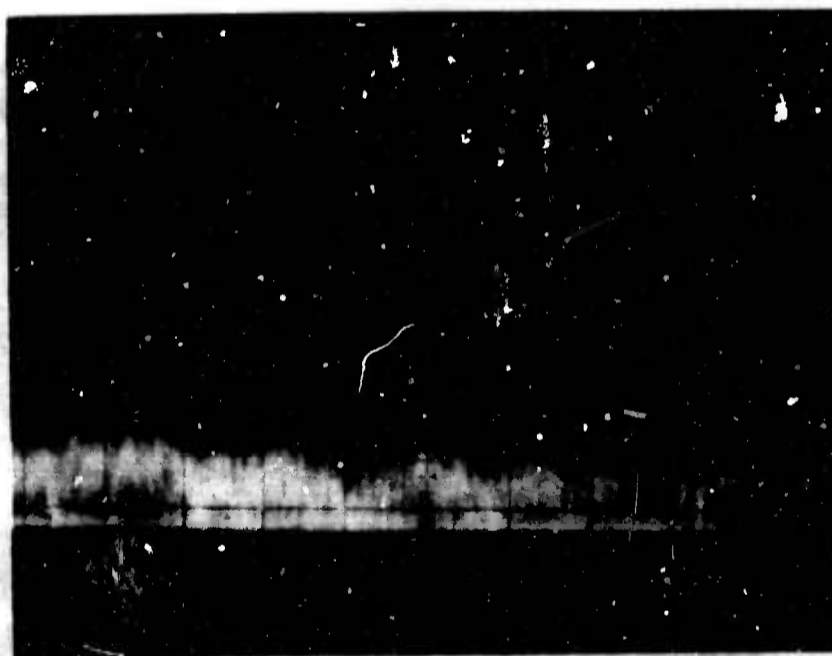
b.   2 GHz spectrum of RF output pulse from
     self-modulated amplifier

FIGURE 17   2 GHz SPECTRA USING 1 MHz BANDWIDTH

These broad band spectra were made using a 1 MHz bandwidth.   Spurious
outputs now appear to be about 35 db below the carrier reflecting the
10 db increase in IF bandwidth used here.   Figure 16 was made using a
100 kHz bandwidth and showed 45 db spurious outputs.   Self-modulation
produces no spurious outputs, indicating that turn off is complete.

the spurious output is clearly more than 30 db below the signal over the 2 GHz spectrum width.

These results show that no degradation in spectral output is caused by the introduction of the bias electrode.

2.4 Pulse Burst Operation

Since one of the principal advantages of completely self-modulated operation over control electrode operation would manifest itself in conditions of either very high pulse repetition frequency (PRF) operation or under conditions of variable pulse width or inter-pulse interval, some experiments were conducted to explore any possible limitations of self-modulation in this regard. The design of the experiments was limited in its complexity by available test equipment, but the results demonstrated clearly that self-modulation was indeed applicable to high PRF systems and would operate quite successfully with variable interpulse intervals. To show this the amplifier was driven by a group of three pulses with an interpulse spacing which was variable from a few microseconds upward. Each of the three pulses was approximately 2 μsec long and the three-pulse group was repeated at a rate of 100 groups per second. In this particular demonstration, the driver magnetron was operated from a hard tube modulator. Shown in Figure 18 are the detected RF envelopes of the amplified three-pulse group. In this photograph the interpulse period is approximately 15 μsec. During the experiment, the interpulse interval could be manually varied at random with no ill effect.

In an effort to simulate as high an intra-burst repetition rate as possible, the interpulse spacing of the three-pulse burst was reduced to the limit of the test equipment, about 1.5 μsec. Under these conditions some inadequacies of the test equipment became evident. The RF drive source in Figure 19 is generating the pulse train shown on the bottom trace at 1 μsec/cm. The pulse shapes unfortunately are

33
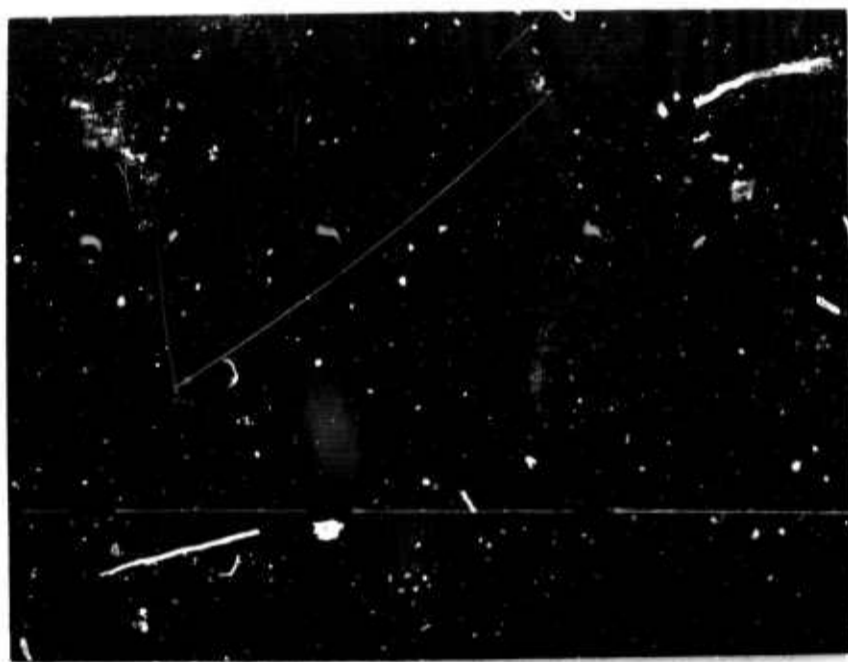
FIGURE 18   RF ENVELOPE OF A THREE-PULSE BURST USING A
SELF-MODULATED AMPLIFIER

The most difficult modulation problem ordinarily arises
with pulse burst operation. This simple illustration of
a three-pulse burst shows that a self-modulated amplifier
can satisfy these requirements. Three 2 µsec pulses are
separated by about 15 µsec each, indicating an intra-
burst repetition rate of 65 kHz. The pulses have clean
and distinct leading and trailing edges.

34
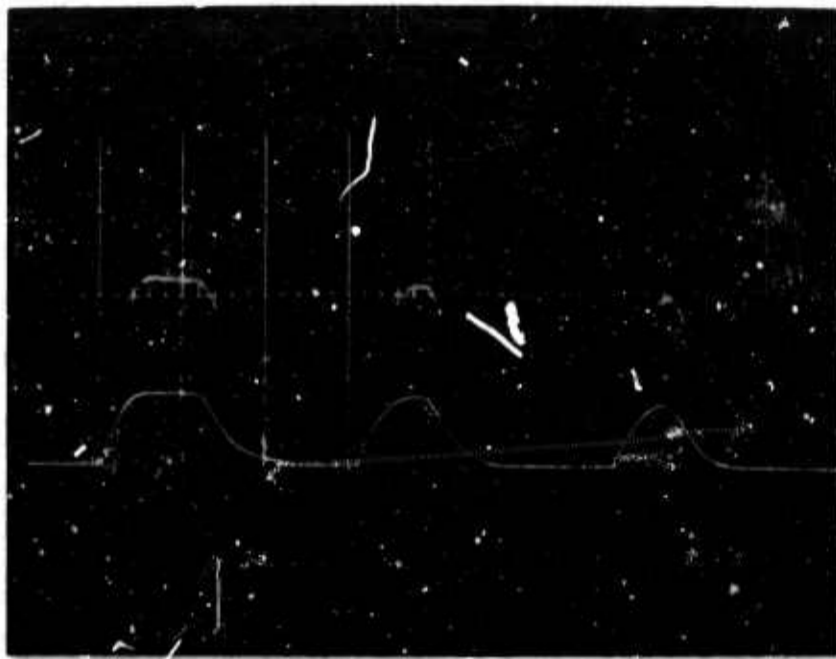
FIGURE 19 RF ENVELOPE OF DRIVE PULSE (LOWER TRACE)
AND OUTPUT PULSE (UPPER TRACE) FOR A
THREE-PULSE BURST FROM SELF-MODULATED
AMPLIFIER

These pulses, on a 1 μsec/cm time base, show the capability
of the self modulation process to amplify with 300 kHz
repetition rates. The amplitude and pulse shape changes
of the RF drive pulse, produced by a capacitor's voltage
droop, are reproduced accurately by the CFA. Differences
in trace intensities are caused by differences in
oscilloscope writing speed.

35

distorted by voltage droop on the energy storage capacitor of the hard tube modulator during the burst. This droop produces both the amplitude change and the pulse shape change. The self-modulated amplifier output in the top trace, however, accurately reproduces both the amplitude change and the pulse shape change. Here the self-modulation process shows itself capable of 300 kHz intra-burst repetition rates. The lower intensity of the amplifier output trace is attributable to the higher writing speed of the oscilloscope under these conditions. The amplifier starts and stops reliably.

2.5 Feedthrough

In addition to making possible the self-modulation process itself, the bias electrode, if required, could be given an additional positive voltage pulse which could prevent the amplifier from turning on at all in order to permit the feedthrough of RF drive power. This type of operation would be quite impossible with linear format distributed emission amplifiers. There appears, therefore, to be no application of which we are aware for which the self-modulation process for a reentrant tube cannot be adapted to advantage.

2.6 Efficiency

What then is the price which must be paid for this successful self-modulation process? The principal area in which overall performance appears to be different from that of the usual SFD-237 is in overall efficiency. In the self-modulated amplifier with a bias electrode, its efficiency has to be redefined to account for some power which is consumed by the bias electrode itself. Since the bias electrode operates at a potential positive with respect to the cathode, it becomes a collector of current during the pulse. There are then two components of collected current, the bias electrode current and the anode current, which make up the bulk of power lost in the amplifier (the remainder

36

is cathode back bombardment power and circuit losses). One can define an anode efficiency, η_a, as

$$\eta_a = \frac{P_o}{E_{dc} i_b}$$

where P_o is the peak output power

   E_{dc} is the anode-cathode voltage

   i_b is the peak anode current

An overall efficiency, η_o, can be defined as

$$\eta_o = \frac{P_o}{E_{dc} i_b + E_{be} i_{be}}$$

where i_{be} is the peak bias electrode current

   E_{be} is the bias electrode voltage

(Still another overall efficiency can be defined by using total cathode current and anode-cathode voltage. This yields the lowest efficiency value but is slightly pessimistic.)

Observations on the first experimental vehicle indicate an anode efficiency of approximately 38% and an overall efficiency of approximately 35%. The deviations of these values from the norm of 50% for the SFD-237 was not believed to be an accurate gauge of the decrease in efficiency resulting from the self-turn off process. The particular experimental vehicle used did not operate as a normal control electrode tube at full 50% efficiency and could be considered below par in that respect. It was believed that the reduced efficiency was a result of a slight difference in the cathode structure used for control electrode operation. A control experiment was performed by rebuilding the test vehicle as a control electrode tube. The efficiency indeed returned to the normal values. Further, visual observations of those vehicles used in the self-turn off experiments also indicated that the loss in

efficiency might be due to perturbations that did not exist or were considerably reduced in a control electrode tube. In other experiments, we reproduced the control electrode cathode structure in the self-turn off test vehicle to confirm these observations, and as expected the overall efficiency was increased. Subsequent experiments, particularly those leading to operation of the bias electrode at lower voltages, also served to increase the overall efficiency of the amplifier so that it was in the vicinity of 45%. It is presently felt that the self-modulation process will not interfere with the achievement of what is considered normal anode efficiency of 50% or greater, and that the power lost to the bias electrode can be made small enough to yield such an overall efficiency as 45%.

2.7 Average Power

The maintenance of the anode efficiency at "normal" 50% or higher levels is important in the additional sense that the achievement of very high average power levels with this self-modulation process imposes no greater burden in terms of dissipation on the slow wave circuit than did control electrode operation. The bias electrode is a collector of electrons and also must be designed with a dissipation capability. It is presently felt that the dissipation capability of the bias electrode can be more readily increased, if necessary, than can the capability of the slow wave circuit because of the fewer boundary conditions which the bias electrode imposes on the problem. The limits of dissipation capability, unfortunately, could not be examined in this set of experiments because a portion of our test equipment set up was limited in duty factor to approximately 0.001.

2.8 Other Experiments

Based upon the results obtained, the next experiments were designed to test our understanding of the mechanism of the bias technique. The geometry of the bias electrode in this series of tests

was varied so as to both reduce and exaggerate the conditions of the previous experiments. It was found that by varying the depth of the bias electrode below the cathode surface, some control of the required minimum bias voltage could be exercised. These experiments indicated that most of the electrons in the interaction region must be forced below the plane of the cathode surface to achieve reliable turn off. It appears that a combination of bias voltage and geometrical perturbation that forces the electrons, which have fallen through approximately 75% to 80% of the anode-cathode potential, below the plane of the cathode surface will provide reliable self-turn off. The three experimental conditions are shown schematically in Figure 20. The anode, cathode, and bias electrode are shown with their respective operating potentials and their resulting equipotential lines. It is seen that when the surface of the bias electrode is located below the cathode surface by a distance equal to the anode-cathode spacing (d), a maximum bias voltage is necessary for turn off. On the other extreme, it is seen that for the bias electrode surface located 3d below the cathode surface, minimum bias voltage is necessary. In practice, it was found that if the spacing were made too great, self-turn off was accomplished at low bias voltage but very high drive power was required and the operating conditions became extremely critical. The cathode behaves as though it is current starved due to the increased bias current and the output power is significantly reduced. The net result is considerably reduced gain and significantly degraded performance. It does appear that the optimum lies between the two extremes and indeed the most gratifying results were obtained with this spacing approximately equal to 2d.
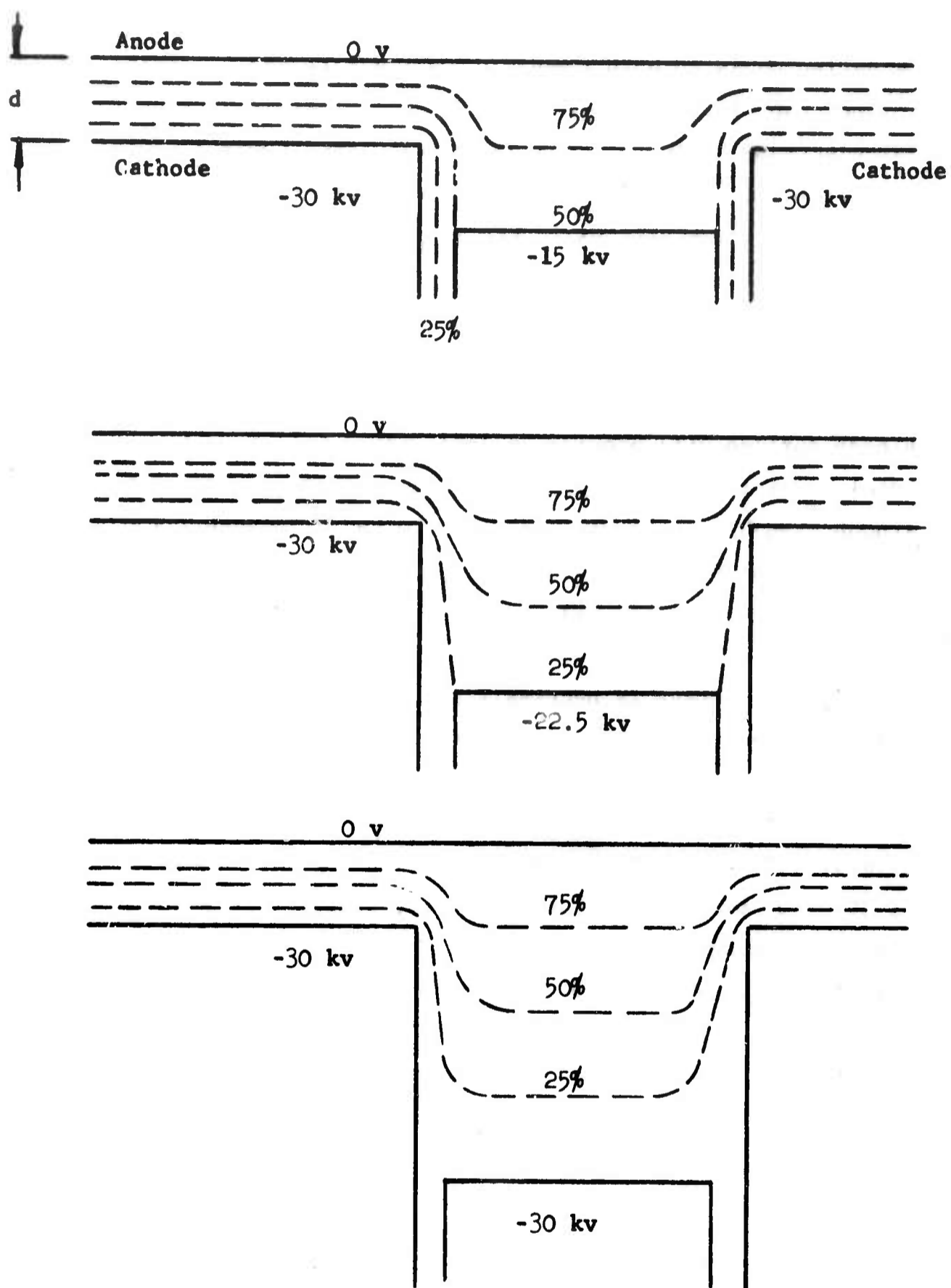
FIGURE 20 EQUIPOTENTIAL LINES FOR THREE DIFFERENT CONTROL ELECTRODE GEOMETRIES

40

3.0 RELATED EXPERIMENTS

During the period from November 1968 until April 1969, S-F-D laboratories acquired data on another program which was pertinent to the goals of Contract F30602-68-C-0055 for the Rome Air Development Center. Inasmuch as these data were obtained during a period when progress was suspended on this RADC contract in order to acquire additional test facilities, and inasmuch as the work on the other program in fact supported the technical goals of the RADC contract, we are presenting the results obtained.

Work was interrupted on the RADC program for several months while additional test equipment was procured by S-F-D laboratories. The additional equipment was found necessary because two aspects of the contract work required some amendment. The first of these was that the aging process for the vehicles under test occupied far too long a period of time. To accelerate the aging, some test equipment was modified to permit the use of a pulse modulator rather than the dc power supply on which the tubes were previously aged. The use of the pulse modulator, it was felt, would considerably shorten the aging period. The necessary modulator was not complete and modifications were required in order to make it ready. The second aspect was that the existing equipment would only permit bias electrode operation with a bias voltage which was fixed at a value of one-half of the applied anode-cathode voltage. It was felt that the inability to vary the bias voltage continued to limit the performance obtained from the vehicles under test. Since the bias voltage is applied between the cathode and the bias electrode, and because the cathode operates normally at a potential of 25 kv or more negative with respect to ground, a variable bias voltage supply must be insulated for 25 kv. Such a supply was then ordered with S-F-D funds as was the modification of the pulse modulator, and test efforts were temporarily suspended on the contract.

41

The transmitter tube on which data had been acquired was
based upon the designs which evolved from the work on the present RADC
contract and from Contract AF 30(602)-4082. For purposes of identifica-
tion, the tube was identified as the SFD-257. The similar tube on the
RADC programs had been designated the SFD-237.

Although the SFD-257 was not identical either in electrical
specification or mechanical outline to the SFD-237 which was being
used for the RADC program, it utilized essentially the same slow wave
circuit and interaction geometry. In addition, the experience acquired
on the SFD-257 program provided a considerable amount of additional
experience which it was felt would permit more effective utilization
of the remaining RADC funds. The SFD-257 program provided a rather
large amount of data which was of interest and value to RADC.

3.1 SFD-257 Specification

The basic performance characteristics of the SFD-257 are
summarized in Table IV. The SFD-257 differs principally from the
SFD-237 in its mechanical configuration and in its operation at
relatively modest average power and pulse length.

3.2 SFD-257 Performance

In its intended application, the SFD-257 operates essentially
at a fixed frequency. It is not required to have a large instantaneous
bandwidth, although it must be capable of operating at rated peak
output power at any frequency in the specified operating band. If the
frequency of operation of the SFD-257 is to be changed in the equipment,
it is possible to readjust operating voltage and current to optimize
the amplifier's performance. Because of this, the presentation of data
shows, for a constant 1 Mw peak output power, the variations which are
required in other parameters. Figure 21 shows the variation with
frequency, under these conditions, of reverse directed power, efficiency,
peak current, and dc voltage. RF input power is maintained at 50 kw.

42

TABLE IV

BASIC PERFORMANCE CHARACTERISTICS OF SFD-257

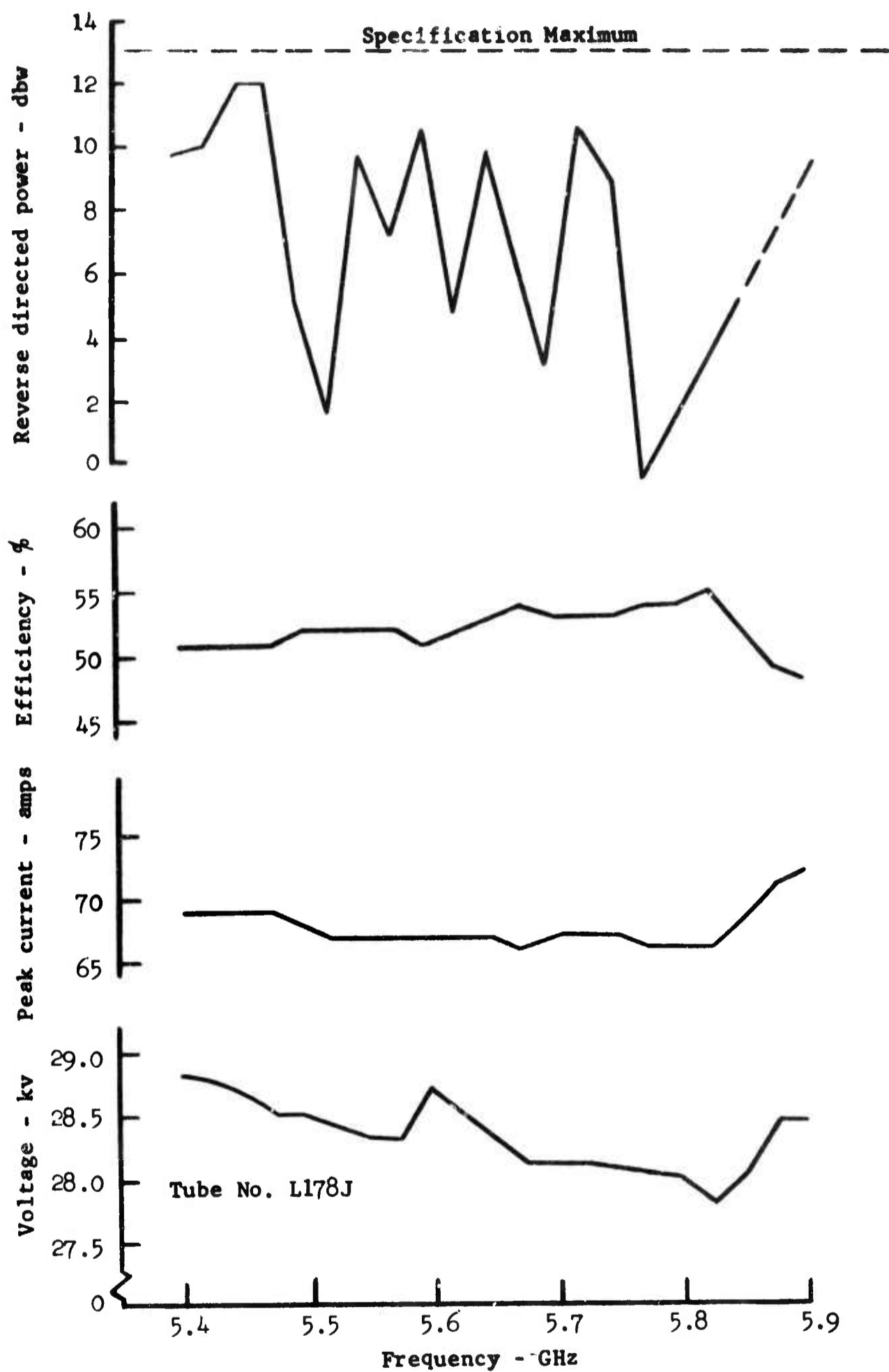|	
Frequency range	5.4 GHz to 5.9 GHz
Peak output power	1 Mw
Peak input power	50 kw
Duty factor	0.001
Pulse length	0.25 μsec and 5.0 μsec
Modulation	Control electrode
Operating voltage	27 kv dc
Control electrode voltage	15 kv
Cooling	Liquid
Focusing	Shielded permanent magnet

FIGURE 21 SFD-257 PERFORMANCE AT 1 Mw PEAK POWER OUTPUT

44

Additional refinements were developed for the SFD-257 slow wave circuit match and have resulted in a substantial reduction in phase non-linearities. These refinements naturally could be applied to the SFD-237 should it ever be required. Figure 22 shows measured phase linearity as a function of frequency for a constant dc voltage. Although these data were obtained at a reduced voltage and a correspondingly reduced peak output power, they are nevertheless much improved over the performance which had been obtained with the SFD-237. The power output for Figure 22 is approximately 500 kw to 600 kw. The peak to peak deviation from linearity appears to be less than 10 degrees. This improvement over the past results is principally due to the additional circuits built on this program and the improved slow wave circuit match. Figure 23 shows the return loss versus frequency for tubes I32H and J35H (both SFD-237s) and the improved curve for tube L178J (SFD-257).

Figure 24 shows the power sensitivity to voltage of the SFD-257. From this characteristic the basic sensitivity of the tube to power supply ripple and intrapulse voltage droop can be extracted. Figure 25 shows the sensitivity of the power output to RF drive under essentially constant voltage operating conditions. Figure 26 shows the phase sensitivity to voltage of the SFD-257. The range of phase changes per voltage which can be expected can be obtained from these curves. The phase sensitivity to voltage, which is usually expressed in degrees per percent change in voltage, corresponds with the slope of the curve shown in Figure 26. This phase sensitivity is a maximum at the upper end of the operating band. Figure 27 shows the phase sensitivity to RF drive of the SFD-257. Again the phase sensitivity is generally expressed in degrees per db variation of RF drive and corresponds with the slope of the curve shown. Phase sensitivity to RF drive is also a maximum at the upper end of the frequency band.

45
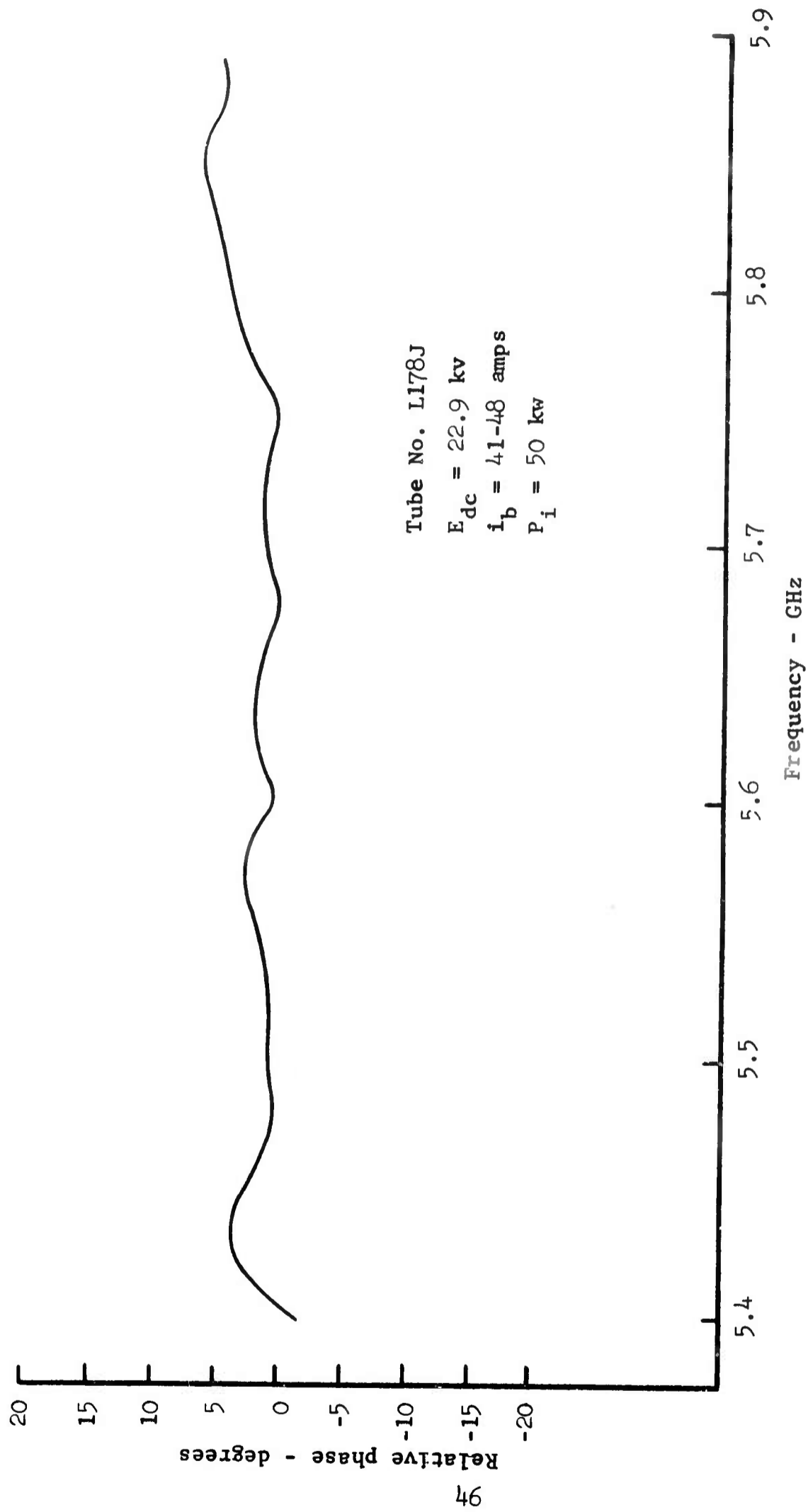
FIGURE 22 SFD-257 PHASE LINEARITY FOR CONSTANT dc VOLTAGE

Tube No. L178J
E_{dc} = 22.9 kv
i_b = 41-48 amps
P_i = 50 kw

Relative phase - degrees

Frequency - GHz

46

I32H, SFD-237

J35H, SFD-237

L178J, SFD-257

Return loss - db

2 3 4 5 6 7 8 9 10 11 12 13 14 15 16 17 18 19 20

5.4 5.5 5.6 5.7 5.8 5.9

Frequency - GHz
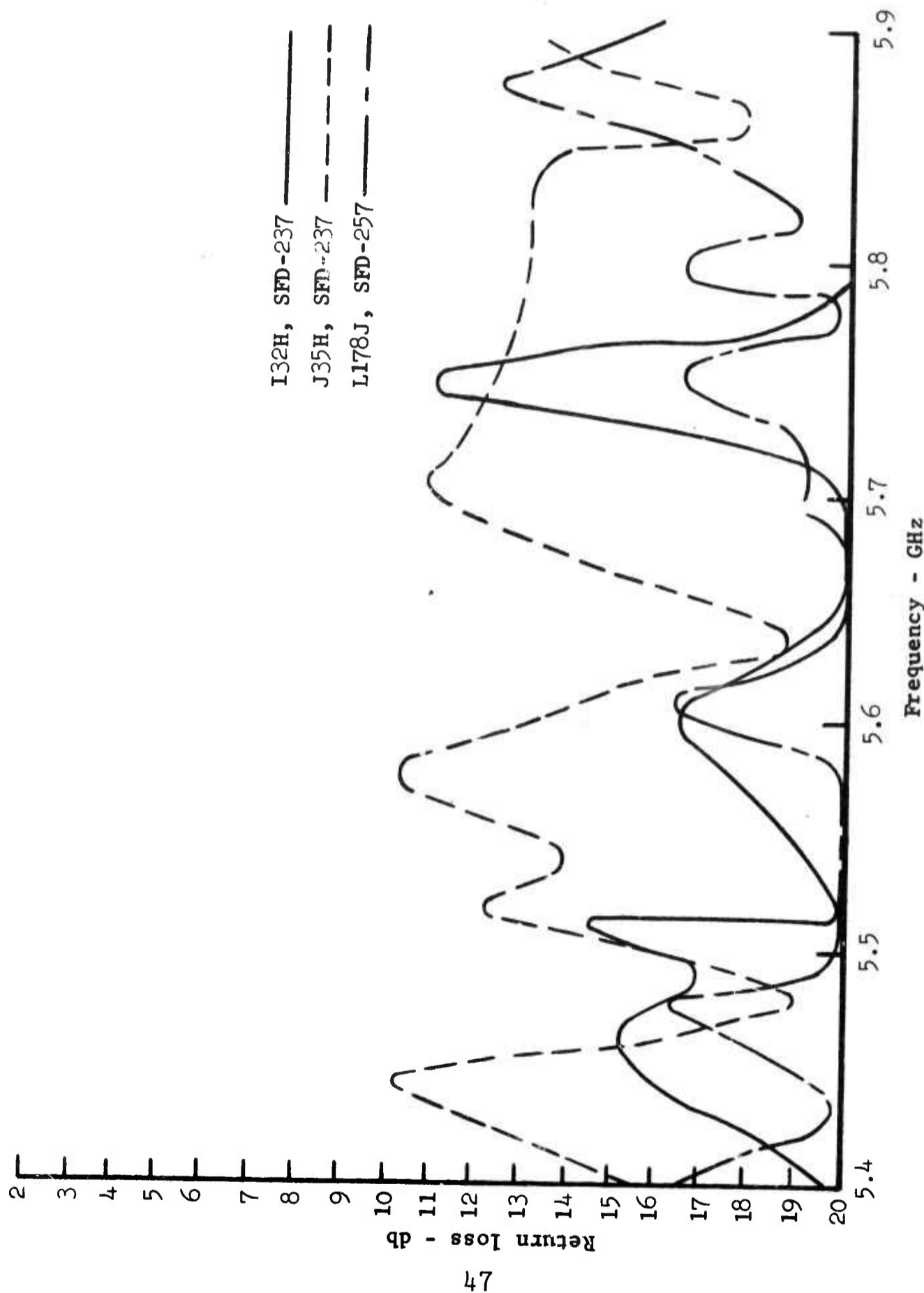
FIGURE 23 COMPARISON OF CIRCUIT MATCHES

47

Tube No. L178J
Conditions

Frequency (GHz)	RF Drive (kw)
5.4	69
5.5	66
5.6	61
5.7	64
5.8	64
5.9	56

FIGURE 24 SFD-257 POWER SENSITIVITY TO VOLTAGE

48
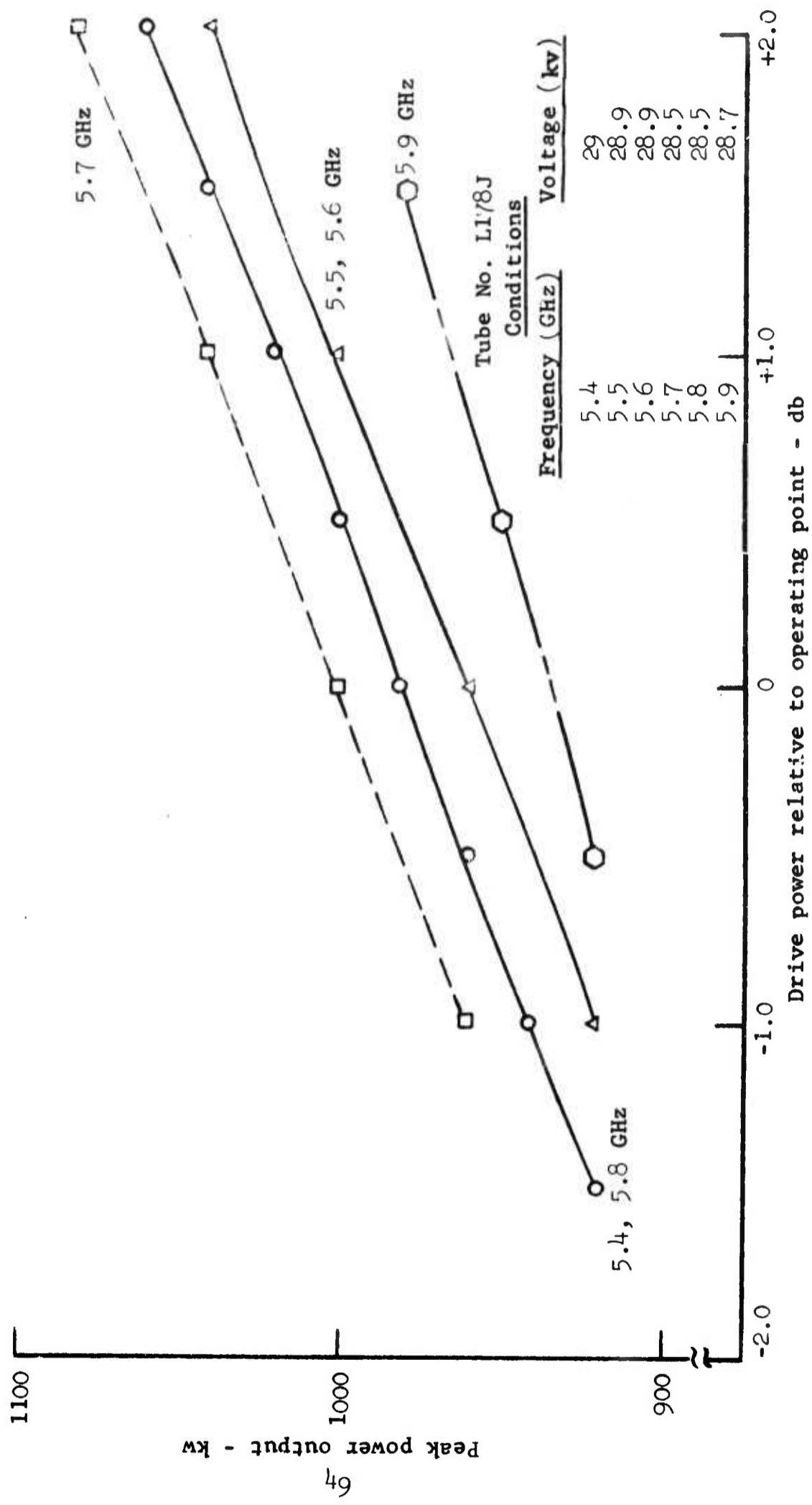
FIGURE 25 SFD-257 POWER SENSITIVITY TO RF DRIVE
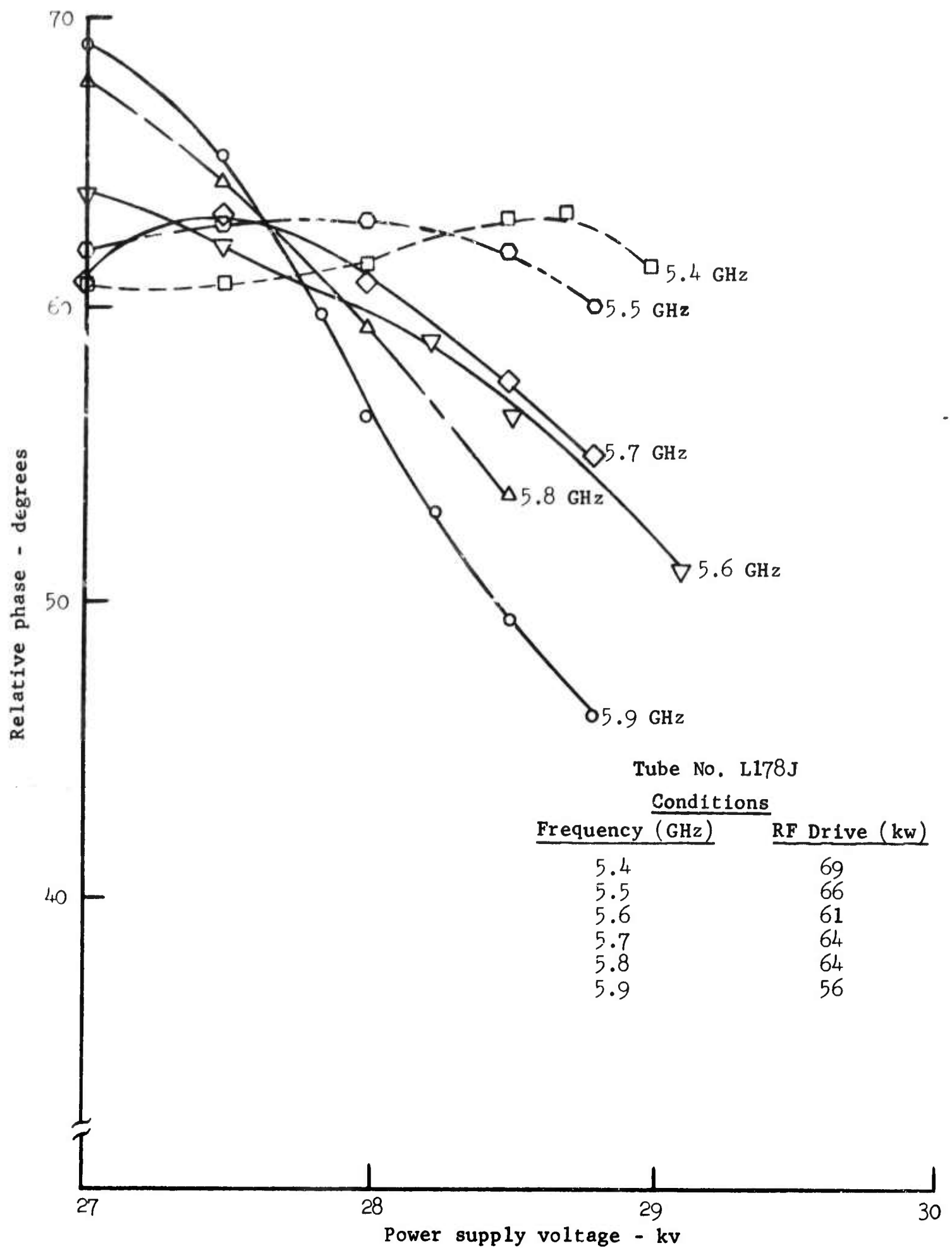
FIGURE 26 SFD-257 PHASE SENSITIVITY TO VOLTAGE

Tube No. L178J

Conditions

Frequency (GHz)	RF Drive (kw)
5.4	69
5.5	66
5.6	61
5.7	64
5.8	64
5.9	56
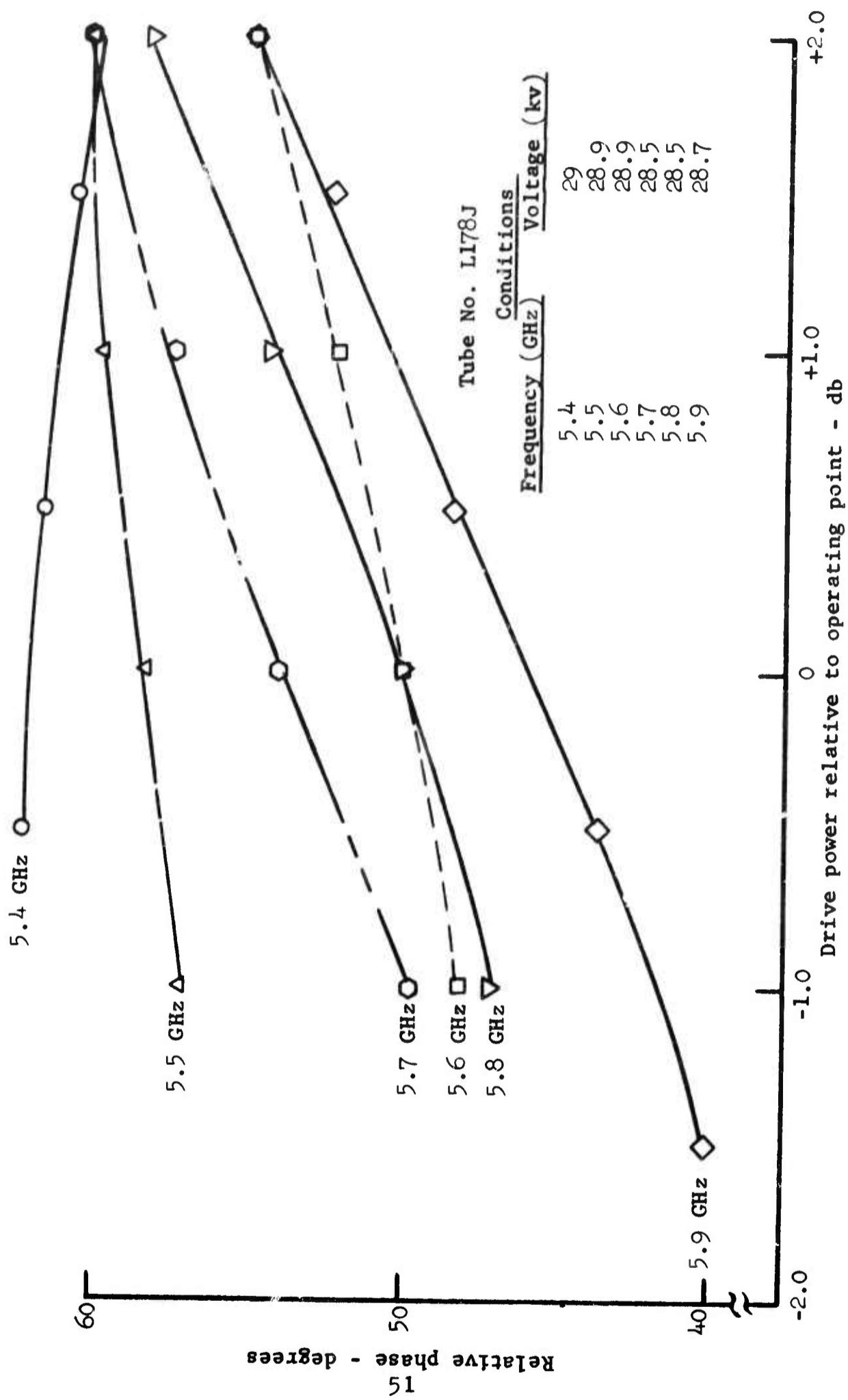
FIGURE 27 SFD-257 PHASE SENSITIVITY TO RF DRIVE

51

Perhaps most interesting and relevant to the objectives of the RADC program is the fact that while the SFD-257 described here was intended for control electrode operation only, it was built using a geometry which would also permit it to operate as an AutoMod amplifier. Therefore, the performance of the SFD-257, as an AutoMod amplifier, was examined briefly.

In these tests, as in AutoMod amplifier tests previously conducted on the RADC program, the bias electrode voltage used was exactly half the applied anode-cathode voltage; that is, the bias electrode operated with a mu of 2.

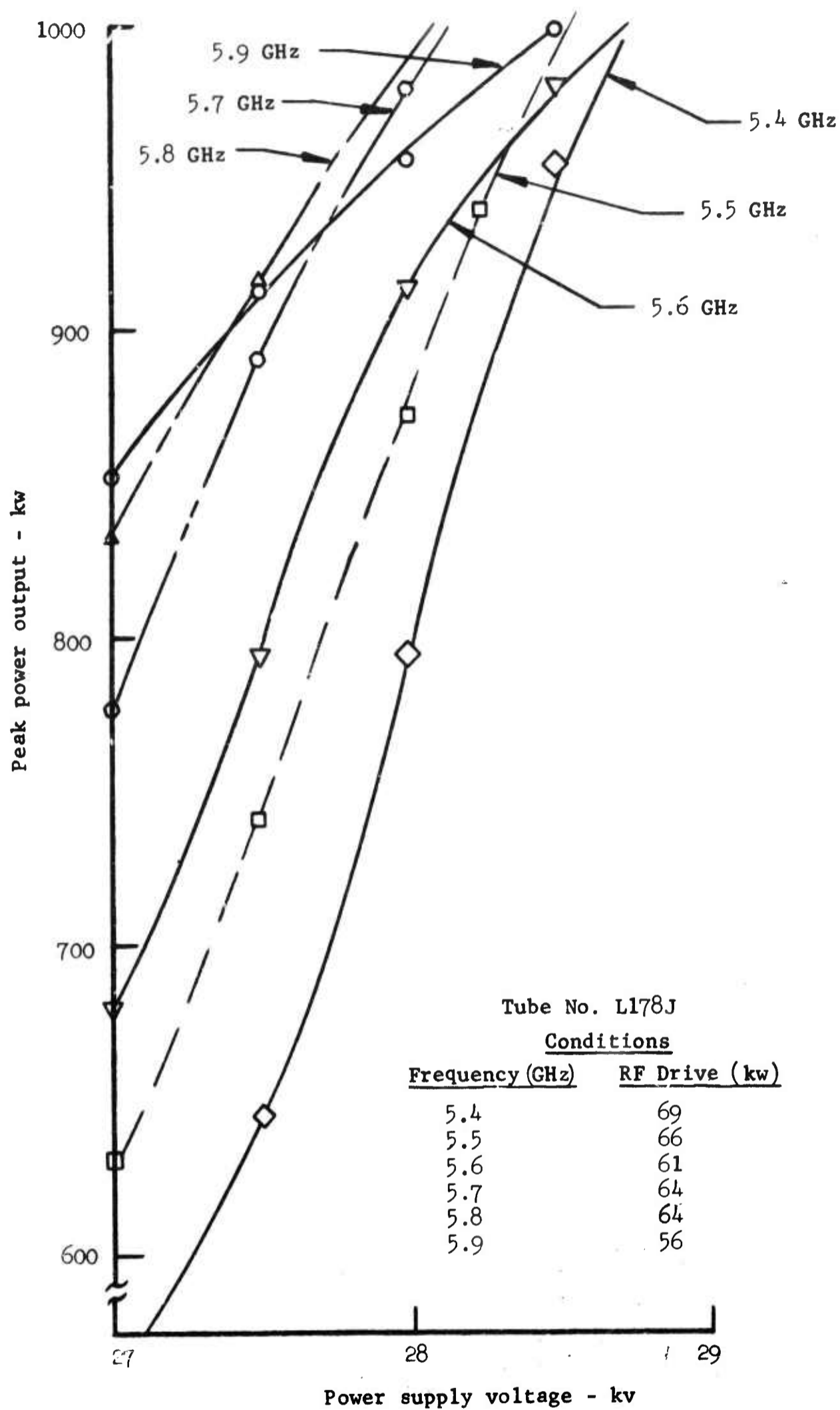Figure 28 shows the RF power output as a function of frequency for this particular SFD-257 under AutoMod operating conditions at a constant voltage. For this test the RF drive power was about 100 kw. The anode voltage was 28 kv, and the bias electrode voltage was 14 kv. The duty factor of operation was 0.002. Figure 29 shows oscillograms of typical cathode current and RF output pulses. These data were obtained under slightly different conditions from the data in Figure 28. Cathode current at the top is 70 amperes peak and the RF output power is 900 kw peak. In Figure 30 are shown the same cathode current pulse at the top with the bias electrode current pulse beneath it. One can see clearly the increase in collected bias electrode current when the amplifier is in the turning off process. The ringing at the trailing edges of all of these pulses is believed to be pickup caused by the turn off transient.

In conclusion we feel that these data constitute a useful supplement to the data which were acquired on this RADC contract, and represent further confirmation of the validity of the techniques which have been developed for AutoMod amplifier operation.

With a slightly reduced bias voltage (12 kv) we were able to achieve a full megawatt across the operating band. However, the 1 Mw peak power output was not achieved at constant voltage; the
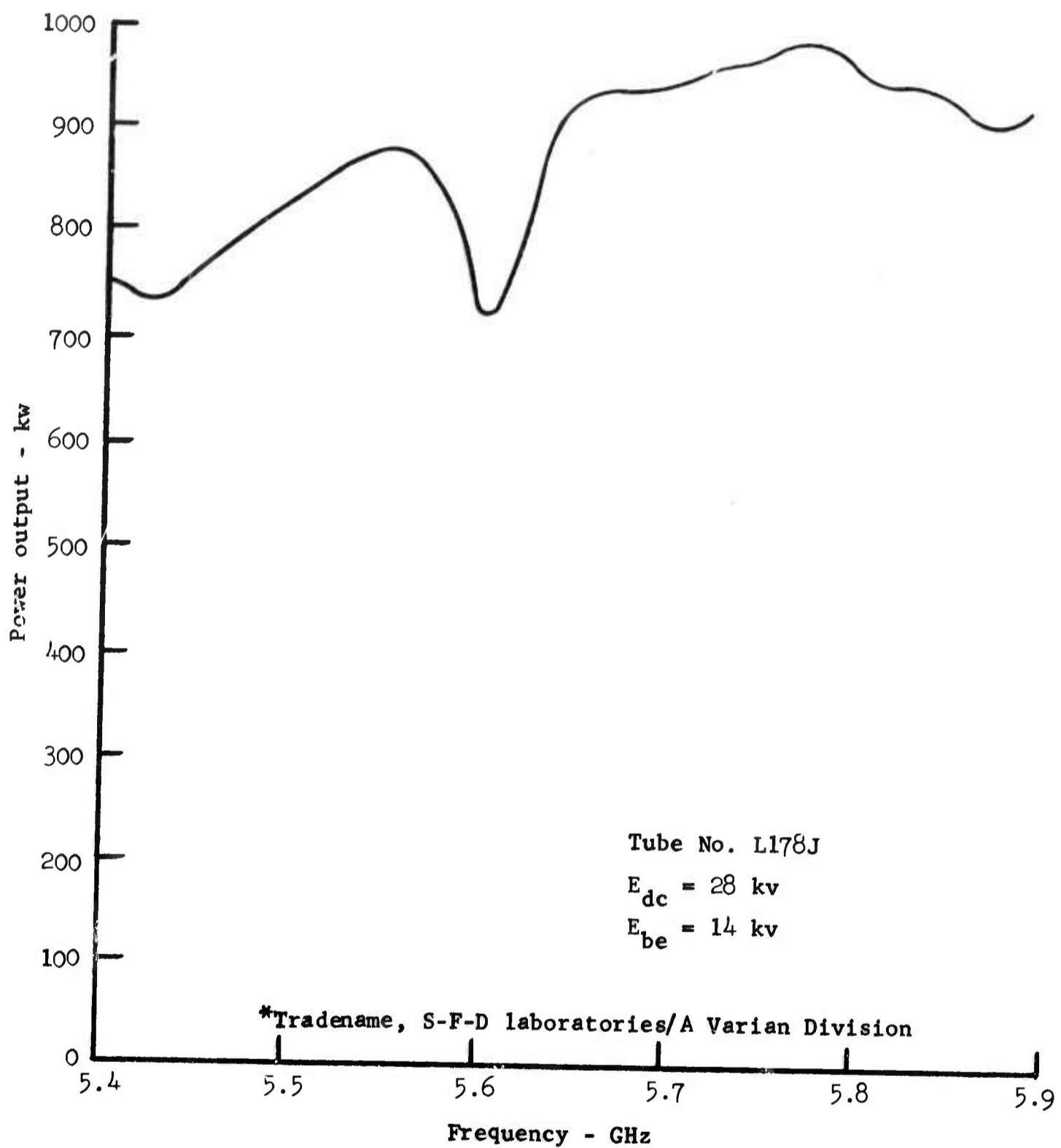
FIGURE 28 SFD-257 AUTOMOD* OPERATION AT CONSTANT VOL?? ??

53
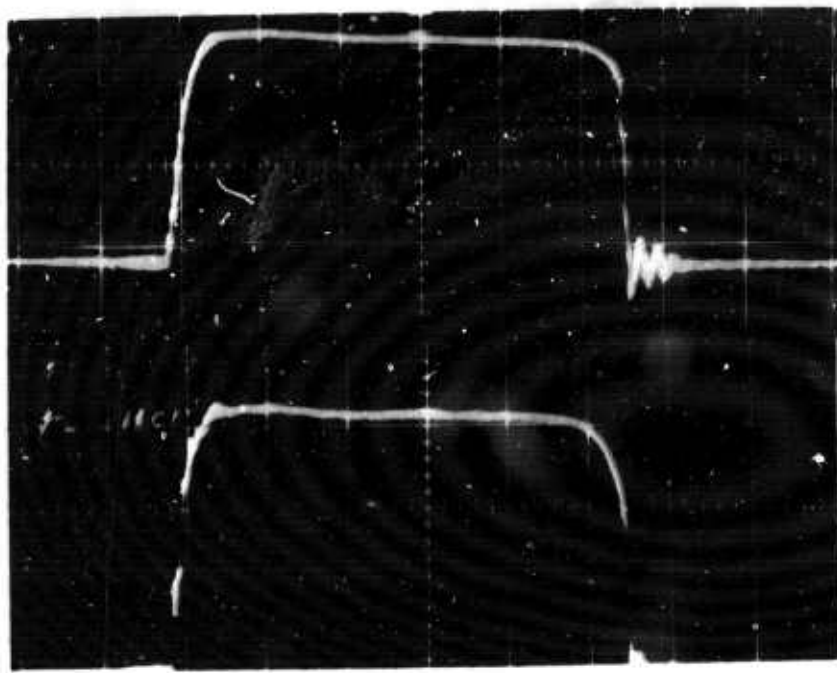
FIGURE 29   TYPICAL CATHODE CURRENT (TOP) AND RF
OUTPUT (BOTTOM) PULSES FOR SFD-257
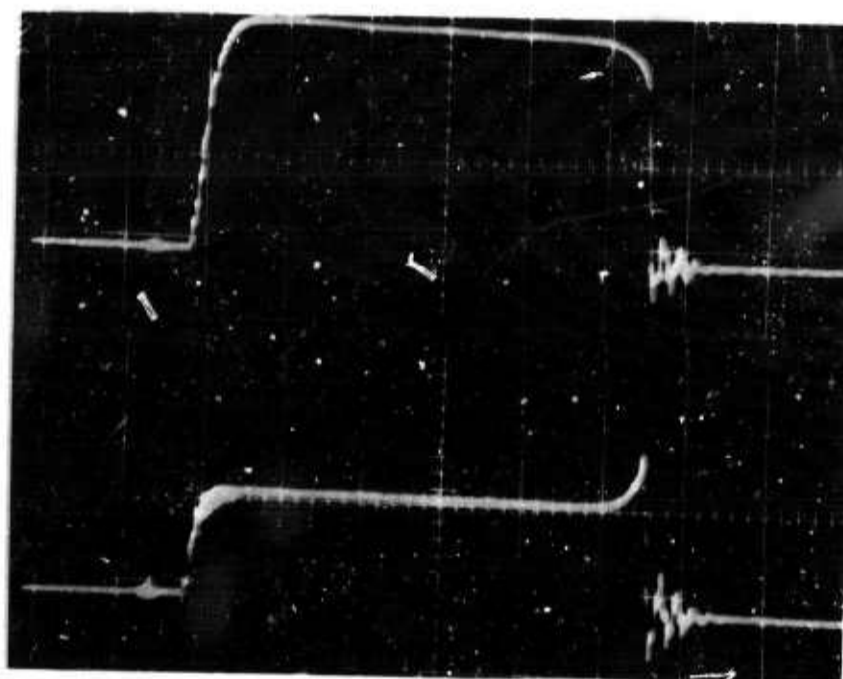
FIGURE 30   TYPICAL CATHODE CURRENT (TOP) AND BIAS
ELECTRODE (BOTTOM) PULSES FOR SFD-257

55

cathode voltage was varied approximately 1.2 kv with the higher voltage used at the lower end of the operating band. The dip in output power appearing at 5.6 GHz is a result of an end space resonance. With a higher voltage applied at this point, the output power was raised to 1 Mw under AutoMod conditions.

4.0 BIAS VOLTAGE EXPERIMENTS

The final experiment started on this program was an attempt to achieve self-modulation with zero bias voltage, that is to obtain self-turn off with only a geometric perturbation. This perturbation was confined to the cathode, and a pulsed control electrode was also incorporated so that the vehicle could be evaluated even if the zero bias attempt proved unsuccessful. The preliminary tests were performed using a pulsed modulator with voltage pulse longer than the RF input pulse to simulate complete dc operation with zero bias. The first results indicated that the attempt for self-modulation with zero bias was not successful. Subsequent tests were made using a dc power supply and a control electrode pulse applied to the auxiliary electrode. These tests indicated that the perturbations of the cathode geometry did not affect the overall performance of this test vehicle; in fact, no difference from typical control electrode operation was seen with the exception that a lower control voltage could be used for successful turn off. The experiments could not proceed beyond this point because all of the funds allowed for this portion of the program were expended. However, this experiment will be continued to its conclusion on another program supported by the U.S. Army Electronics Command under Contract DAAB07-69-C-0343. Zero bias turn off was not achieved in the preliminary test. However, the low control voltage observed under these conditions suggested that it may be possible to achieve a much lower bias voltage with a considerably reduced bias current resulting in higher operating efficiency and increased power output.

5.0 HIGH POWER AMPLIFIER DESIGN (SFD-252)

The goal of this development program was to demonstrate a reentrant stream, crossed-field amplifier capable of operating with an RF power output level of 2 Mw peak, 20 kw average over a 500 MHz band at C-band. The amplifier would be capable of operating with a 50 μsec pulse at the specified power levels. The tube was to be liquid cooled using distilled deionized water as the coolant for both anode and cathode. As a design objective, the amplifier was intended to provide the performance specifications listed in Table I. The program required the delivery of an experimental tube model.

5.1 General Description of the Amplifier Design

The tube is a forward wave, crossed-field, reentrant stream amplifier capable of operating from a dc power supply. The internal anode structure is a forward wave, slow wave circuit composed of a number of bars which are coupled by a helical transmission line. The combination of bars and helix form a non-reentrant, non-resonant RF transmission network which has its pass band between 3 GHz and 7 GHz. (The RF circuit is non-reentrant but the electron stream is reentrant.) The anode bars, which must be capable of dissipating 30 kw of power, are cooled by passing the coolant directly through the bars. The cathode is cylindrical and concentric with the anode and contains an electrode which is used to turn the amplifier off. The self-turn off feature could be included in the high power experimental tube. The cathode is also cooled by passing the coolant directly beneath its surface. The electron space charge clouds which interact with the RF wave on the anode circuit, while traveling in the same direction as the circuit wave, are bunched during amplification but are demodulated or debunched by passing the cloud through a drift space before the electrons emerge into the input section of the interaction space. The drift space is relatively free of RF fields so

58

that debunching of the cloud takes place rapidly under the influence of the crossed electric and magnetic fields present. The drift space is also designed to isolate the RF input and RF output sections on the slow wave circuit from each other.

5.2 Design Criteria

All of the operating specifications are interdependent to some degree and design tradeoffs are necessary. In the design of this 2 Mw, 20 kw amplifier, some of the more restricting parameters are the operating voltage, the peak and average powers, and the pulse length.

The peak and average power, pulse length, and efficiency of the amplifier determine the power which is dissipated on the anode and the cathode. The operating temperature rise which this dissipation will produce depends upon the anode (or cathode) area over which it impinges and the thermal impedance between the surface of the anode and the heat sink. For the high dissipation level expected in this tube, it is necessary to make the area as large as possible and the thermal impedance as small as possible.

The physical size of the structure, and therefore the area, is governed primarily by the frequency of operation, the range of phase shift per section on the dispersion characteristic over which the amplifier operates, the operating voltage, and the number of circuit sections used in the tube. The operating frequency, of course, is not variable. The range of phase shift per section in principle is variable, but experience with the design of these amplifiers has shown a particular range which yields the best performance and operation generally is restricted to that range. In practice, then, the phase shift per section is not variable. The remaining factors, operating voltage and the number of circuit sections, are the variables which must be selected.

The slow wave circuit may be shown in a plan view as in Figure 31. It is a periodic structure made up of N elements spaced by
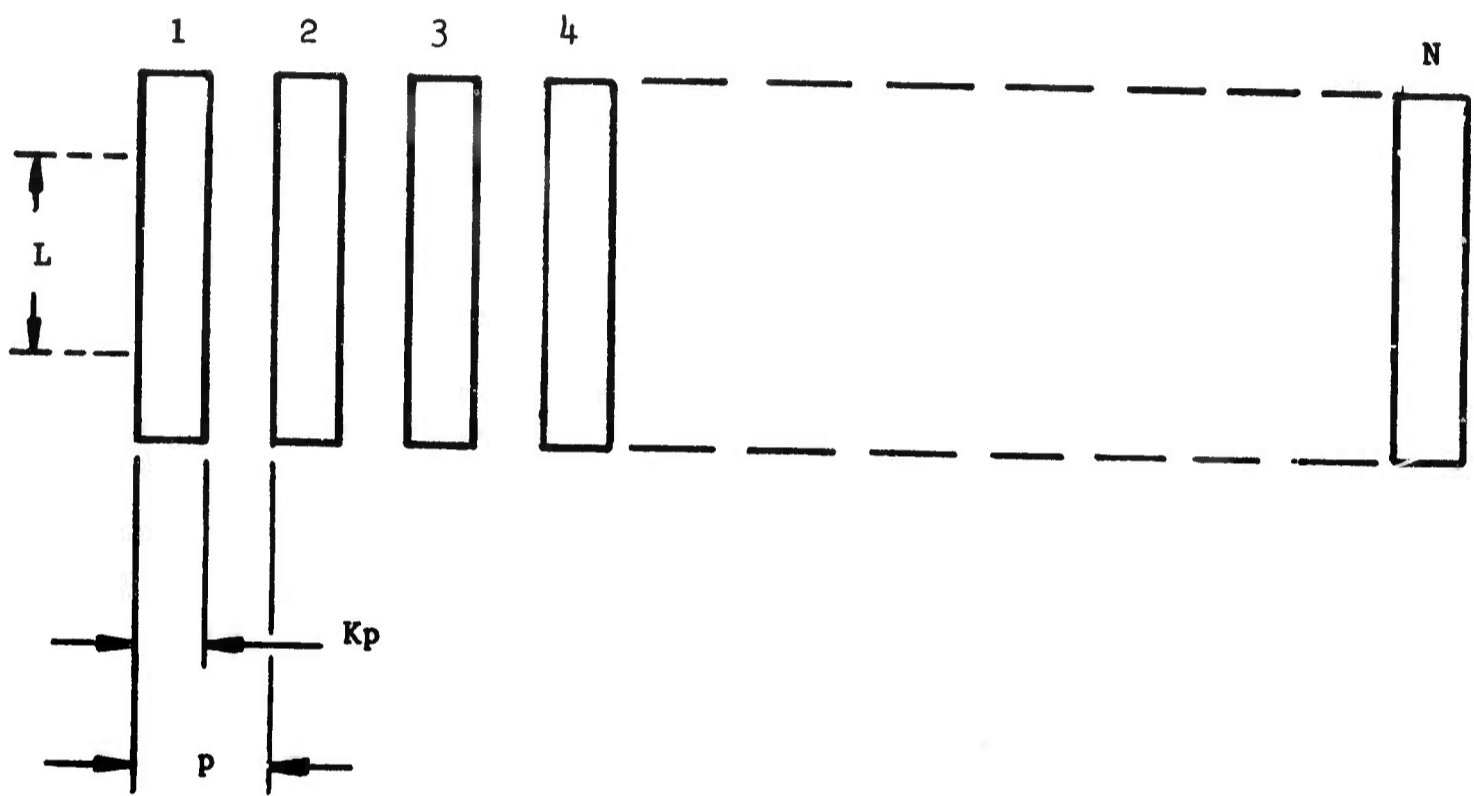
FIGURE 31 PLAN VIEW OF SLOW WAVE CIRCUIT

the pitch, p. The dissipation occurs over a length, L, of each element. The width of each element is some fraction, K, of the pitch, usually $(0.5)p$. The area available for dissipation, therefore, is

$$A = NLKp$$

The effect of operating voltage on the available area can be seen from the dependence of the pitch on voltage, given by

$$p = \frac{\theta \sqrt{2\eta V_o}}{9.16(f)}$$

where θ is the phase shift per section

η is the electronic charge to mass ratio

f is the frequency

V_o is the synchronous voltage of the slow wave circuit

The operating voltage of the amplifier is usually 8 to 10 times V_o. To maximize the area, therefore, it is desirable to operate the tube with as high a voltage as possible.

Two limits on voltage appear in the design analysis. The first is related to the RF drive power which is available and the second to the maximum voltage gradients permissible in the structure. As the operating voltage (and the synchronous voltage of the circuit) is increased, the minimum RF drive power required for stable operation also increases. The drive power for this program was 100 kw. From experience with slow wave circuits similar to the one used (in terms of interaction impedance), operating voltages of at least 40 kv could be used without encountering RF drive power limitations. The practical limit on operating voltage was expected to be the maximum permissible voltage gradient. This gradient is considerably smaller for dc operated tubes, in which voltage appears on the tube continuously, than it is for the pulse modulated tubes. Prior experiments to establish this

61

maximum gradient in similar structures indicated that voltage levels up to 35 kv would be safely attainable in a design without an excessive arcing rate.

The choice of K, which defines the metal-to-space ratio (which is 1:1 for a K of 0.5) is limited to a maximum of about 0.6 in order to avoid too large a decrease in interaction impedance. The interaction impedance strongly affects efficiency, gain, and minimum RF drive power.

The choice of N is also limited by the goal of a 10 inch maximum tube diameter. The inside circumference of the slow wave circuit is given by

$$Np$$

and the circuit diameter is given by

$$\frac{Np}{\pi}$$

Values of N of 100 or more are practical, although the insertion loss of the slow wave circuit may be prohibitive for such a value. For high powered tubes of this general design, N is usually chosen to be between 50 and 100.

5.3 Anode Circuit Design

Based on the considerations outlined in Section 5.2, a tentative design was made in which a new slow wave circuit was used (i.e., different from that used on AF 30(602)-4082) in addition to increasing the operating voltage to 35 kv. The circuit modification was made and the operating voltage was increased to increase the thermal capability of the anode and to reduce the cathode loading. The anode circuit is generically a helix derived circuit in which the interaction

height, L, was extended and the thermal impedance was reduced. More specifically, it is a helix coupled bar circuit. Some of the design parameters are shown in Table II.

5.4 Thermal Properties

Once the circuit design was fixed, the thermal properties of the circuit were analyzed to determine the coolant requirements for the expected dissipation power. The initial calculations based on some relatively simple assumptions indicated that flow rates in the order of 0.4 gal per min per bar would be required to maintain reasonable temperatures at the vane tips near the output. The corresponding pressure drop was in the order of 75 psi. However, when measurements were made on an actual anode bar, these estimates were found to be conservative. Actual measurements indicated that the flow rate could be reduced safely to less than 0.3 gal per min per bar with a corresponding pressure drop of 42 psi. The experiment consisted of passing a controlled quantity of coolant through an anode bar while power was applied to the bar over the expected heat transfer area. The heat transfer area is that area on which the electrons will be collected. The power applied to this area was measured with a calorimeter and temperatures at various points on the bar were monitored with thermocouples. With the indicated flow rates and with the applied power approximately 10% greater than that expected in the actual amplifier, the face of the vane attained a temperature of approximately 250°C. (The temperature at the coolant-wall interface indicated that the coolant had just reached the nucleate boiling regime.) When considering operation at full power at a 50 µsec pulse length, the transient temperature rise is expected to be an additional 450°C at the end of the pulse. This results in a maximum anode vane tip temperature of approximately 700°C which is quite reasonable when a refractory metal is used on the vane tip. Figure 32 shows schematically how the vane temperature varies during the 50 µsec pulse at full average power output.
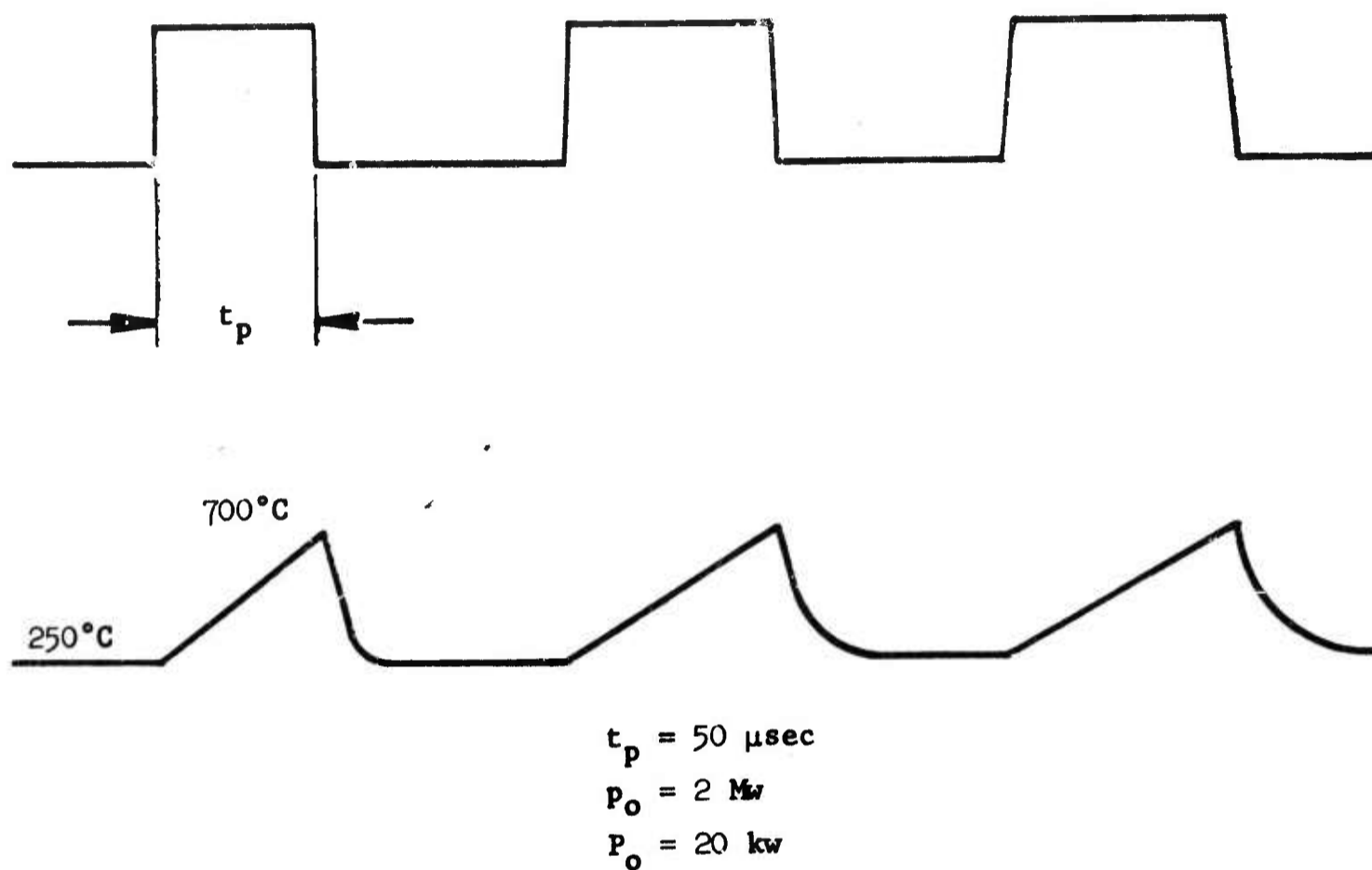
63

$$t_p = 50 \ \mu sec$$
$$P_o = 2 \ Mw$$
$$P_o = 20 \ kw$$

FIGURE 32   VANE TIP TEMPERATURE WITH 50 μsec PULSED OPERATION

Some experiments were planned to optimize the coolant channel geometry to reduce the coolant requirements. At this stage in the preliminary design, the quantities stated above appeared to be quite adequate.

5.5 Cold Test Results - Linear Slow Wave Circuit

The initial cold test results were obtained on a linear version of the anode circuit shown in Figure 33. A linear version is used at first because of the ease of construction. The dimensions of the first linear tester are derived theoretically. Several different circuits may be needed before the proper dimensions for the operating frequency and phase shift per section are achieved. The dispersion curve for the tentative design is shown in Figure 34. The "cold" band pass of the circuit extends from approximately 3.2 GHz to 7.0 GHz with the hot operating band (5.425 GHz to 5.925 GHz) placed between 115 degrees per section and 132 degrees per section.

5.5.1 Interaction Impedance

The interaction impedance of this circuit was measured to be 38 ohms at the lower frequency to 31 ohms at the upper frequency. The variation of interaction impedance as a function of frequency is shown in Figure 35. The variation of RF field strength across the height of the anode was also measured and is shown in Figure 36.

5.5.2 Transitional Match

The first attempts to obtain the transitional match were made by first matching to a short section of coaxial line which in turn will be matched to the standard waveguide. The first matches from circuit to coaxial line are shown in Figures 37 and 38. Figure 37 shows the input return loss and transmission through the circuit with the output terminated in a matched load. Figure 38 shows the results when the
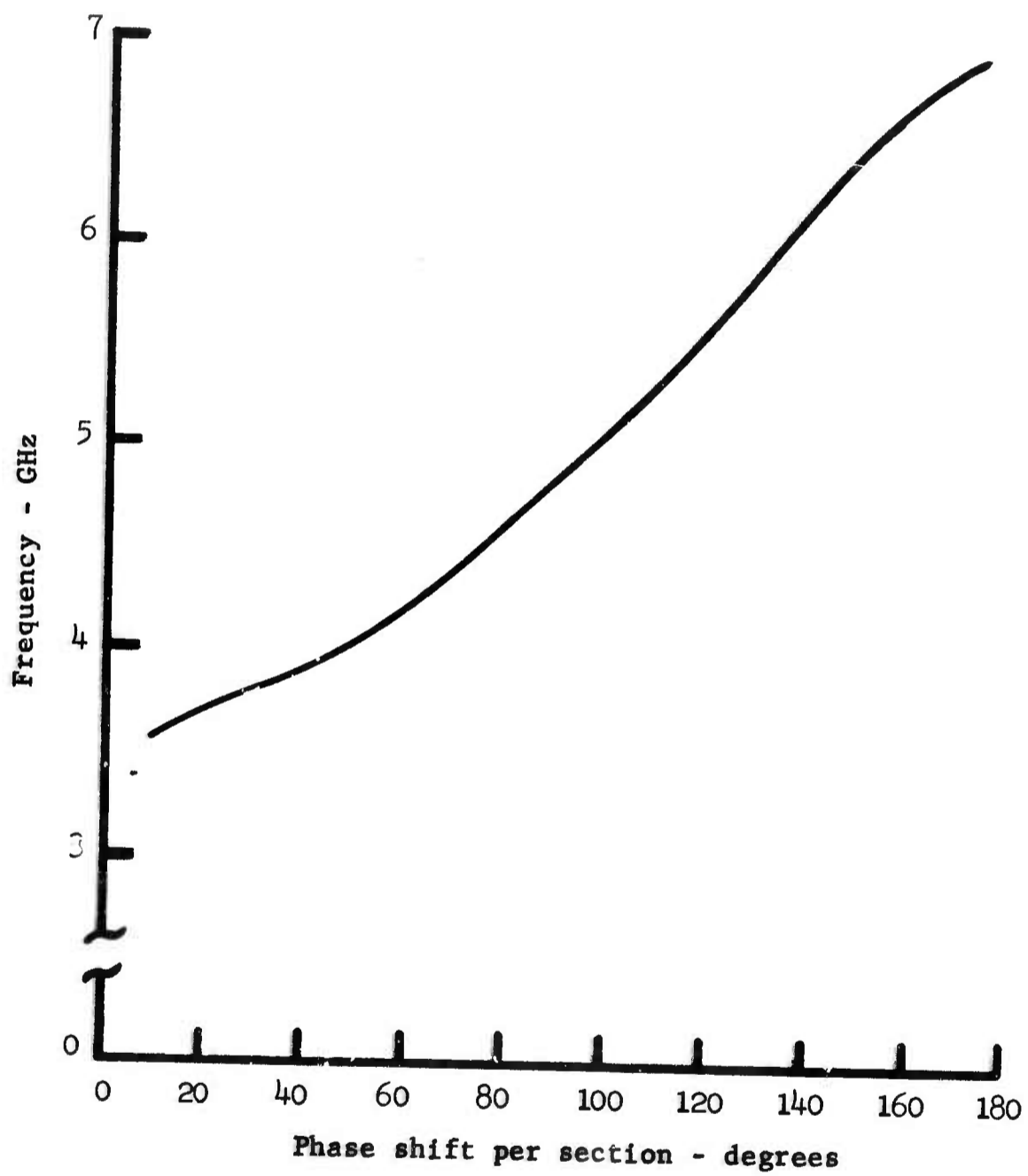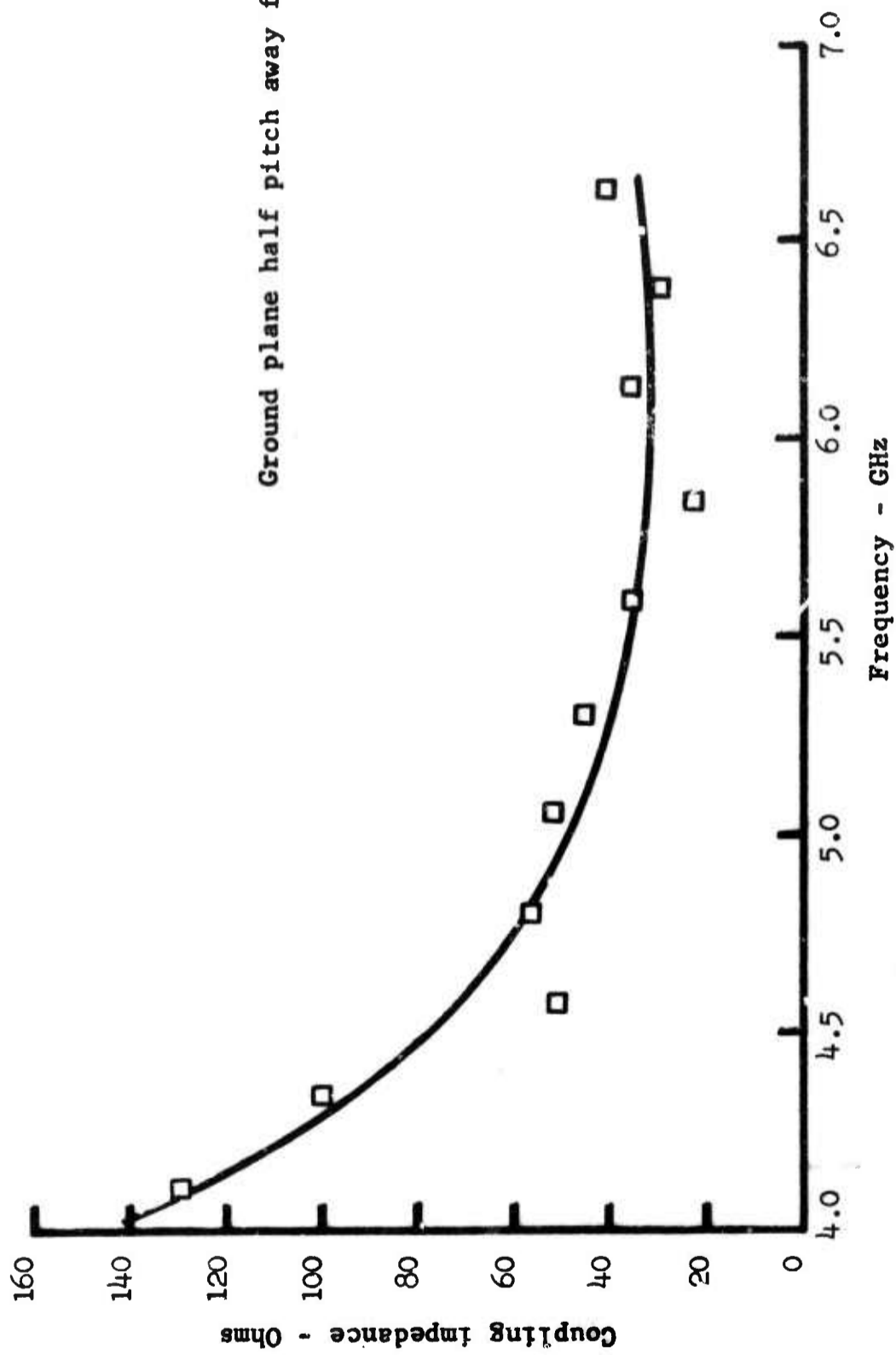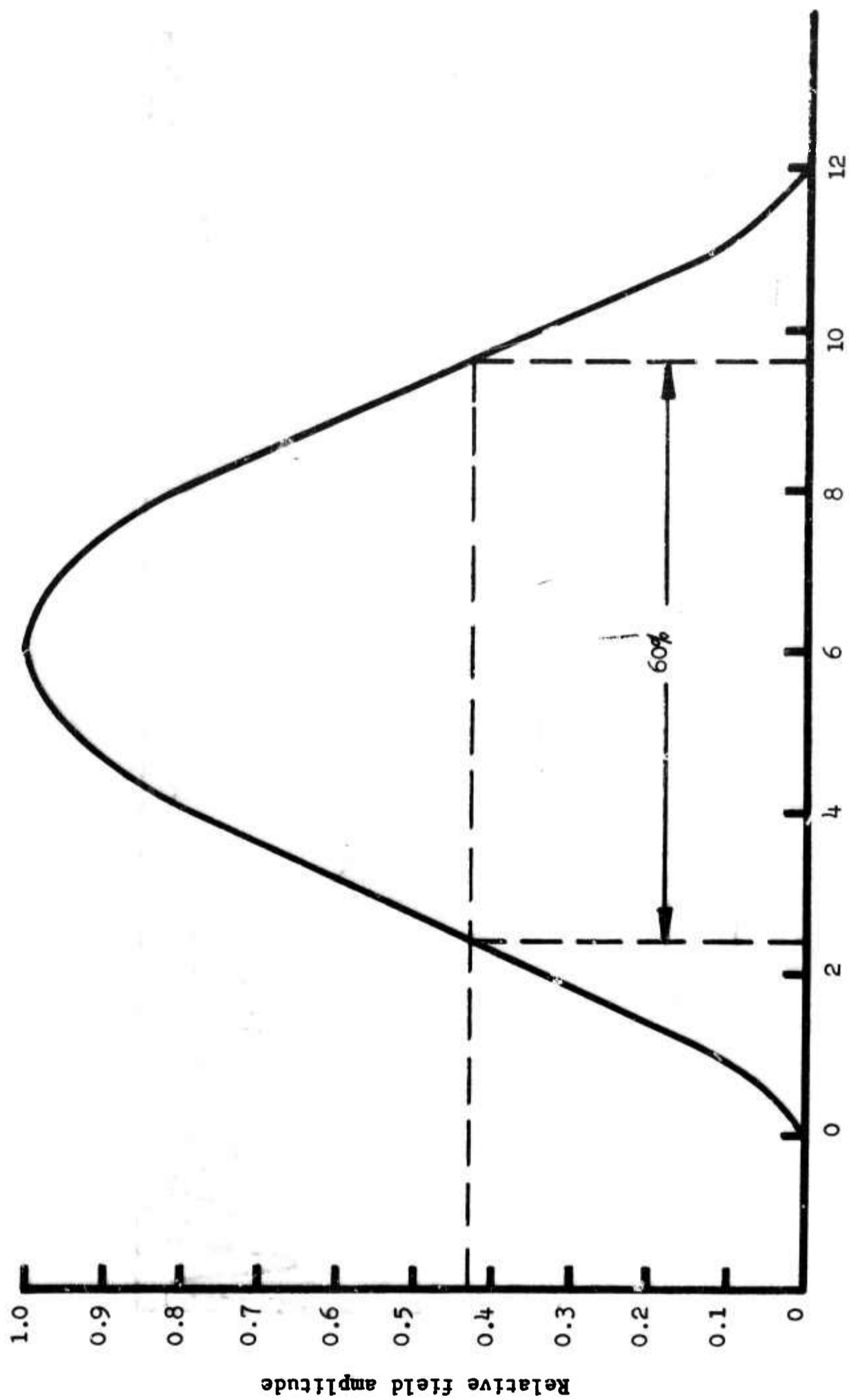
65

FIGURE 33   LINEAR VERSION OF SLOW WAVE ANODE CIRCUIT

FIGURE 84 DISPERSION CURVE FOR INITIAL DESIGN CIRCUIT

67

Ground plane half pitch away from helices

FIGURE 35 INTERACTION IMPEDANCE

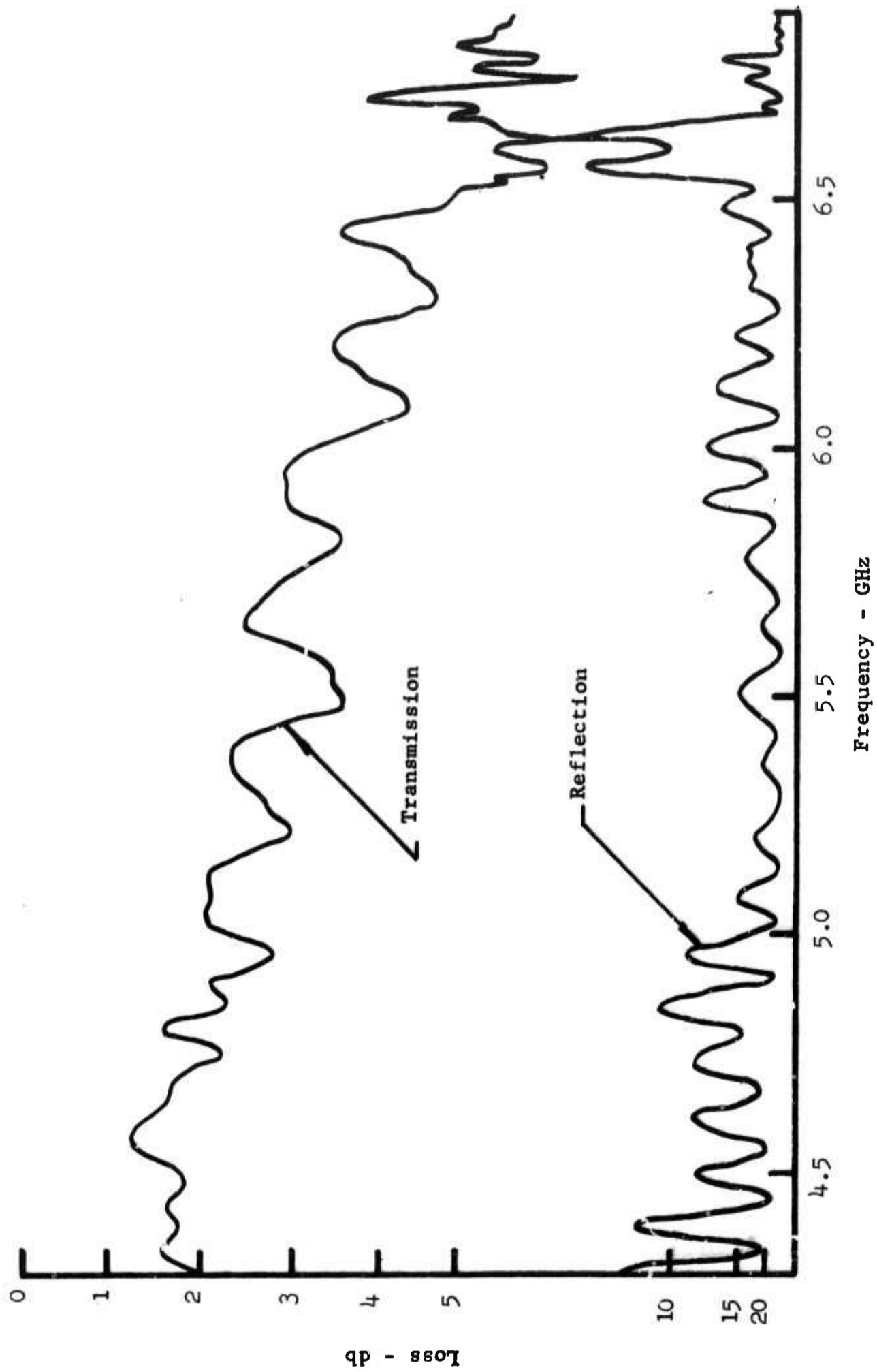FIGURE 36 FIELD VARIATION ALONG ANODE HEIGHT

69

FIGURE 37 INPUT RETURN LOSS AND TRANSMISSION WITH OUTPUT TERMINATED
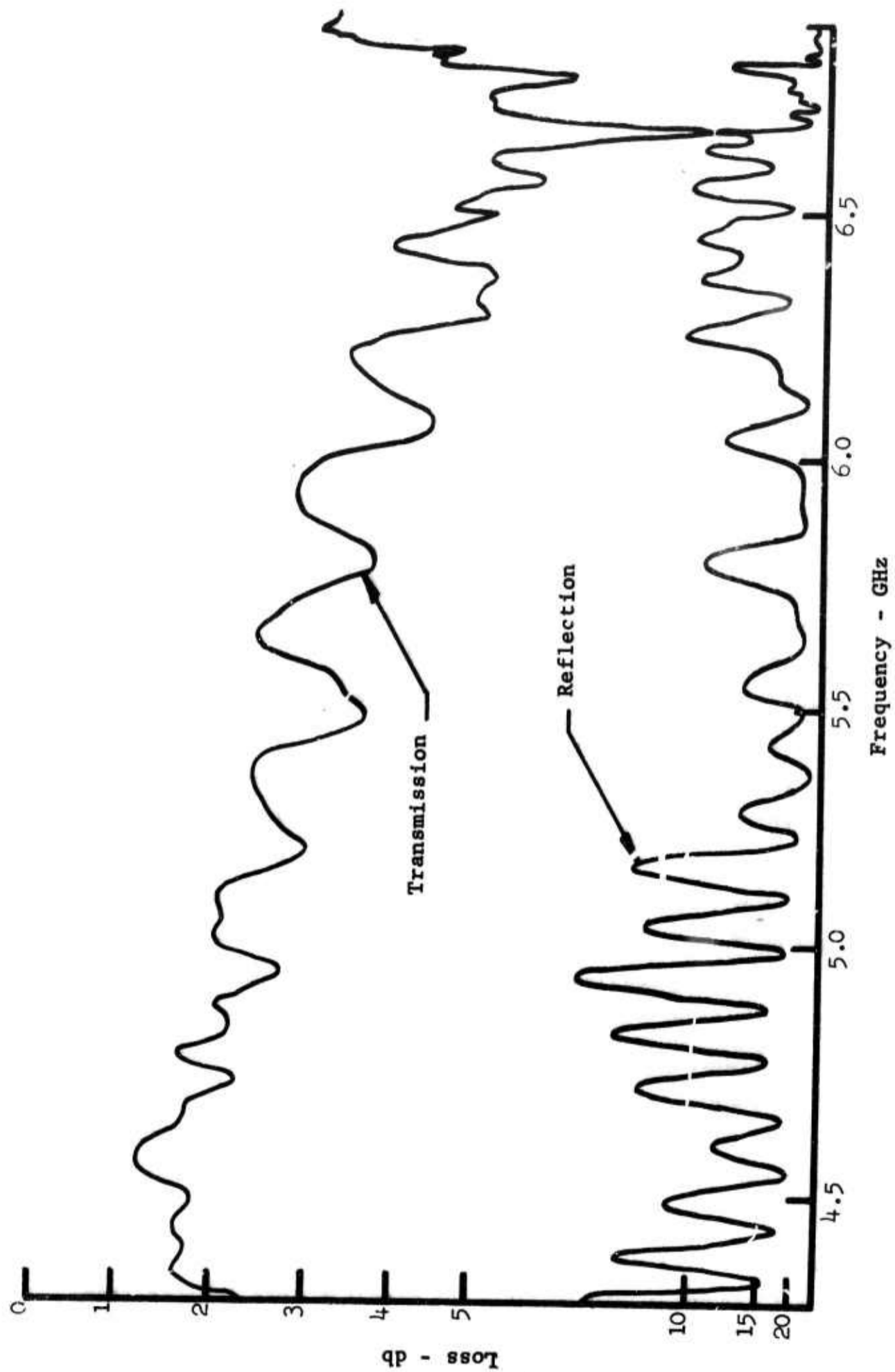
70

FIGURE 38 RETURN LOSS AND TRANSMISSION WITH INPUT TERMINATED

71

input is terminated and the output is illuminated in a matched load. The transmission loss is seen to be approximately 2 db to 3 db, as was expected. The transitional match from coaxial line to waveguide had not been attempted; however, since this was a relatively common transition, no great difficulty was anticipated.

Based upon the results obtained with the linear cold tester, a circular version which duplicated the amplifier anode was ordered.

5.6 Cold Test - Circular Slow Wave Anode

The circular version of the cold test vehicle was evaluated, and the results were found to be identical with those obtained with the linear version. The dispersion curves for both the linear and circular versions were identical and are shown, compared to the calculated curve, in Figure 39. The interaction impedarce and field distribution also appeared to be quite similar.

Since the anode circuit properties seemed to be well under control, the next step was to incorporate the matching transitions using the technique developed with the linear version. The match obtained with the linear version was accomplished using small coaxial lines to accommodate the existing test equipment. The technique for launching the energy onto the slow wave circuit was valid, but the physical size of the coaxial lines was not considered adequate for the anticipated power levels in a hot tube. In order to incorporate the matching transitions to be used in a hot tube, a broad band waveguide to coaxial transition had to be designed using components capable of handling the high average and peak powers anticipated. The method used for this transition was a capacitive post design which was capable of being water cooled to insure safe operation at the high power levels. The match obtained with the waveguide to coaxial line transition is shown in Figure 40. The mismatch loss is less than 0.1 db across the required band.
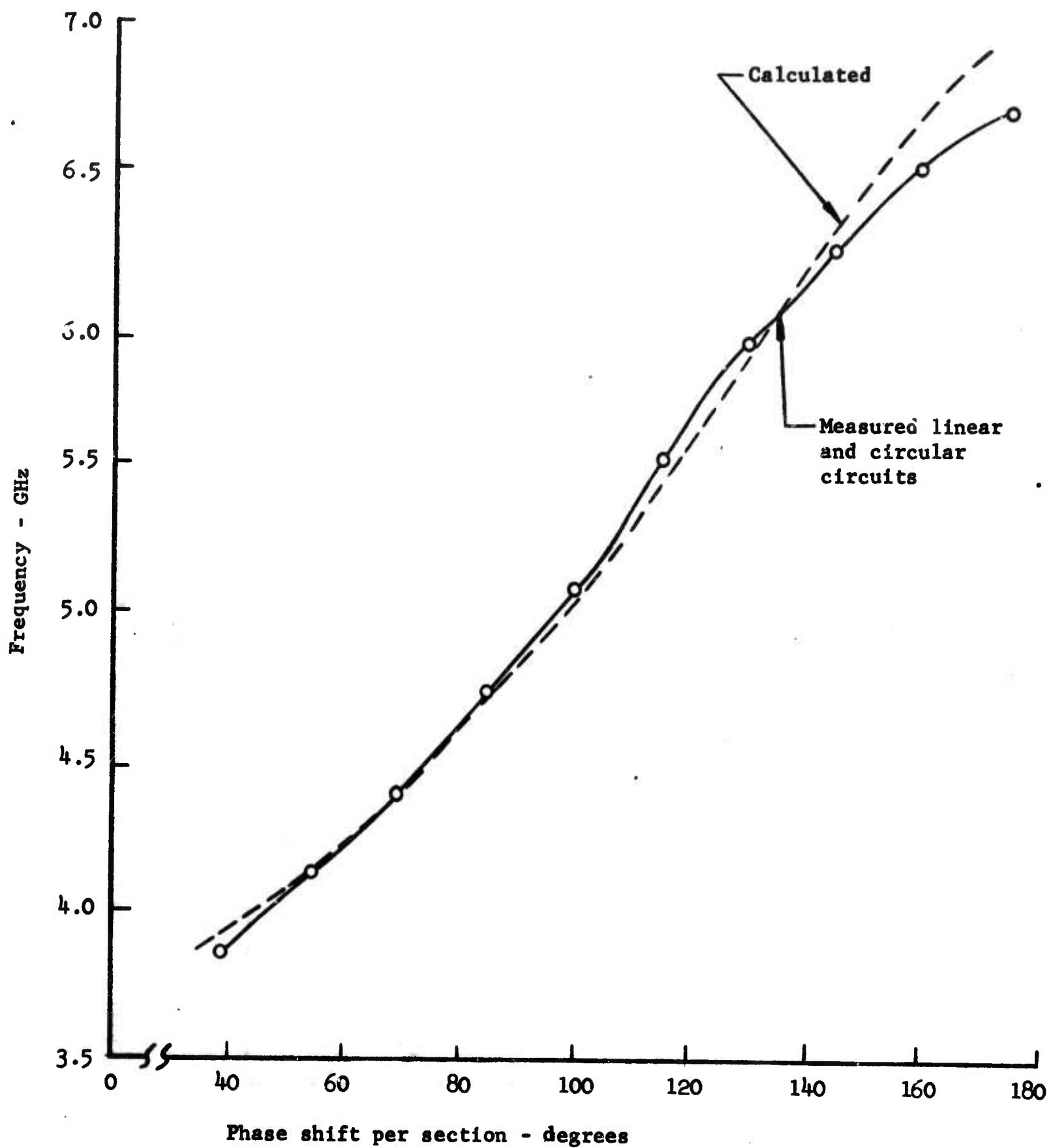
FIGURE 39 DISPERSION CURVES FOR LINEAR AND CIRCULAR SLOW WAVE CIRCUITS
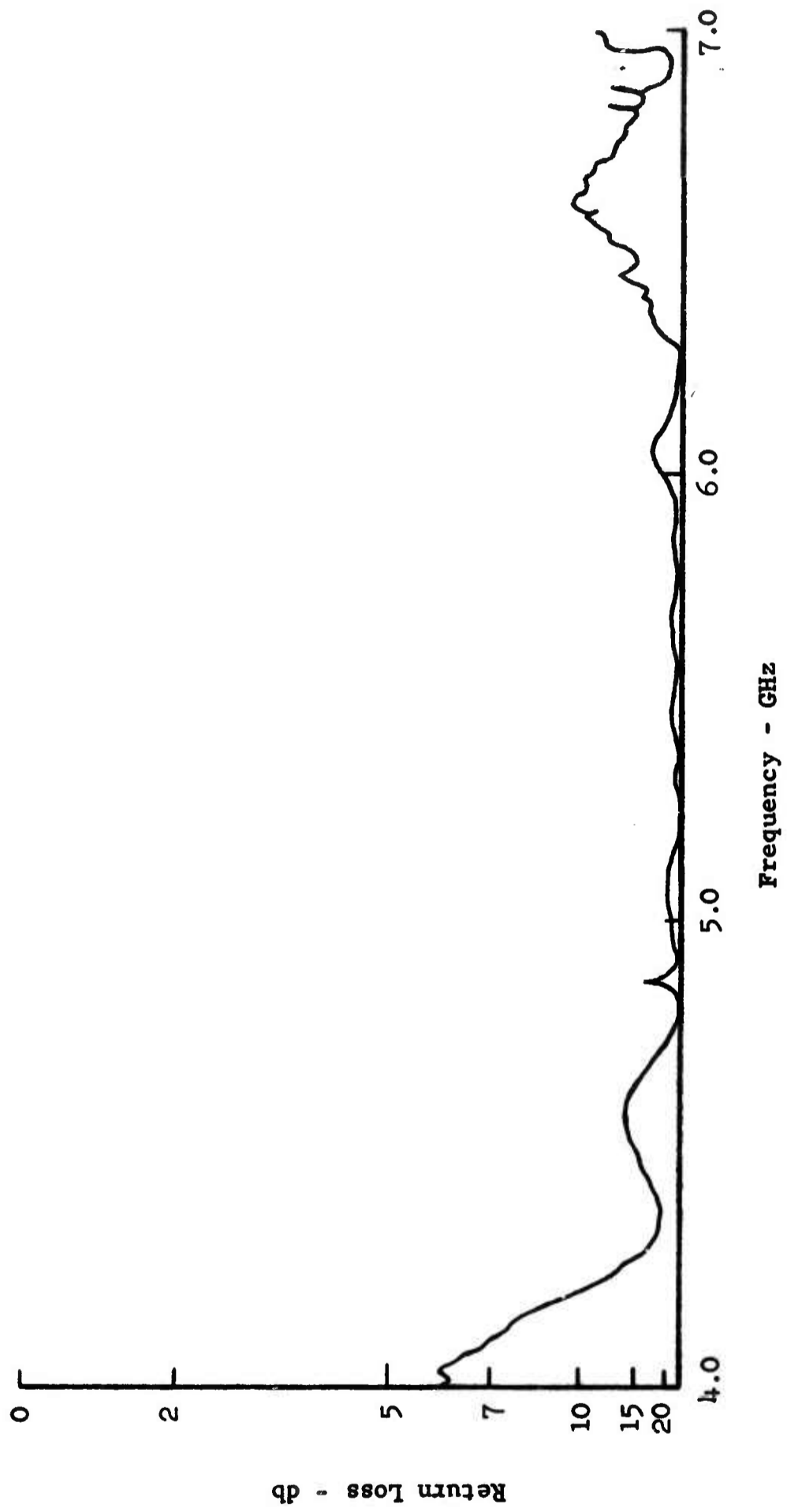
73

Return Loss - db

Frequency - GHz

FIGURE 40 WAVEGUIDE TO COAXIAL TRANSFORMER RETURN LOSS - CAPACITIVE POST DESIGN

74

Using the waveguide to coaxial transition and the technique for launching the energy onto the slow wave circuit, we proceeded to optimize the overall match to the cold te.. vehicle. Figure 41 shows a photograph of the circular cold test assembly and the waveguide input and output arms. In the photograph, the waveguides are parallel and extend in the same direction; this was done to facilitate testing. Since the transition from waveguide to the slow wave circuit was coaxial, either waveguide could be oriented in any position around 360 degrees in the plane of rotation. In the hot tube, the waveguides were to be attached for "in line" operation; that is, the waveguides would be parallel but 180 degrees apart and separated by approximately the tube body diameter.

The overall match obtained with the transitions described is shown in Figure 42. The return loss from the illuminated port is seen to be at least 15 db over the range from approximately 4.8 GHz to 6.0 GHz.

5.7 Cold Test - Circular Cold Test Vehicle

The initial circular cold test vehicle had its match adjusted with an absorber on the circuit. The next step was to adjust the match with no absorber on the circuit and with the circuit's output port properly terminated. This technique would show interfering mismatches from both input and output transitions as well as any circuit non-uniformities. The tube was then reversed and the observation was repeated for the other port. A similar technique was used to look at the transmission through the tube, and an indication of insertion loss was observed and recorded. The initial results of the match, both from return loss and insertion loss information, indicated that there was an interfering mode or modes in the tube.

A display of either return loss or transmission loss as a function of frequency will normally show small periodic variations across the band of the tube. The variations in return loss will
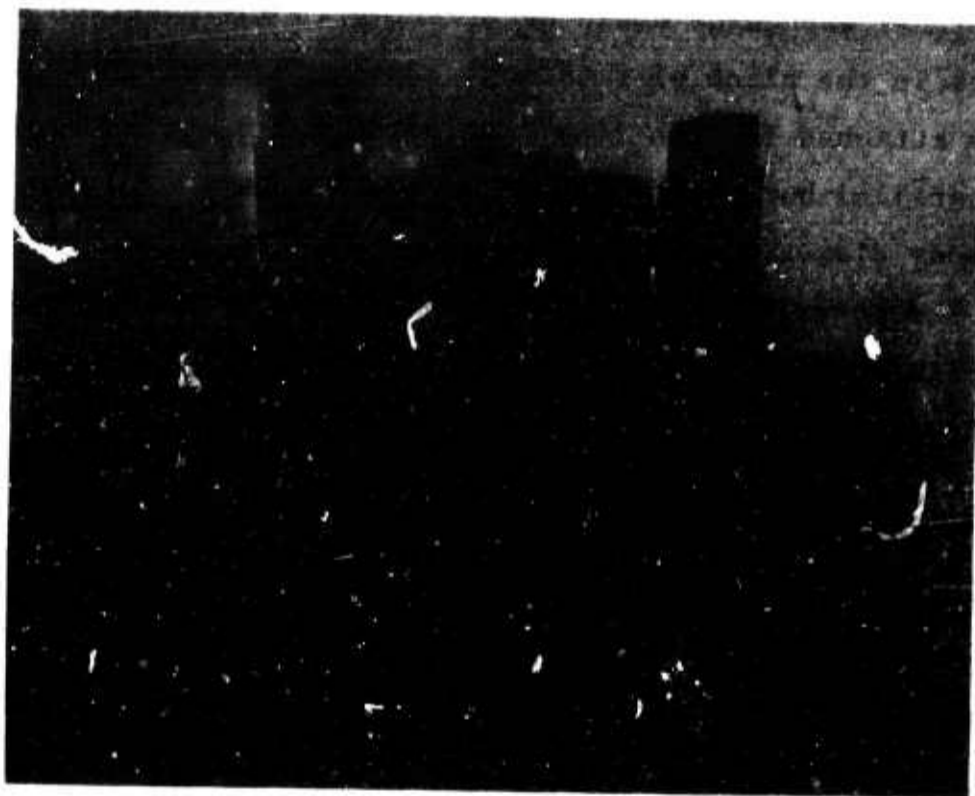
75

FIGURE 41   CIRCULAR COLD TEST ASSEMBLY WITH
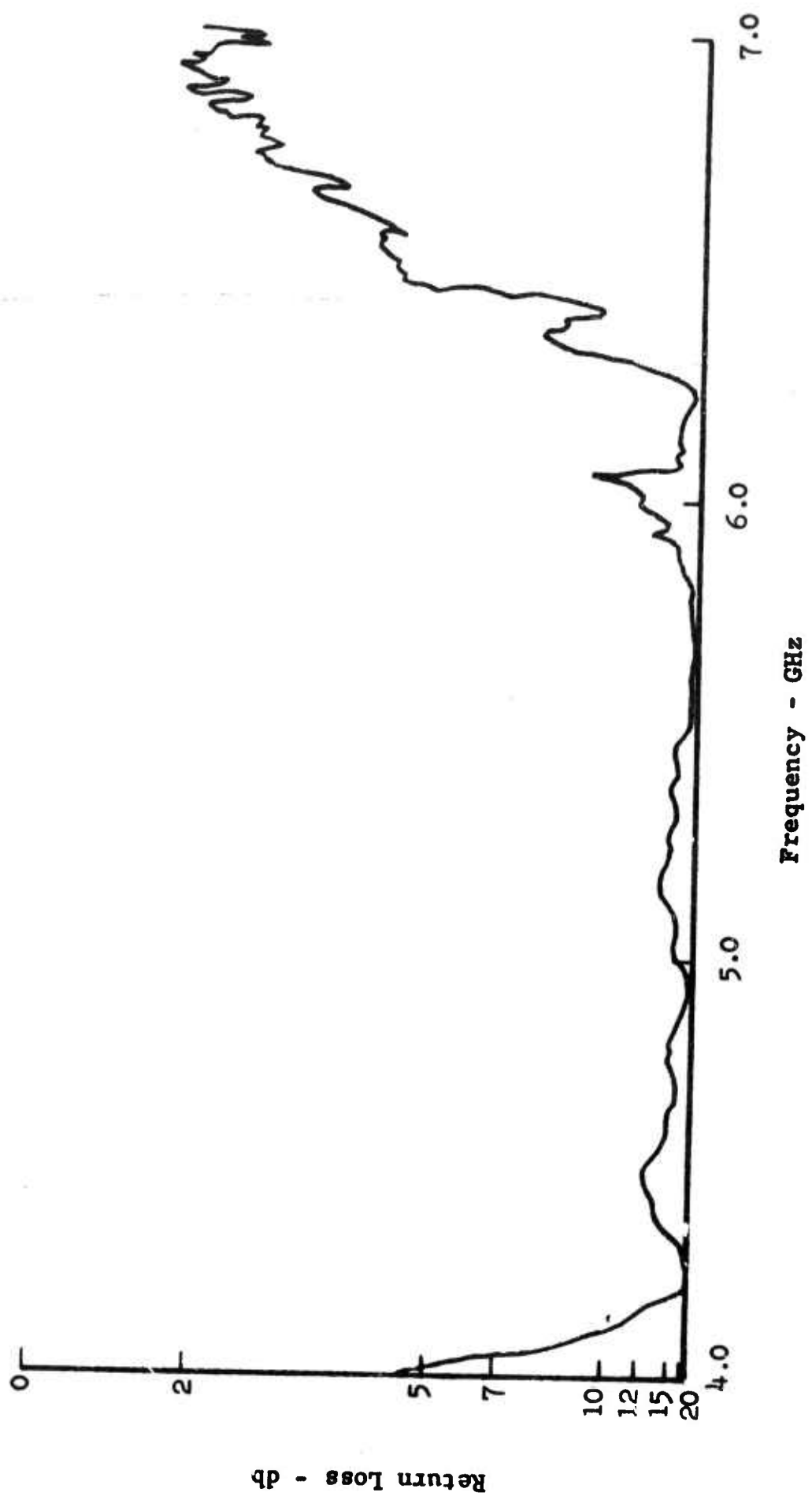   WAVEGUIDE INPUT AND OUTPUT ARMS

FIGURE 42 RETURN LOSS OF INPUT TRANSITION

77

normally correlate with the variations in transmission loss. The
initial results showed these small variations plus other variations
which were larger than expected. However, these larger variations did
not show correlation between return loss and transmission loss.

There are several effects which could produce the results
observed. The small variations arise from periodic imperfections in
the slow wave circuit; e.g., differences in element spacing or the
existence of non-uniform braze joints on the circuit. These usually
appear and are easily remedied.

The pattern observed in this instance, however, showed
pronounced dips in the transmission through the circuit, but without
corresponding mismatches as shown in Figure 43. This pattern indicates
an absorptive rather than a reflective type of loss. Only a small
fraction of the incident power is reflected back through the input,
but a significant amount of power is lost in transmission. If we
expand a small portion of Figure 43 in the region around 5.0 GHz, we
can illustrate this effect. In Figure 44 we show the return loss and
transmission loss from Figure 43 and also show the transmission loss
which would be produced by the reflections alone. That is, the 6.5 db
reflection at 5.0 GHz would normally produce a corresponding 1.1 db of
transmission loss. The observed transmission loss is 5 db. (The
transmission losses shown in Figure 43 include a 4 db circuit loss
which is taken as a reference.) The large transmission loss shows
clearly that some energy is being absorbed in the particular geometry
of this tester.

The cause was an exchange of energy between the slow wave
circuit and the region between the circuit and the back wall of the
anode assembly. This effect did not show up in the return loss in the
previous test simply because the absorber on the slow wave circuit
damped out this exchange of energy between the back wall and the
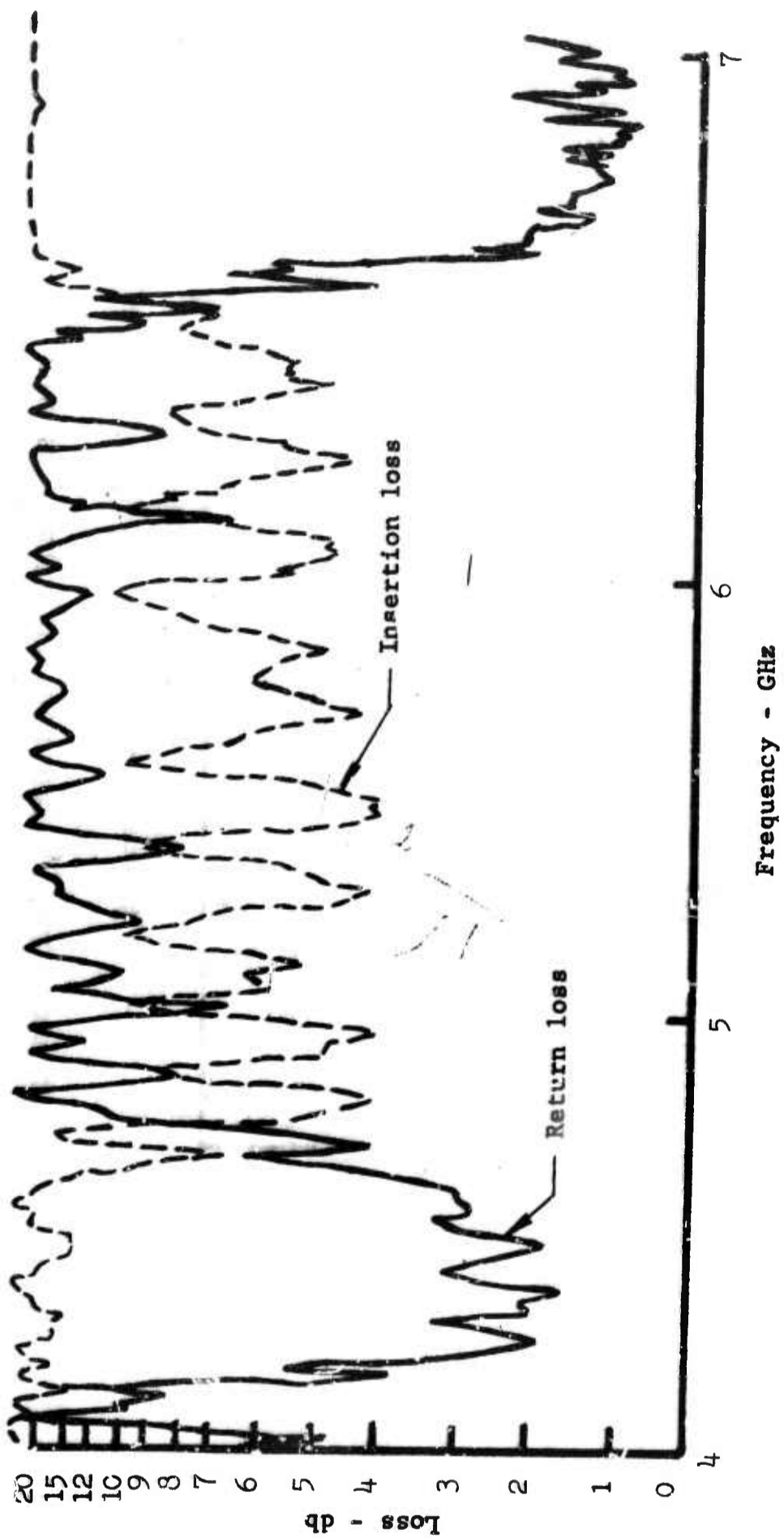circuit.

78

FIGURE 43 TRANSMISSION AND RETURN LOSS FOR CIRCULAR COLD TEST MODEL
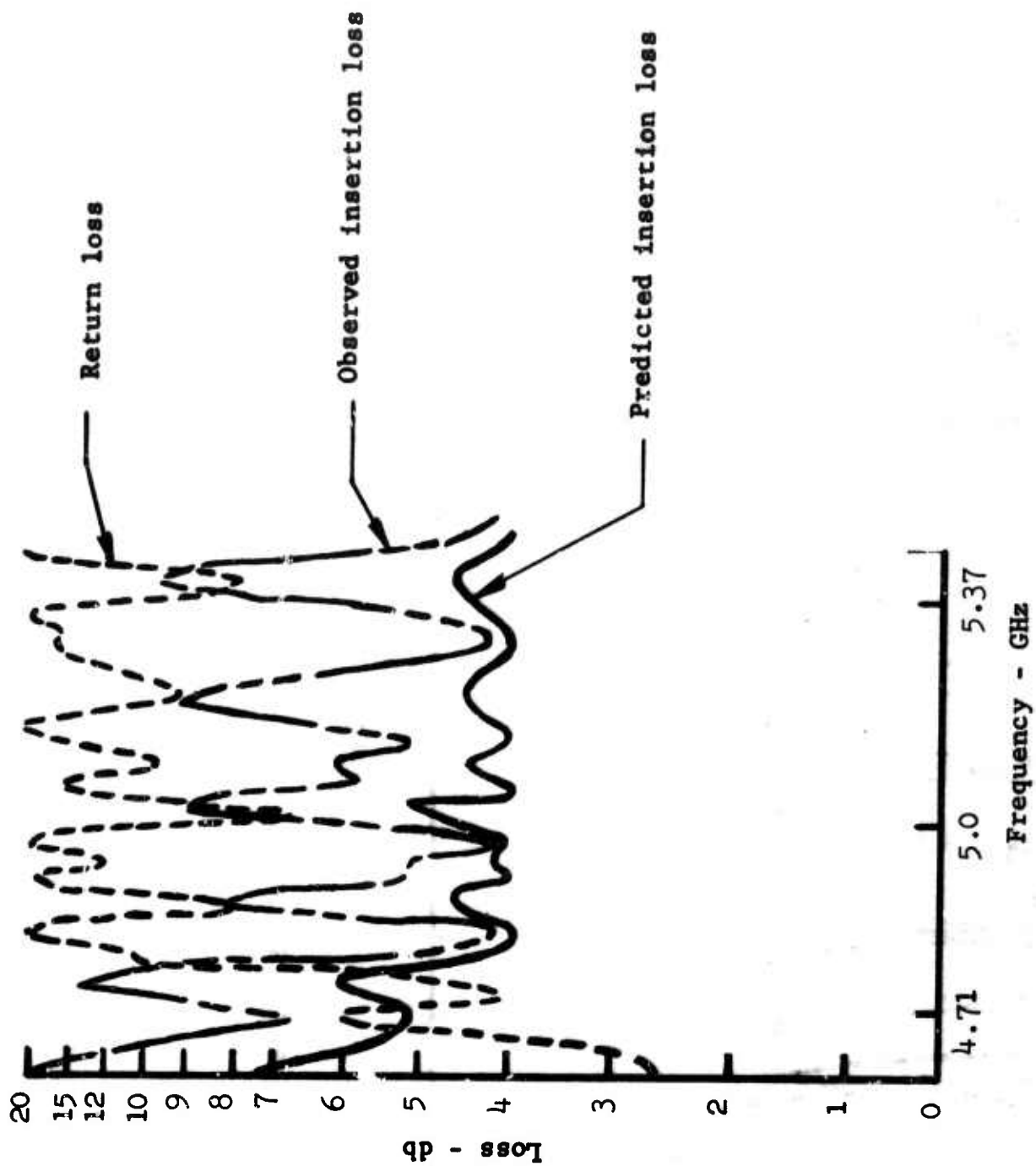
79

FIGURE 44 EXPANDED VIEW OF INSERTION AND RETURN LOSS FROM FIGURE 43 WITH PREDICTED INSERTION LOSS

There are several ways in which these effects can be reduced or eliminated. To reduce or eliminate some of the small periodic variations, the elements of the slow wave circuit are carefully checked and realigned to achieve maximum mechanical uniformity. The more prominent effects with this circuit are the exchange of energy between the slow wave circuit and the back wall region. It was found that the energy propagating between the slow wave circuit and the back wall behaved very much like that which propagates in a ridged waveguide. The method used to reduce or eliminate the coupling between the two propagating systems was to alter the cut off wavelength of the ridged guide such that its cut off frequency would fall above the pass band of the slow wave circuit. This was accomplished by altering the geometry of the back wall as shown schematically in Figure 45.

Another effect which was observed is sometimes difficult to reduce or eliminate. This effect is a cavity resonance. The field must be altered in order to shift the resonance out of the slow wave circuit pass band. The field distribution must be known in order to accomplish this. Again by changing the geometry, the boundary conditions that set up the field can be altered which will shift the resonant frequency.

As a result of these cold tests, changes were made in the geometry of the hot test vehicle. The results will be discussed in the following section.

5.8 Hot Test Vehicle

Techniques for assembling the slow wave circuit evolved through the construction of the cold test model and the initial hot test model. Both of these models had defects in some of the brazed joints which were formed simultaneously. Efforts to correct these defects by rebrazing resulted in mechanical non-uniformities. The non-uniformities upset the circuit to line match and could not
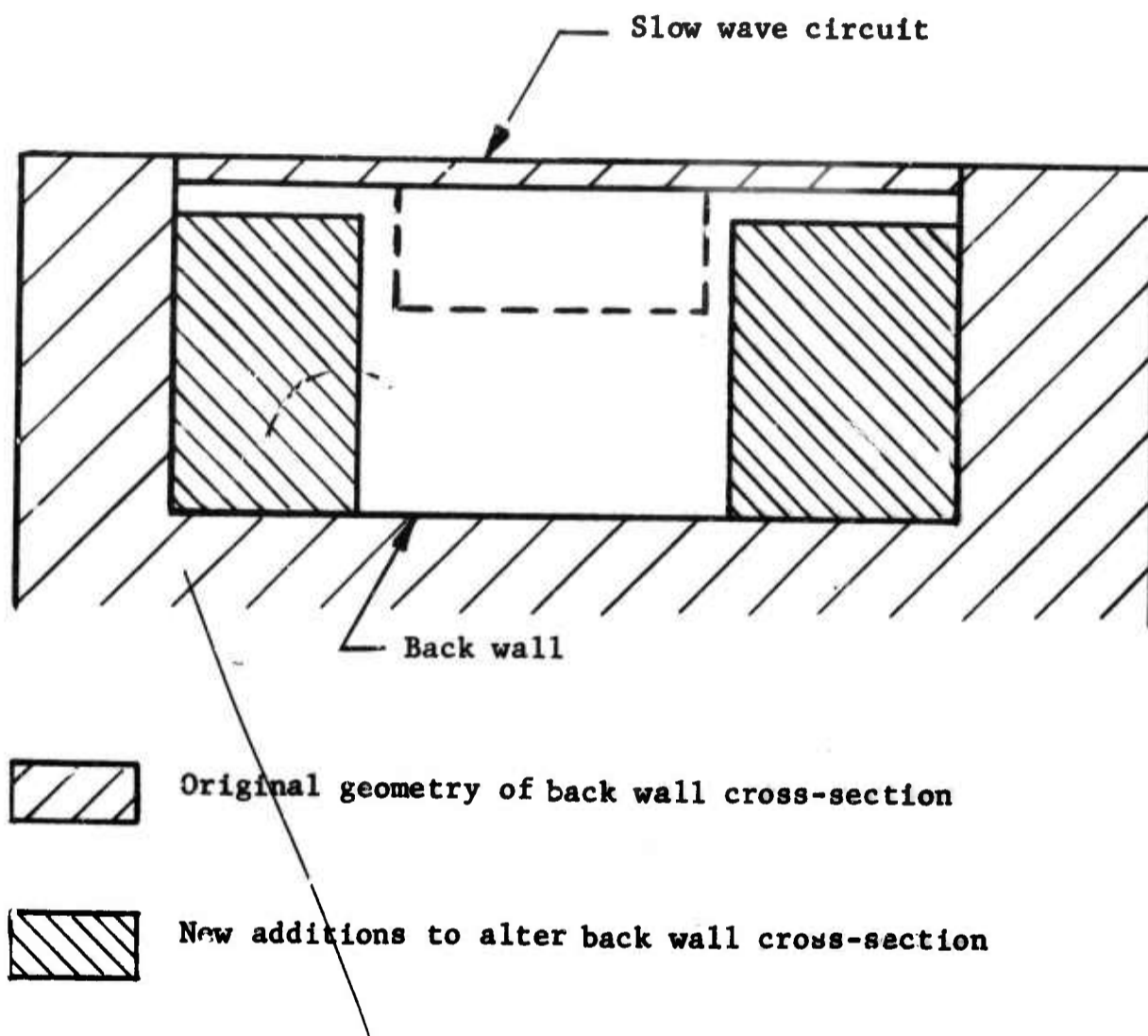
FIGURE 45   SCHEMATIC OF BACK WALL GEOMETRY SHOWING ALTERATIONS

subsequently be corrected. The assembly of the second hot test model was successful. Photographs of this assembly are shown in Figures 46 and 47.

The anode is first brazed into the tube body, after which the cathode and pole pieces are put in place. At this time, the match is observed and recorded as shown in Figures 48 and 49 for return loss, and Figures 50 and 51 for insertion loss. Because of the manner in which the hot test vehicle is assembled, provisions were made for making final adjustments to the match prior to final seal in of the tube.

The cathode assembly shown in Figures 52 and 53 is essentially a coaxial structure made of double wall tubing so that the coolant can pass directly under the cathode proper. This method provides a continuous flow of coolant to remove the heat developed at the cathode and control electrode while proper electrical insulation between the electrodes is maintained. This technique was developed and used quite successfully on the previous program under Contract AF 30(602)-4082.

Figure 54 shows the complete assembly of the hot test vehicle. Three coolant paths are provided in the tube. The anode body has one coolant path with all circuit bars cooled in parallel. This can be seen in Figure 54. The input and output connections for this path are shown at the top of the anode block. The output waveguide, output window, and output transformer make up a second coolant path. The cathode has the third coolant path (not shown). The tubulation seen coming out of the side of the tube body is the pumping port. The ceramic high voltage bushing can be seen (to the left) on the RF input side of the tube.

Figures 55 and 56 are the end view and side view of the hot test vehicle. The coolant system for the cathode and control electrode can be seen. The cathode assembly contains two coolant ports, which also serve as high voltage connections to the cathode and control

83

FIGURE 46   ANODE ASSEMBLY FOR HOT TEST MODEL
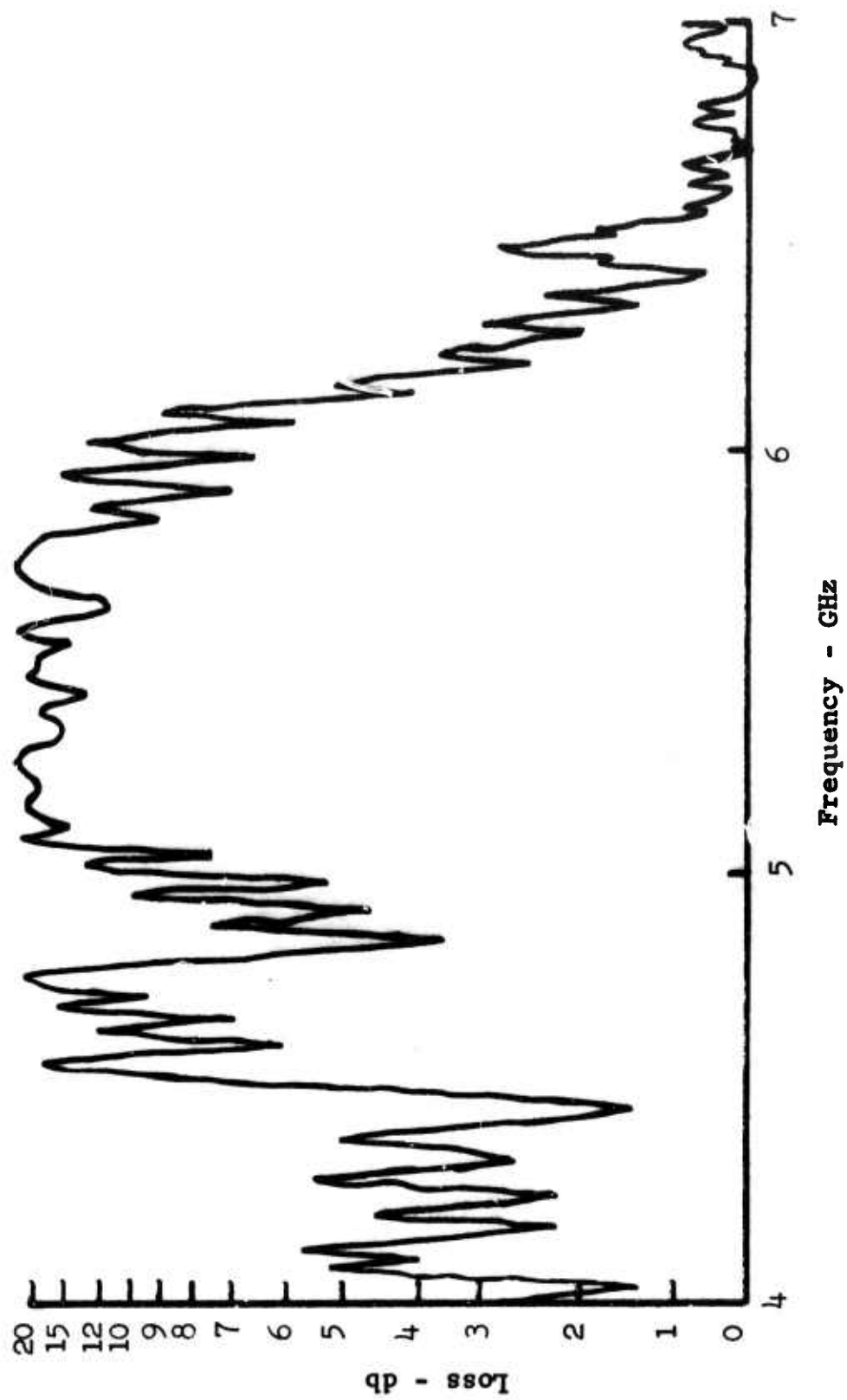
FIGURE 47   ANODE FOR HOT TEST MODEL

85

FIGURE 48 INPUT RETURN LOSS FOR HOT TEST VEHICLE
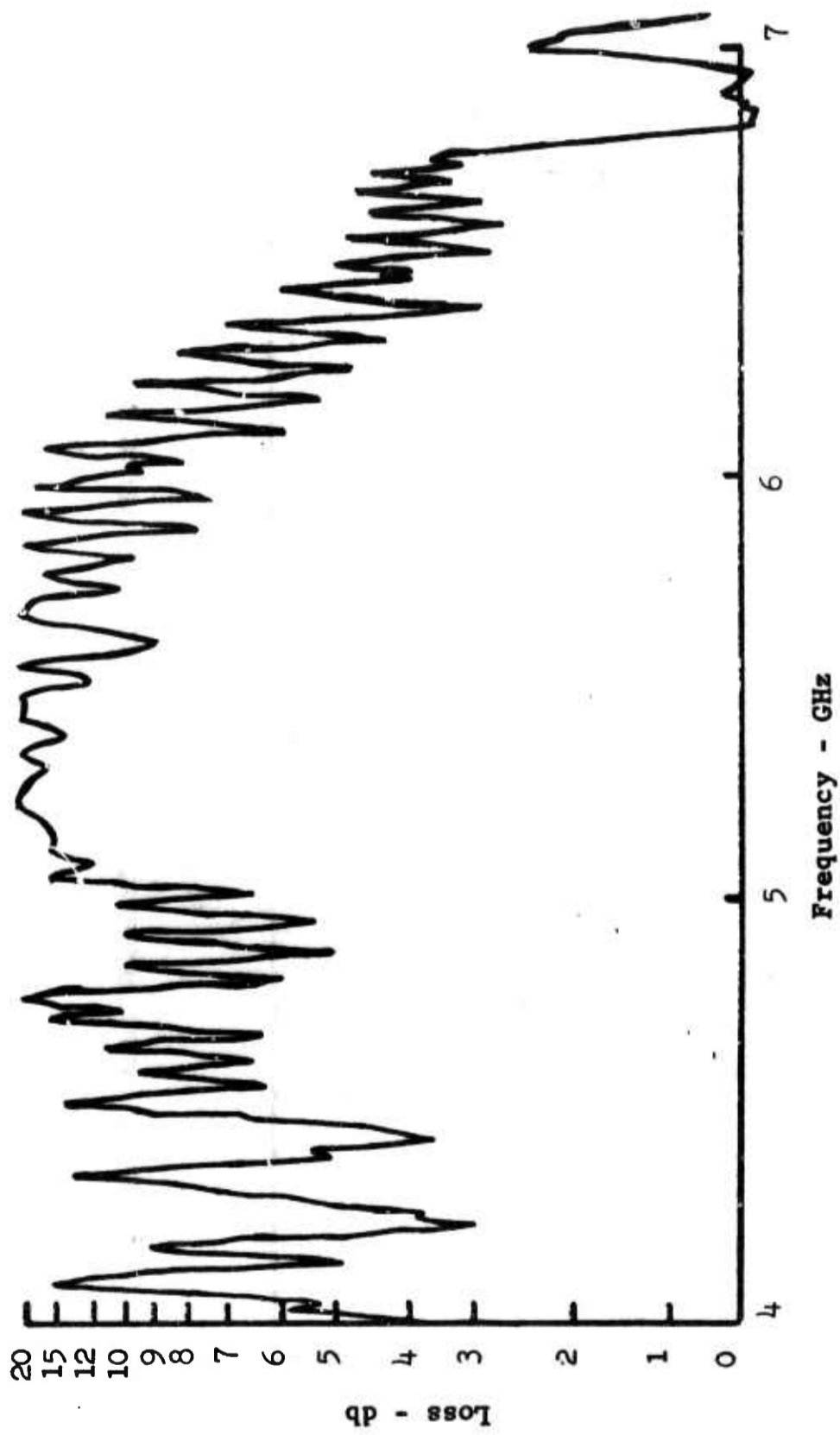
FIGURE 49 OUTPUT RETURN LOSS FOR HOT TEST VEHICLE

87
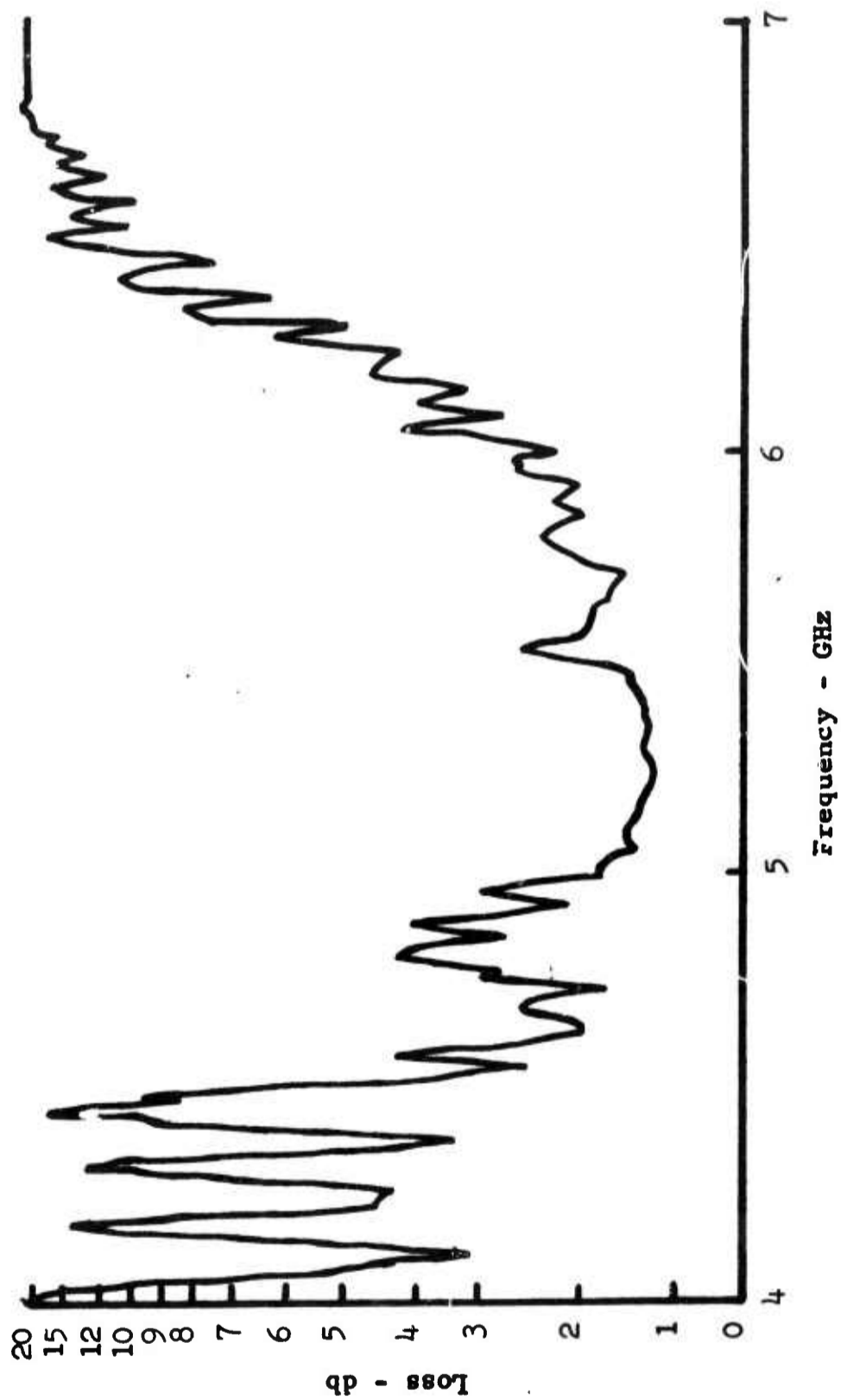
FIGURE 50 INPUT INSERTION LOSS FOR HOT TEST VEHICLE

88
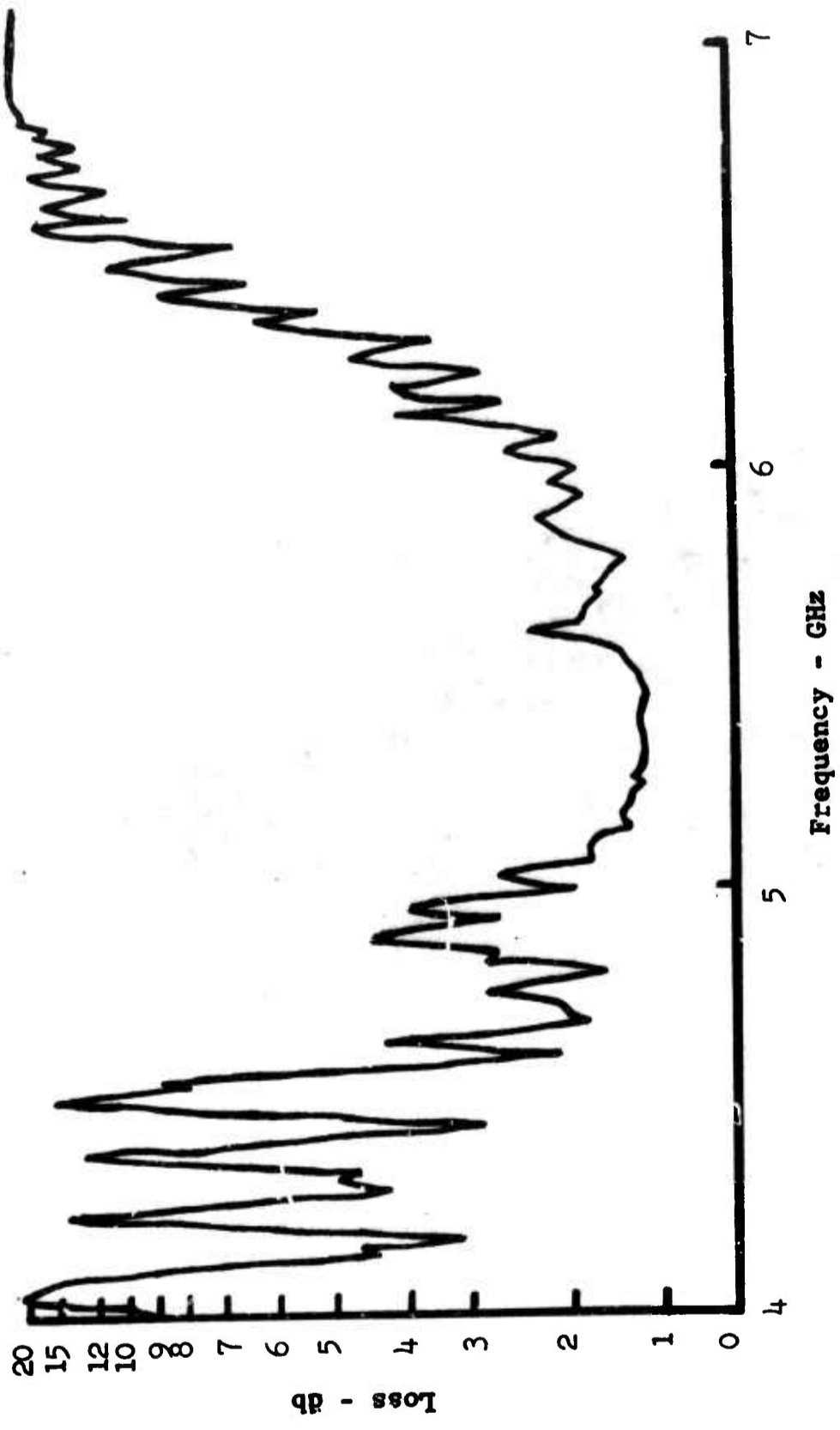
FIGURE 51. OUTPUT INSERTION LOSS FOR HOT TEST VEHICLE

89

FIGURE 52   CATHODE SUBASSEMBLIES
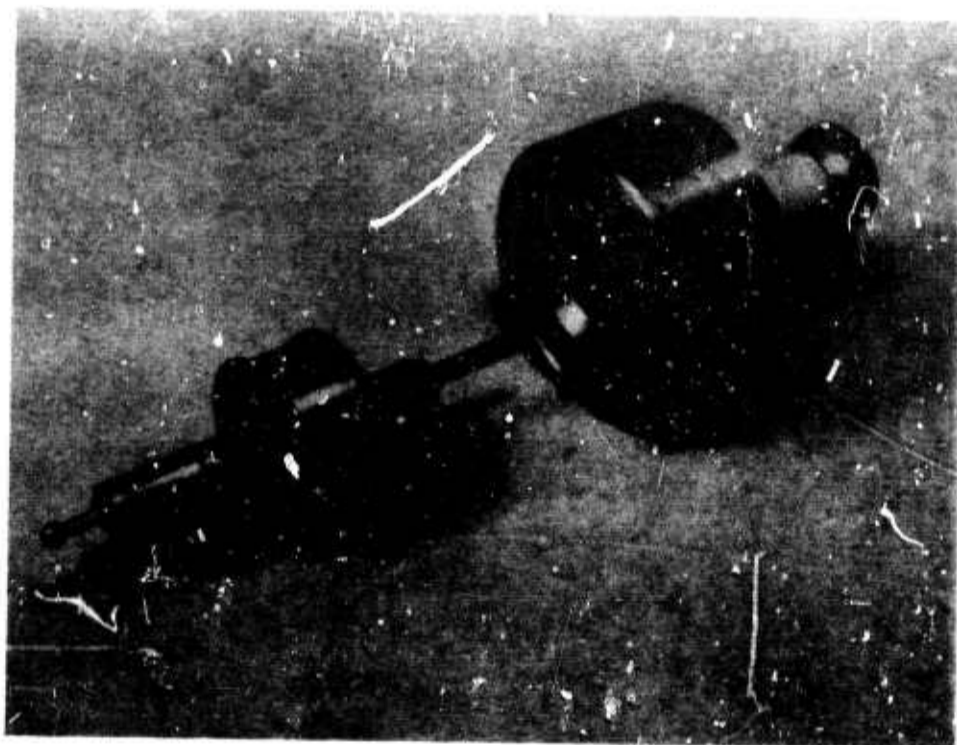
FIGURE 53   CATHODE AND POLE PIECE

91

FIGURE 54   COMPLETE HOT TEST VEHICLE ASSEMBLY

Coolant input
to circuit manifold

Impedance
section

Septum

Drift space
section

Control
electrode

Input

Coolant output

Cathode and
control electrode
coolant input

Control electrode
terminal

End hat
radius

Cathode
surface

Helix

Observation window
(pinched off)

Hollow circuit bar
(with coolant passage)

FIGURF 55 END VIEW OF HOT TEST VEHICLE

93

Impedance matching
section

Output window
coolant

Liquid cooled coaxial line to
waveguide transition

de

Output

Cathode terminal

Molybdenum facing

Ion pump port
(pinched off)

circuit bar
olant passage)

β

Coolant input to
circuit manifold

Input

Coolant output

Control electrode
terminal

Cathode terminal

Cathode and control electrode
coolant input

Ion pump port
(pinched off)

Obse
(pi

FIGURE 56 SIDE VIEW OF HOT TEST VEHICLE

94

A

Coolant output

Output window coolant

Output

Liquid cooled coaxial line
to waveguide transition

Observation window
(pinched off)

B

electrode. The breakaway on the upper right of the tube body in
Figure 55 shows the general matching scheme. The dashed lines across
the output waveguide and the dotted lines, which show the taper into
the circuit, constitute the waveguide to coaxial transformer. The
output side of the two matching transformers is liquid cooled. The
input and output are separated by a septum across the coaxial line
above the drift space section. An observation port is provided at
the bottom of the body of the hot test vehicle so that a small part
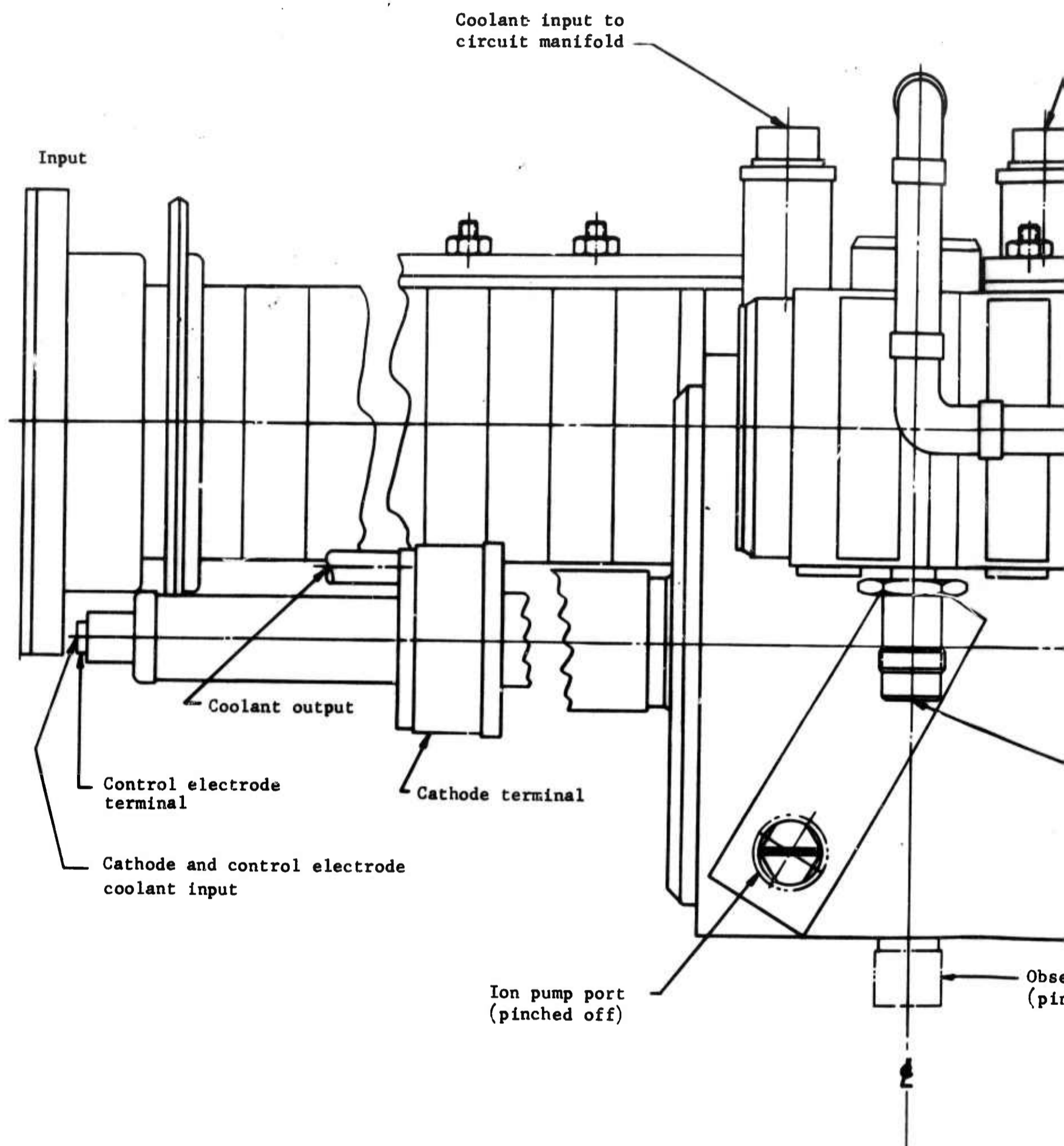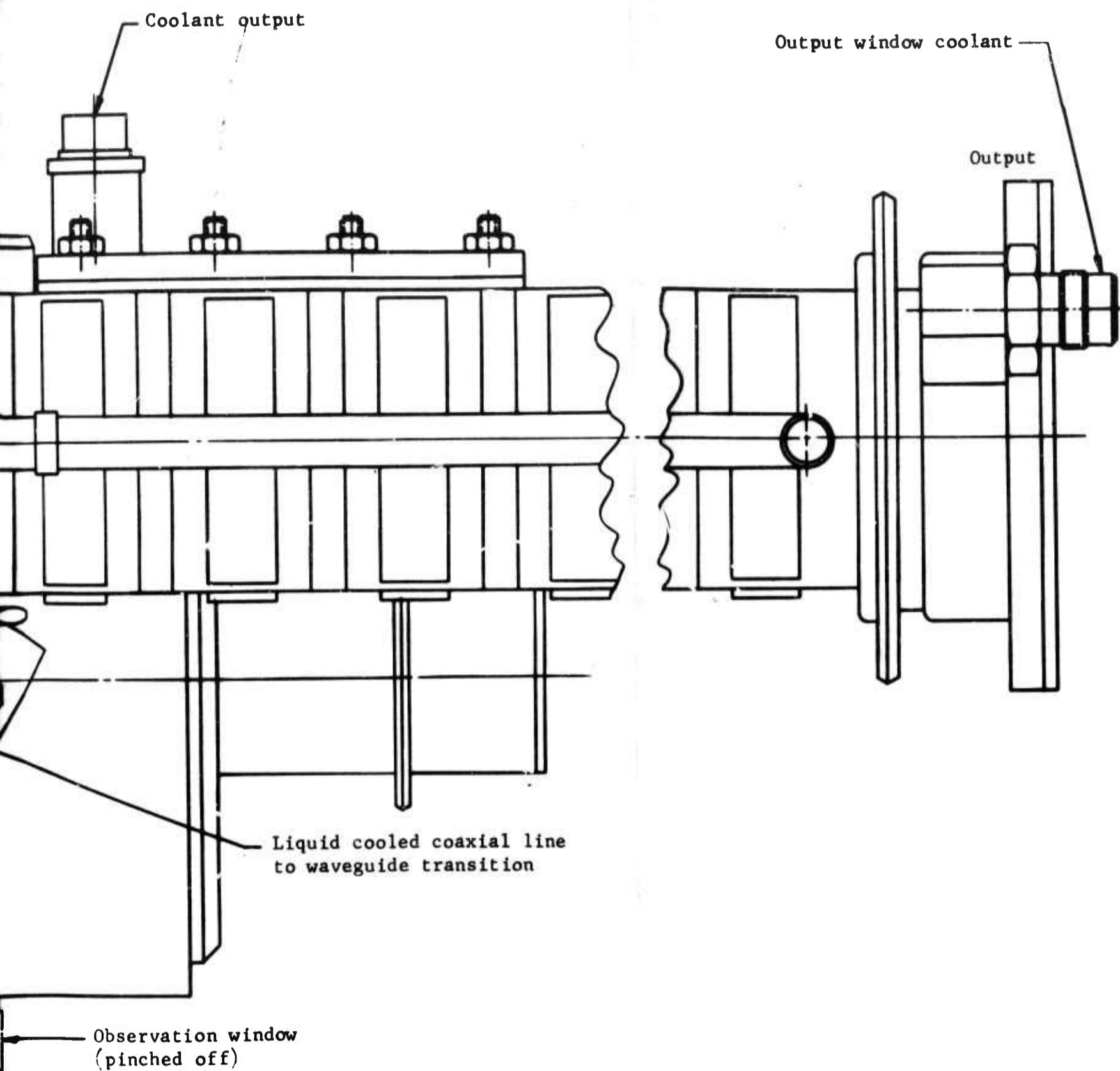of the circuit and cathode surface can be seen during operation.

5.9 Magnetic Circuit

The magnetic field uniformity produced by the pole piece
geometry was first evaluated with electrolytic field plots and then
checked with a magnetic probe using a cold test magnetic pole piece
tester shown in Figure 57.

The pole pieces were shaped in order to provide a fairly
uniform flux density in the interaction space. This was verified by
the measurements taken. The results of these measurements are shown
in the flux density field plot in Figure 58. As can be seen, the
field is fairly uniform in the shaded area which represents the
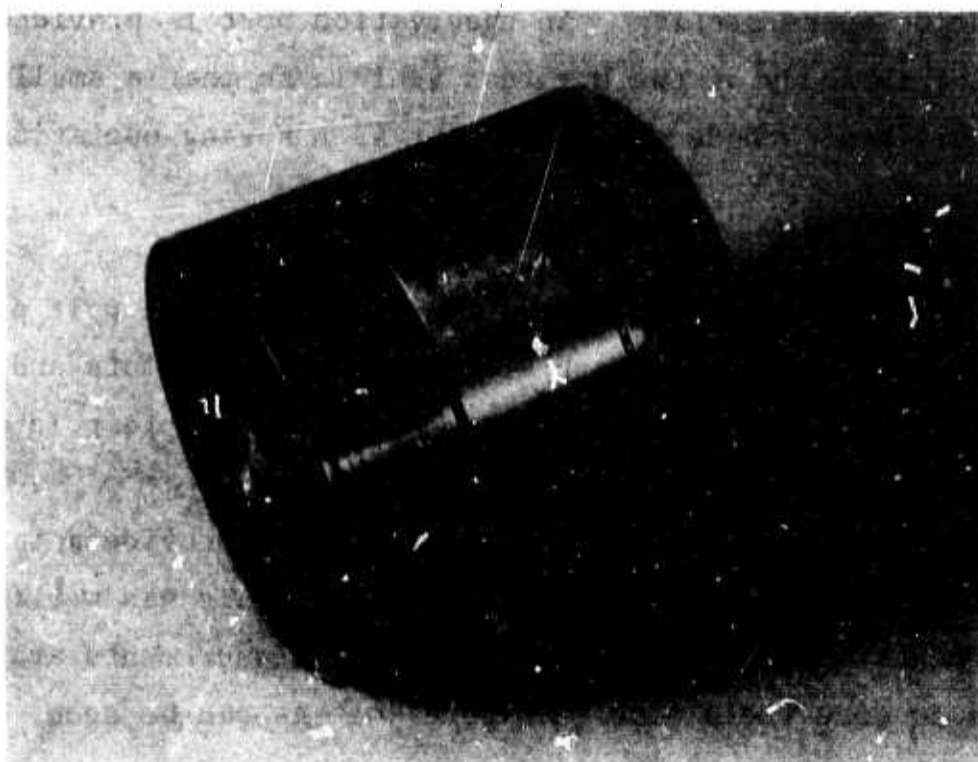interaction space.
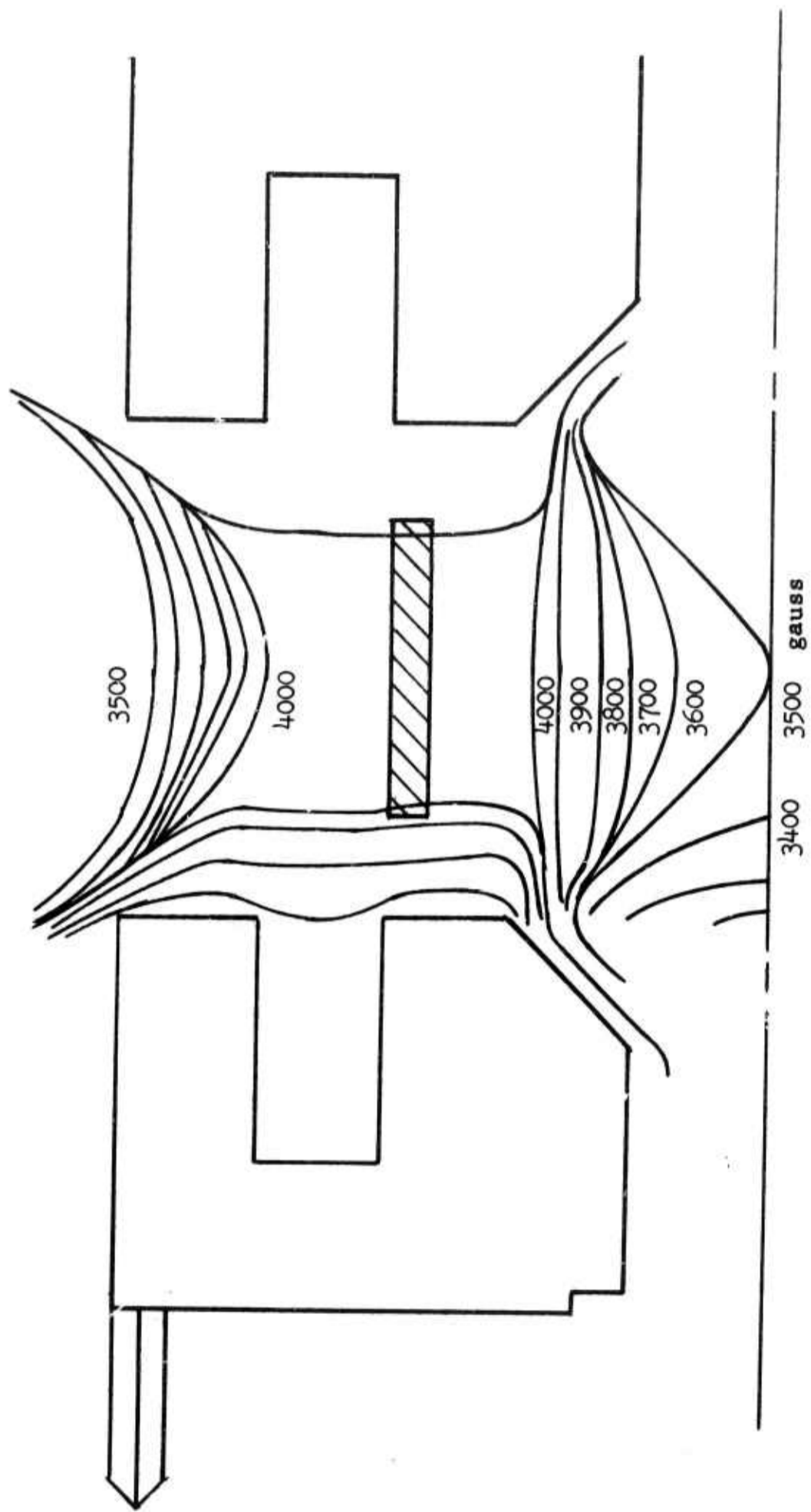
FIGURE 57   MAGNETIC CIRCUIT COLD TESTER

FIGURE 58 FIELD PLOT OF MAGNETIC FLUX DENSITIES USING MAGNETIC COLD TESTER

97

6.0 HOT TEST RESULTS (SFD-252)

Because of the complexity of this type of vehicle and the limited funds available, only one vehicle was constructed. A number of fabrication difficulties which were encountered during the construction of the amplifier had to be overcome. Consequently the amount of hot testing was limited. The hot tests which were performed essentially confirmed the initial design and proved the feasibility of operating with this new RF slow wave anode. Figure 59 is a photograph of the SFD-252 mounted in the test bed.

The initial evaluation was performed using a hard tube pulse modulator. The experience obtained on the previous program involving high power dc operated amplifiers has shown that the initial aging and evaluation under cathode pulsed conditions could be obtained quickly. On the other hand, dc operation always required a second and longer period of aging and seasoning before the vehicle could be operated at full power.

Under cathode pulsed conditions, the amplifier was operated to a limit imposed by the modulator. The amplifier was operated at approximately 29.5 kv over the 500 MHz band between 5.4 GHz and 5.9 GHz. Figure 60 shows the power output obtained across this band with essentially constant voltage. This power output curve was generated by sweeping the band very slowly and recording the output of a thermopile on a strip chart. Some variations in power output were observed and are generally attributed to the interaction with the circuit resonances which had not been completely removed during cold test. Figure 61 is a photograph of the RF output envelope at a randomly selected point. This photograph shows the power output as viewed through a broad band detector and also through a transmission type wavemeter to show that the output power is at the signal frequency. Figure 62a is a photograph of the RF output and the current pulses obtained under these conditions. The pulse length was then
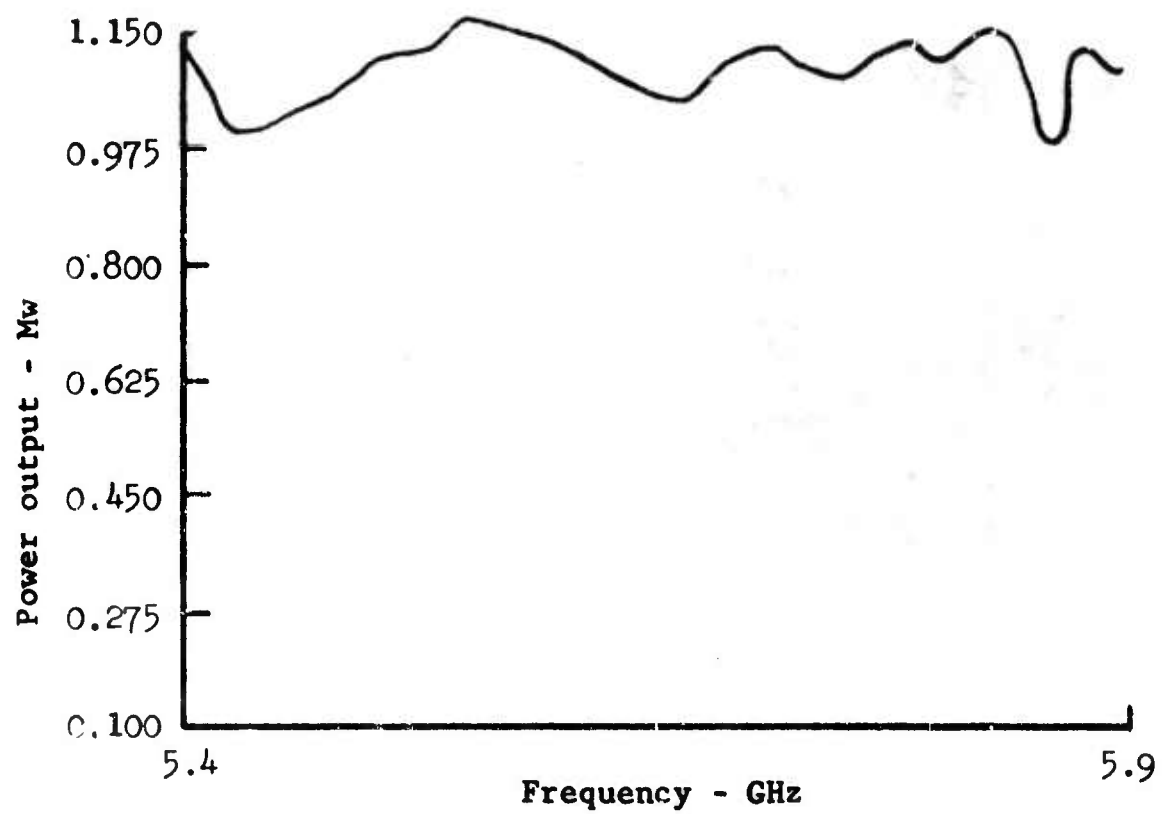
98

FIGURE 59   SFD-252 MOUNTED IN TEST BED

FIGURE 60 POWER OUTPUT OF SFD-252 OPERATING UNDER CATHODE PULSED
CONDITIONS AT CONSTANT VOLTAGE

FIGURE 61   RF OUTPUT ENVELOPE FOR SFD-252
AT RANDOMLY SELECTED POINTS

a. Same pulse length conditions as for Figure 61

b. Longer pulse length

FIGURE 62   RF OUTPUT (TOP) AND CURRENT (BOTTOM) PULSES
FOR SFD-252

increased to observe the effect of longer pulse operation as shown in Figure 62b. The storage capacity of the modulator limited the pulse length as can be seen by the drooping current in the photograph.

The next series of tests were to operate the amplifier with dc voltage applied between anode and cathode and with a control electrode used for turn off. As previously mentioned, a second aging and seasoning was required before this operation could be achieved. This seasoning process began at reduced magnetic field and comparatively low voltage. As the aging progressed, the magnetic field was increased and correspondingly higher voltages were used until the full operating level was reached. The design level for this vehicle was a magnetic field of 3400 gauss and an operating voltage of 35 kv.

The performance under dc operating conditions was terminated with less dc aging than would have been desired. The first reliable operation was obtained at a magnetic field which was approximately three-quarters of the design value with a corresponding low voltage and power output. Figure 63 shows the RF output of the amplifier and the current pulse operating under these conditions and Figure 64 shows the RF output compared to the unamplified feed through signal. The vehicle was operated at essentially a constant voltage of 26.5 kv at a peak cathode current of 135 amperes with a control voltage pulse of 12 kv applied at the end of the RF pulse to turn the tube off. Under such conditions of low magnetic field, the efficiency of the operation was rather low, as would be expected.

The next series of tests was to observe the performance of this vehicle under complete RF modulation conditions. This series of tests utilized some of the preliminary information obtained during the other phase of this program and was extremely encouraging, especially since this vehicle had not yet been properly aged. Under the AutoMod conditions, the amplifier was operated with only dc voltage applied. The RF turn on and turn off were accomplished.

103

FIGURE 63   RF OUTPUT (TOP) AND CURRENT (BOTTOM)
PULSES FOR SFD-252 UNDER dc
OPERATING CONDITIONS

104

FIGURE 64   RF OUTPUT PULSE (TOP) AS COMPARED TO
UNAMPLIFIED FEED THROUGH SIGNAL (BOTTOM)
FOR SFD-252 UNDER dc OPERATING CONDITIONS

Figure 65 shows the amplified RF output pulse compared to the
unamplified RF feed through signal. Again the tests were made at
reduced magnetic field and voltage and except for the slightly
reduced power output, the performance obtained reproduced that
obtained with dc voltage and pulsed control voltage operation. An
operating voltage of 26.5 kv and a total cathode current of 128 amperes
produced approximately 600 kw as compared to the 850 kw obtained with
control voltage operation. The amplified RF output and the total
cathode current are shown in Figure 66. The reduced power output
resulted from some of the cathode current being collected on the bias
electrode and consequently not contributing to the signal amplification.
Figure 67 shows the total cathode current and the bias current
obtained during the AutoMod type of operation. The total cathode
current was measured at 128 peak amperes and the bias current at
23 peak amperes or approximately 18% of the total cathode current.
The current available for the amplification interaction was
approximately 105 peak amperes. The bias voltage used was 8 kv which
represents an approximate 3 to 1 ratio of operating voltage to bias
voltage. The average power operation was increased as each series of
tests was performed, culminating with the AutoMod operation at
approximately 1500 watts at the peak values described above. At this
point, no adverse effects had been observed and it is felt that a
significant increase in peak and average power output would be
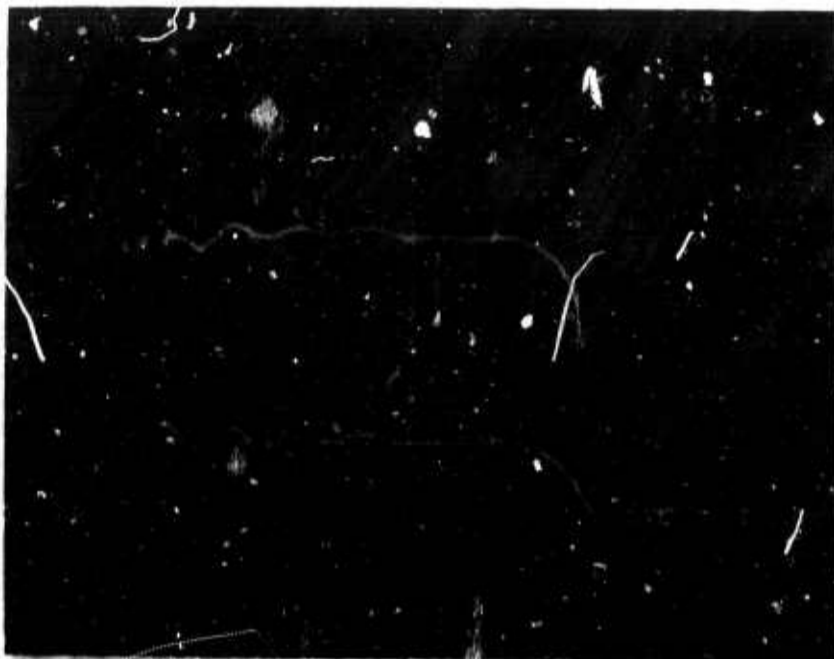obtained with further aging and seasoning.

FIGURE 65   RF OUTPUT (TOP) COMPARED TO UNAMPLIFIED
FEED THROUGH SIGNAL (BOTTOM) FOR SFD-252
UNDER AUTOMOD CONDITIONS
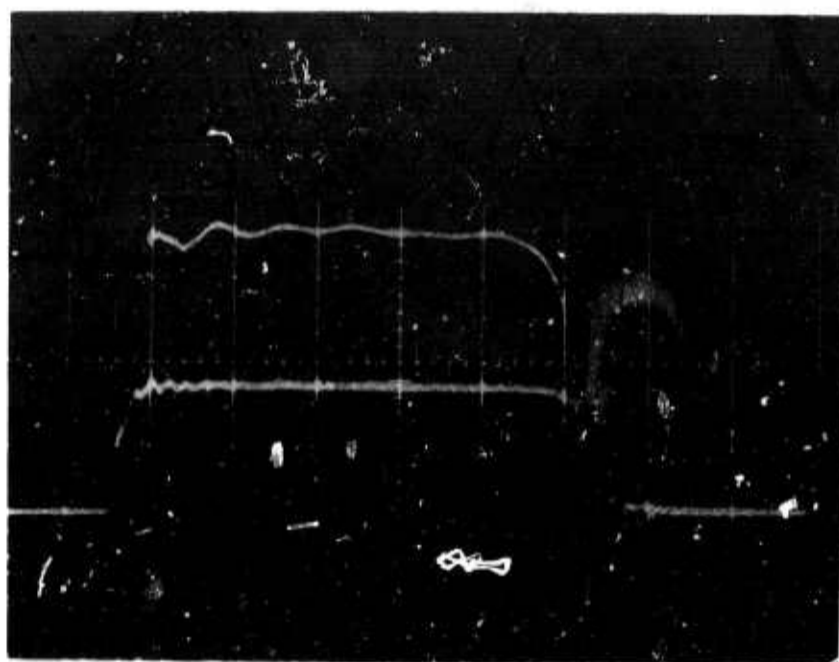
FIGURE 66   AMPLIFIED RF OUTPUT (TOP) AND TOTAL
             CATHODE CURRENT (BOTTOM) FOR SFD-252
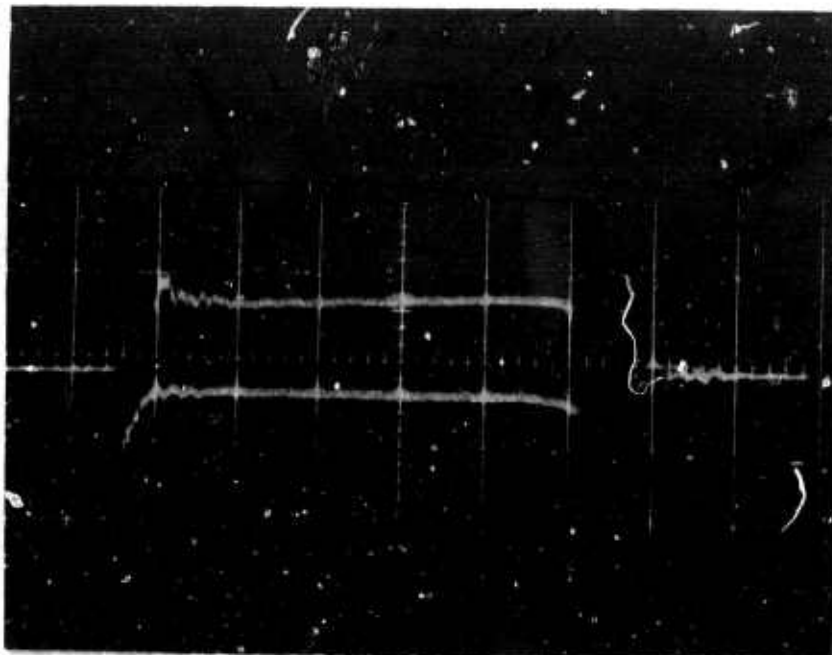   UNDER AUTOMOD CONDITIONS

FIGURE 57   BIAS CURRENT (TOP) AND TOTAL CATHOD_
CURRENT (BOTTOM) FOR SFD-252 DURING
AUTOMOD OPERATION

109

7.0 CONCLUSIONS

There were two main objectives for this program effort. The first was to demonstrate the feasibility of complete RF modulation (that is, RF turn on and RF turn off). The second was to demonstrate the feasibility of a high peak and average power slow wave anode circuit which uses a directly water cooled helix coupled bar circuit

The first objective, that is complete RF modulation of the amplifier, was met very successfully. The complete RF modulation or AutoMod operation was demonstrated in seven of the twelve experiments performed using the SFD-237 amplifier developed on the preceding contract, as well as in the SFD-252 amplifier which was being developed on this contract. AutoMod operation has been demonstrated in the SFD-237 to power levels of 800 kw to 1000 kw peak with constant cathode voltage and to 1000 kw or better at fixed cathode current (where cathode voltage is adjusted for constant current). Both modes of operation were accomplished with a fixed bias voltage and RF input power across a frequency band of 500 MHz from 5.4 GHz to 5.9 GHz. Average power output was limited to 3.5 kw by the equipment being used. It is believed that this vehicle can achieve at least twice this value of average power output without modifications. AutoMod operation was also successfully demonstrated in the SFD-252 using the preliminary information obtained with the SFD-237. In this case, power levels under AutoMod conditions were approximately 600 kw across the band at an average power of approximately 1500 watts. These results on the SFD-252 are considered to be preliminary as its evaluation was not as extensive as would be desired. At this level of operation, no obvious defects were observed, and it is believed that essentially full power operation could be achieved with additional effort.

The second objective of this effort, to demonstrate a new directly cooled slow wave circuit capable of high peak and average

power, has also been accomplished with considerable success. Although the full power operation was not demonstrated, the results obtained were significant. A peak power output of more than 1 Mw was demonstrated across a 500 MHz operating band between 5.4 GHz and 5.9 GHz at a constant voltage of approximately 29 kv. The peak power output was limited by the length of time which was available for aging. The SFD-252 appears to be quite capable of attaining the full peak power output when operated at the design level of 35 kv. The average power output demonstrated was only 1500 w. This low average power output demonstration cannot be considered a meaningful evaluation of the average power capability of the tube. In general it is viewed with a high degree of confidence that this vehicle can achieve the full power ratings with further aging.

DOCUMENT CONTROL DATA - R & D

(Security classification of title, body of abstract and indexing annotation must be entered when the overall report is classified)

1. ORIGINATING ACTIVITY *(Corporate author)*	2a. REPORT SECURITY CLASSIFICATION
VARIAN/EASTERN TUBE DIVISION *formerly* 800 Rahway Avenue Union, NJ 07083 SFD Labs., Inc. Union, N.J.	UNCLASSIFIED
	2b. GROUP N/A

3. REPORT TITLE

C-BAND PHASED ARRAY CROSSED-FIELD AMPLIFIER DEVELOPMENT

4. DESCRIPTIVE NOTES *(Type of report and inclusive dates)*

Final Report, 24 Jul 67 - 30 Nov 69

5. AUTHOR(S) *(First name, middle initial, last name)*

A. Wilczek

6. REPORT DATE	7a. TOTAL NO. OF PAGES	7b. NO. OF REFS
July 1970	112	-
8a. CONTRACT OR GRANT NO. F30602-68-C-0055	9a. ORIGINATOR'S REPORT NUMBER(S) 118-F	
b. PROJECT NO.		
c. ARPA Order No. 136	9b. OTHER REPORT NO(S) *(Any other numbers that may be assigned this report)* RADC-TR-70-132	
d.		

10. DISTRIBUTION STATEMENT

This document is subject to special export controls and each transmittal to foreign governments or foreign nationals may be made only with prior approval of RADC (EMATE) Griffiss AFB, NY 13440.

11. SUPPLEMENTARY NOTES	12. SPONSORING MILITARY ACTIVITY
RADC Project Engineer: Dirk T. Bussey (EMATE) AC 315 330-4251	Rome Air Development Center (EMATE) Griffiss Air Force Base, NY 13440

13. ABSTRACT

This program has two main objectives. The first is to demonstrate the feasibility of an RF turn on, RF turn off, reentrant stream crossed-field amplifier. The second objective of this program is to increase the power output capability previously demonstrated under Contract AF 30(602)-4082 by a factor of two.

The first objective was met very successfully as RF turn on and RF turn off were demonstrated reliably in a number of experiments in two different amplifier types. The second objective was partially accomplished with very significant results.

DD FORM 1473 (1 NOV 65)

14. KEY WORDS	LINK A		LINK B		LINK C	
	ROLE	WT	ROLE	WT	ROLE	WT
Microwave Tubes						
C-Band						
Power Amplifier						
Crossed-field						
Control Electrode Modulation						
Self-biasing						

END